
**Enzyme tRNA interaction and (t)RNA conformation
probed via
environmentally sensitive cyanine dyes**

Dissertation

zur Erlangung des Grades

“Doktor der Naturwissenschaften”

im Promotionsfach Pharmazie

am Fachbereich Chemie, Pharmazie und Geowissenschaften

Der JOHANNES GUTENBERG-UNIVERSITÄT

in Mainz

vorgelegt von

Felix Michael Spenkuch

geb. am 08.04.1984 in Bergisch Gladbach

Mainz, im September 2014

Dekan:

1. Berichterstatter:

2. Berichterstatter:

Datum der mündlichen Prüfung: 17.10.2014

D77 (Dissertation Mainz)

Die vorgelegte Dissertation wurde ... in Mainz zur Erlangung des Grades
"Doktor der Naturwissenschaften", unter Betreuung von _ angefertigt.

Erstgutachter:

Zweitgutachter:

Hiermit versichere ich eidesstattlich:

1. Ich habe die jetzt als Dissertation vorgelegte Arbeit selbst angefertigt und alle benutzten Hilfsmittel (Literatur, Apparaturen, Material) in der Arbeit angegeben.
2. Ich habe oder hatte die jetzt als Dissertation vorgelegte Arbeit nicht als Prüfungsarbeit für eine staatliche oder andere wissenschaftliche Prüfung eingereicht.
3. Ich hatte weder die jetzt als Dissertation vorgelegte Arbeit noch Teile davon bei einer anderen Fakultät bzw. einem anderen Fachbereich als Dissertation eingereicht.

Ort, Datum

Felix Spenkuch

“IF WE KNEW WHAT IT WAS WE WERE DOING,
IT WOULD NOT BE CALLED RESEARCH, WOULD IT?”

- *Albert Einstein (1879-1955)*

Für meine Familie.

Abstract

Nucleoside modifications influence RNA dynamics and function and act in epigenetics. However, conformational dynamics and modification enzyme recognition of the most densely modified RNA tRNA are still ill understood. Furthermore, the influence of the presumed covalent mechanistic inhibitor 5-fluorouridine (5FU) on Ψ synthase enzymes, which generate pseudouridine (Ψ) is as enigmatic as ever.

This work uses tRNAs labeled with the cyanine fluorophores Cy3 and Cy5 and applies thermophoresis and advanced fluorescence spectroscopy. A remarkable tolerance of dye-labeling and for the detected dye Cy5 an increase of fluorescence lifetime upon enzyme binding were revealed in thermophoresis binding assays. Moreover, thermophoresis assays could detect conformational differences in mutants of human mitochondrial tRNA^{Lys} and SAM binding by SAM-I riboswitch RNA.

To elucidate the action of 5FU-RNA on Ψ 55 synthase TruB, thermophoresis and time-resolved fluorescence binding assays were applied using Cy5-labeled tRNA. In agreement with gel shift experiments all results reveal reversible binding with a similar affinity of TruB for U55- and 5FU55-tRNA over the time span of several hours. A reevaluation of the SDS-stable 5FU-RNA TruB complex, previously interpreted as covalent adduct resulting from catalytic suicide action of 5FU, revealed a fast complex formation in high yield even for the poor substrate U33 tRNA. More stringent incubation conditions did not change complex yield. Thus the SDS stable band represents the initial contact of RNA and enzyme and not a suicide adduct resulting from catalysis.

Zusammenfassung

Nukleosidmodifikationen beeinflussen Dynamik und Konformation von RNA und sind epigenetisch wirksam. Wenig verstanden sind konformationelle Dynamik und enzymatische Erkennung von tRNA, sowie der Einfluss des mutmaßlichen kovalenten Inhibitors 5-Fluorouridine (5FU) auf Ψ Synthasen, die Pseudouridin (Ψ) erzeugen. Frühere Arbeiten nutzten mit den Fluorophoren Cy3 und Cy5 markierte tRNA, um diese Fragen zu adressieren.

Die vorliegende Arbeit weitet Cy3-Cy5-Markierung auf Hefe tRNA^{Phe} aus und nutzt Thermophorese und fortschrittliche Fluoreszenzspektroskopie. In der Thermophorese zeigte sich eine hohe Toleranz gegenüber Fluoreszenzmarkierung bei gleichzeitiger Erhöhung der Cy5 Fluoreszenz durch Enzymbindung. Zudem konnte die Konformation verschiedener Mutanten human mitochondrialer tRNA^{Lys} und die Bindung von SAM durch SAM-I Riboswitch RNA untersucht werden.

Um etwaige Unterschiede in der Interaktion von Ψ 55 Synthase TruB mit Cy5-gelabelter U55- bzw. 5FU55-tRNA aufzudecken, wurde eine Kombination aus Thermophorese, zeit- und polarisationsaufgelöster Fluoreszenzspektroskopie und 'gel shift' Experimenten genutzt. Alle Ergebnisse zeigten übereinstimmend eine reversible Bindung ähnlicher Affinität für beide tRNAs und widersprechen somit einer kovalenten Inhibition durch 5FU. Folgerichtig wurde der SDS-stabile Komplex von TruB mit 5FU-tRNA neu evaluiert, da er bisher als kovalent interpretiert wurde. Es erfolgte eine schnelle Komplexbildung in hoher Ausbeute auch für schlechte Substrate, außerdem ließ sich die Komplexausbeute nicht durch andere Reaktionsbedingungen beeinflussen. Somit kann der SDS stabile Komplex nur den ersten, nicht-kovalenten Kontakt von Enzym und 5FU55-tRNA darstellen und repräsentiert kein kovalentes Addukt späterer Katalyse.

Contents

Abstract	ix
Zusammenfassung	xi
List of Tables	xvi
List of Figures	xvii
Abbreviations and symbols	xxiii
1. Introduction	1
1.1. The changing dogma of molecular biology	1
1.2. RNA function, conformation and dynamics	3
1.2.1. What makes RNA different from DNA and proteins	3
1.2.2. tRNA conformation, modification and function	3
1.2.3. RNA conformation in riboswitches	8
1.3. Pseudouridine	10
1.3.1. General aspects	10
1.3.2. Occurrence in tRNA	11
1.3.3. Effects of 5-fluoropyrimidines on RNA and DNA	12
1.3.4. 5-Fluorouridine in the investigation of pseudouridine syn- thases	13
1.4. Sensitivity of cyanines towards their biomolecular environment . .	16
1.4.1. Protein induced fluorescence enhancement of cyanines . . .	16
1.4.2. Interaction of cyanine fluorophores with nucleic acids	18
1.5. Theory of Microscale Thermophoresis	19
1.5.1. General Theory	19
1.5.2. Experimental Implementation	21

2. Goal of this Work	23
3. MST on RNA	25
3.1. Evaluation of RNA protein interactions	25
3.1.1. MST detects binding of many tRNA modifying enzymes . .	25
3.1.2. Influence of dye labels on tRNA upon TruB binding	30
3.1.3. MST to evaluate binding mode of Mouse Ψ synthase I . . .	34
3.2. MST to evaluate conformation of hmt tRNA ^{Lys}	38
3.3. MST of a SAM binding riboswitch	43
4. Interaction of TruB with 5FU55-tRNA	49
4.1. Introduction	49
4.2. Gel shift and LC-MS/MS analysis	50
4.3. Microscale thermophoresis	54
4.4. Spectroscopy of Cy5-tRNA TruB interaction	59
4.4.1. Spectroscopic change upon TruB binding	59
4.4.2. Spectroscopic titrations	60
4.5. Discussion	63
4.5.1. Dye label interference with tRNA structure and with TruB turnover	63
4.5.2. Spectroscopic effects of protein binding	65
4.5.3. TruB interaction with 5FU55- vs. U55-tRNA	67
4.5.4. Comparison with other cases of 5FU inhibition	68
4.5.5. Comparison with tRNA-guanine transglycosylases	70
4.5.6. Effect of SDS on proteins	72
4.5.7. Possible effects of fluorine on TruB binding	73
4.6. Conclusion	75
5. Single molecule FRET on tRNAs	77
5.1. Tolerance of dye positions in ribosome smFRET	77
5.1.1. Introduction	77
5.1.2. Aminoacylation and EF-Tu complexation	78
5.1.3. tRNA-Ribosome FRET	78
5.2. SmFRET reveals two conformations of hmt tRNA ^{Leu(CUN)}	80
5.2.1. Construct design and idea	80

5.2.2.	At 2 mM Mg ²⁺ hmt tRNA ^{Leu(CUN)} is in a dynamic extended conformation	81
6.	Conclusion & Outlook	85
6.1.	Conclusion	85
6.1.1.	Microscale thermophoresis on RNA	85
6.1.2.	Protein induced fluorescence enhancement	85
6.1.3.	5FU55-tRNA TruB interaction	86
6.1.4.	Single molecule FRET	86
6.2.	Outlook	87
6.2.1.	MST on hmt tRNA ^{Lys}	87
6.2.2.	Single molecule fluorescence studies of tRNA-TruB interaction	87
6.2.3.	Turnover studies and binding kinetics on tRNA-TruB interaction	88
7.	Experimental Details	89
7.1.	Material	89
7.1.1.	Buffers:	89
7.1.2.	Enzymes	90
7.1.3.	Consumables	90
7.1.4.	Instruments	93
7.2.	RNA ligation constructs	94
7.2.1.	Yeast tRNA ^{Phe}	94
7.2.2.	Human mitochondrial tRNA ^{Lys}	95
7.2.3.	Human mitochondrial tRNA ^{Leu(CUN)}	96
7.3.	Methods	97
7.3.1.	RNA synthesis	97
7.3.2.	Protein synthesis	99
7.3.3.	Microscale thermophoresis	101
7.3.4.	Gel shift experiments	104
7.3.5.	Coomassie staining procedure	105
7.3.6.	Bulk fluorescence measurements	105
7.3.7.	Single molecule fluorescence measurements	106

A. Appendix	109
A.1. Appendix to chapter 3	109
A.1.1. subsection 3.1.1	109
A.1.2. subsection 3.1.2	110
A.1.3. Appendix to section 1.5	112
A.2. Appendix to chapter 4	113
A.2.1. Pseudouridine formation analyzed by LC-MS/MS	114
A.2.2. All features of MST curves are sensitive to TruB binding	115
A.2.3. Additional MST experiments	115
A.2.4. tRNA-TruB binding investigated by urea PAGE	116
A.2.5. tRNA-TruB interactions investigated on SDS PAGE	120
A.2.6. Spectra on tRNA-TruB interaction	120
A.2.7. Effects of tRNA-TruB binding on fluorescence anisotropy	121
 Bibliography	 123
 B. Publications	 143

List of Tables

3.1. Results of a screen for protein binding using microscale thermophoresis.	29
4.1. Comparison of thermophoretic properties of free, TruB bound and chased tRNA samples.	58
4.2. Changes in spectroscopic properties upon TruB binding.	59
5.1. Preliminary results of smFRET ribosome assays.	79
7.1. Enzymes used in this work.	90
7.3. Instruments used in this work.	93
7.4. Oligonucleotides applied in yeast tRNA ^{Phe} synthesis.	95
7.5. Oligonucleotides applied in human mitochondrial tRNA ^{Lys} synthesis.	96
7.6. Oligonucleotides applied in human mitochondrial tRNA ^{Leu(CUN)} synthesis.	97
7.7. Recipe for 6% stacking and 10% resolving SDS PAGE.	105
A.1. Changes in anisotropy upon TruB binding	121

List of Figures

1.1. Epigenetic mechanisms.	2
1.2. Structure of yeast tRNA ^{Phe}	4
1.3. Modified nucleosides of yeast tRNA ^{Phe}	5
1.4. Structure of human mitochondrial tRNA ^{Leu(CUN)}	6
1.5. Structure of human mitochondrial tRNA ^{Lys}	7
1.6. Schematic representation of the types of riboswitches.	8
1.7. Ligand binding of the SAM I riboswitch aptamer domain.	9
1.8. Scheme representing the formation of pseudouridine (Ψ) by pseudouridine synthases.	10
1.9. Distribution of pseudouridine in tRNAs.	11
1.10. Inhibition mechanisms of 5-fluoropyrimidines.	12
1.11. Mechanisms proposed for pseudouridine synthases.	14
1.12. Products generated by pseudouridine synthases.	15
1.13. Protein influence on spectroscopic properties of cyanine dyes.	17
1.14. Influence of single nucleotides or DNA attachment on the fluorescence lifetime of Cy3.	18
1.15. Readout and analysis of MST titrations.	21
3.1. Modification enzymes used in a thermophoresis screen on fluorescently labeled yeast tRNA ^{Phe}	25
3.2. MST Traces of the protein screen.	26
3.3. Percental increase in fluorescence upon protein binding.	27
3.4. Enzyme tRNA binding isotherms as determined by MST.	28
3.5. Docking model of <i>E. coli</i> TruB to yeast tRNA ^{Phe}	31
3.6. Normalized thermophoresis curves of tRNA-TruB interaction.	31
3.7. MST titration curves of tRNA TruB interaction.	32
3.8. Results of MST titration of various yeast tRNA ^{Phe} FRET constructs with TruB.	33

3.9. Tertiary structure of the tRNA ^{Leu(CUN)} constructs.	35
3.10. Normalized MST curves of titrations with mPus1p.	36
3.11. MST titration curves of tRNA ^{Leu(CUN)} mPus1p interaction.	37
3.12. Results from MST titrations of tRNA ^{Leu(CUN)} constructs with mPus1p. 37	
3.13. Secondary structures of fluorescently labeled human mitochondrial tRNA ^{Lys} mutants.	39
3.14. Normalized MST curves of tRNA ^{Lys} Mg ²⁺ titrations.	40
3.15. MST titration of tRNA ^{Lys} mutants with MgCl ₂	41
3.16. Structure of SAM-I riboswitch constructs.	43
3.17. Normalized MST curves of SAM titrations.	44
3.18. MST titration curves from SAM SAM-I riboswitch interaction. . . .	45
3.19. Conclusions from MST titration on SAM-I riboswitch interaction. . .	46
4.1. Tertiary (above) and secondary (below) structure representations of the yeast tRNA ^{Phe} constructs.	50
4.2. Analysis of SDS-stable complex formation of TruB with unlabeled tRNA.	51
4.3. Comparison of the kinetics of SDS stable complex formation with enzymatic turnover for labeled and unlabeled tRNA.	52
4.4. Normalized MST curves for tRNA TruB interaction.	55
4.5. MST titration curves of tRNA TruB interaction.	56
4.6. Representative unnormalized MST curves fitted to a two phase ex- ponential decay.	57
4.7. Exemplary representation of spectroscopic changes caused by TruB binding.	60
4.8. Spectroscopic titration curves of TruB tRNA interaction.	61
4.9. Overview of determined K _d s for the tRNA TruB interaction.	62
4.10. Conformation and TruB interaction of yeast tRNA ^{Phe}	64
4.11. Tertiary and secondary structure of yeast tRNA ^{Phe} in canonical or lambda conformation.	66
4.12. Comparison of 5FU action in m ⁵ U methyl transferases (a) and a proposed similar action in Ψ synthases.	69
4.13. Comparison of tRNA-guanine transglycosylase mechanism with the glycol mechanism of Ψ formation.	71

4.14. Crystal structures showing structural differences and different protein-RNA interactions in the active site of the wild type and a catalytically inactive <i>E. coli</i> TruB bound to 5FU RNA.	74
5.1. Crystal structure of yeast tRNA ^{Phe} with typical vs. applied labeling positions for ribosome FRET.	78
5.2. Arrival of an EF-Tu(GTP)-tRNA ternary complex at the A site of the ribosome.	80
5.3. Construct design and immobilization procedure for smFRET.	81
5.4. Single molecule FRET efficiency histogram of human mitochondrial tRNA ^{Leu(CUN)} at 2 mM Mg ²⁺	82
5.5. Tertiary interaction in canonical hmt tRNA ^{Leu(CUN)} and in the 'T slip' conformation.	83
7.1. Ligation system for of yeast tRNA ^{Phe}	94
7.2. Ligation system for of hmt tRNA ^{Lys}	95
7.3. Ligation system for of hmt tRNA ^{Leu(CUN)}	96
7.4. Chromatograms from Ni ²⁺ -NTA HisTrap chromatography of TruB.	100
7.5. Chromatograms from size exclusion chromatography of TruB.	100
A.1. Dissociation constants of TruB and tRNA constructs as resulting from different thermophoresis curve readouts.	109
A.2. Labeling chemistries for different yeast tRNA ^{Phe} constructs.	110
A.3. MST curve set of C49-U17-U55 tRNA TruB interaction.	111
A.4. Dissociation constants of TruB and tRNA constructs as resulting from different thermophoresis curve readouts.	112
A.5. Dissociation constants of mPus1p and tRNA constructs as resulting from different thermophoresis curve readouts.	113
A.6. Measurements performed by LC-MS/MS analysis for verification of turnover efficiency.	114
A.7. Dissociation constants of TruB and tRNA constructs as resulting from different thermophoresis curve readouts.	115
A.8. Influence of protein inhomogeneity on MST experiments.	116
A.9. TruB-C49-tRNA interaction assessed by 8 M Urea PAGE.	117
A.10. TruB-tRNA interaction assessed by urea PAGE.	118

A.11. TruB-tRNA interaction assessed by native PAGE.	119
A.12. TruB-C49-5FU55-tRNA interaction assessed by SDS PAGE for the different incubation times and temperatures.	120
A.13. Representative spectra from tRNA TruB titrations.	120
A.14. Detail of tRNA-TruB docking model.	122

Abbreviations and symbols

5FhPsi	5-fluoro–6-hydroxy-pseudouridine
5FU	5-fluoro-uridine
ASL	anticodon stem loop (part of tRNA structure)
ATP	Adenosin triphosphate
bp	base pair
BSA	Bovine Serum Albumin
Cy3	Reactive dye for labeling of amino-modifiers on RNA was: 3H-Indolium,2-[3-[1-[6-[(2,5-dioxo-1-pyrrolidinyl)oxy]-6-oxohexyl]-1,3-dihydro-3,3-dimethyl-5-sulfo-2H-indol-2-ylidene]-1-propenyl]-1-ethyl-3,3-dimethyl-5-sulfo-,inner salt
Cy5	Reactive dye for the labeling of aminomodifiers on RNA was: 3H-Indolium,2-[5-[1-[6-[(2,5-dioxo-1-pyrrolidinyl)oxy]-6-oxohexyl]-1,3-dihydro-3,3-dimethyl-5-sulfo-2H-indol-2-ylidene]-1,3-pentadien-1-yl]-1-ethyl-3,3-dimethyl-5-sulfo-,inner salt
DNA	Deoxy nucleic acid
DTT	Dithiothreitol
E. coli	Escherichia coli
EC50	half maximal effective concentration
EF-Tu	Elongation Factor Tu
FRET	Förster (or Fluorescence) Resonance Energy Transfer
GTP	Guanosine triphosphate
hDnmt2	enzyme Dnmt2 of human
hmt	human mitochondrial
IPTG	Isopropyl beta-D-1-thiogalactopyranoside
Kd	dissociation constant
mPus1p	mouse Pus1p

MST	Microscale Thermophoresis
n	Hill coefficient
NA	numerical aperture
OD600	optical density at 600 nm
pabTrmi	enzyme Trmi of <i>Pyrococcus abyssi</i>
PAGE	polyacrylamide gel electrophoresis
PBS	Phosphate buffered saline
PDB	Protein database entry
PIFE	Protein Induced Fluorescence Enhancement
Pseudouridine	5-(beta-D-ribofuranosyl)pyrimidine-2,4(1H,3H)-dione
RNA	Ribonucleic acid
s. c.	<i>saccharomyces cerevisiae</i>
SAM	S-Adenosylmethionin
scPus4p	enzyme Pus4p of <i>Saccharomyces cerevisiae</i> (yeast)
SDS	sodium dodecyl sulfate
smFRET	single molecule Förster (or Fluorescence) Resonance Energy Transfer
<i>T. thermophilus</i>	<i>Thermus thermophilus</i>
tmTruB	<i>Thermotoga maritima</i> TruB
Tris	tris(hydroxymethyl)-aminomethan
tRNA	transfer ribonucleic acid
tRNA ^{Leu} (CUN)	transfer ribo nucleic acid recognizing the codon CUN coding for the amino acid leucine (Leu)
tRNA ^{Lys}	transfer ribo nucleic acid recognizing the codon for the amino acid lysine (Lys)
tRNA ^{Phe}	transfer ribo nucleic acid recognizing the codon for the amino acid phenylalanine (Phe)
Trolox	6-hydroxy-2,5,7,8-tetramethylchroman-2-carboxylic acid
TruB	pseudouridine synthase generating Psi55 in eubacteria
TSL	T stem loop, a part of transfer ribonucleic acid

1. Introduction

1.1. The changing dogma of molecular biology

Completion of the human genome project definitely caused a considerable acceleration of research in life sciences [1]. But with the genetic code being available in plain writing, the real challenge only began: How is this code actually put to use, which portions of it are important and when? The question seemed simple when Francis Crick coined the 'central dogma of molecular biology' in 1970: 'DNA makes mRNA (messenger RNA) and mRNA makes protein' [2]. A fixed hierarchy was established: The permanent information carrier DNA (genome), was to be transcribed into its transient offspring RNA that functions as a template for the synthesis of proteins, which build the actual functional elements of life.

However, there is a necessity of dynamic gene regulation, which becomes especially apparent in the development of multicellular organisms: To cause the right cellular differentiation specific proteins have to be synthesized in the right cells at a specific time in a specific amount [3]. This genetic regulation is investigated by the rapidly expanding field of epigenetics: Epigenetics describe mechanisms that regulate gene activity, thereby affecting a cell's fate and the development of a whole organism without actual alteration of the genetic code [3, 4]. Since they govern cellular fate, mechanisms of epigenetics are thought to be of paramount importance in diseases [5].

The mechanisms of epigenetics are too numerous to be discussed here, especially as they act reversibly on various levels (see Fig.1.1) in a complexity that warrants dedicated reviews for each of them [6–12]. The most enigmatic epigenetic mechanisms may involve base modification of RNA, where bases are tuned by adding or changing functional groups. At present about ~150 modified nucleosides are known [13–15] but only the epigenetic mechanism of m⁶A incorporation

in mRNA is about to be fully established (see Fig.1.1) [11].

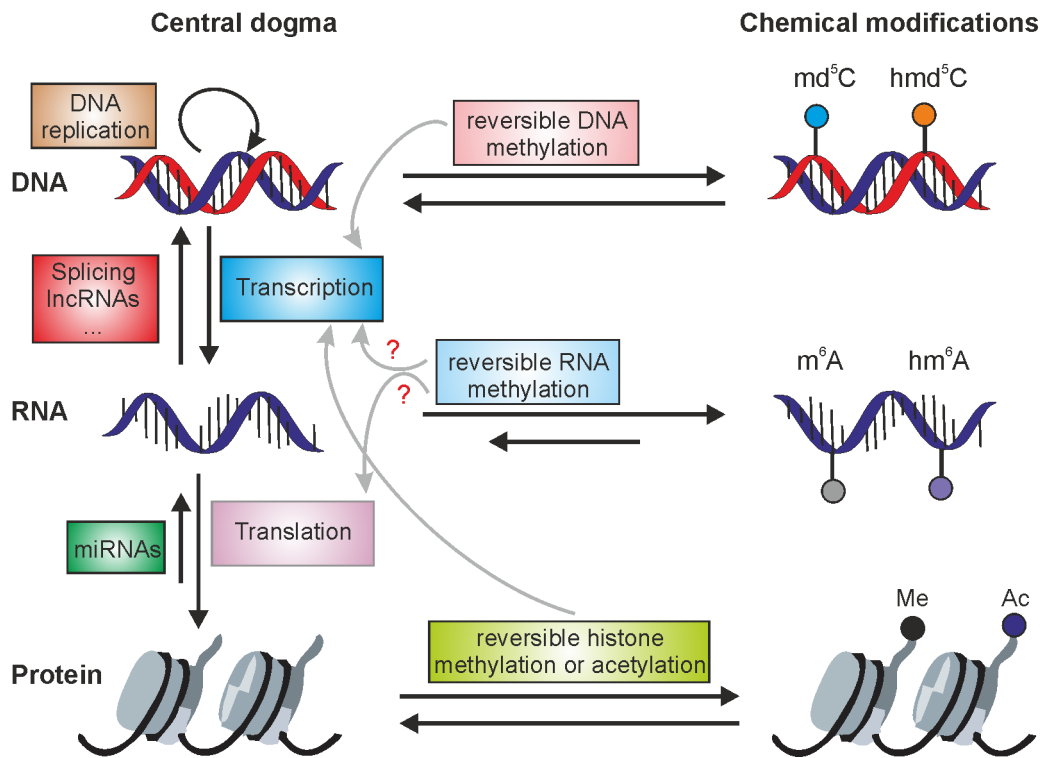


Figure 1.1.: Epigenetic mechanisms and their action on various stages of the 'central dogma of molecular biology'. Figure based on [7, 11, 16].

Two other modifications come into focus of epigenetics:

- m^5C in tRNA was shown to promote tRNA stability and protein synthesis in mice and in human fibroblasts [17, 18], while regulating the function of long non-coding (lnc) RNAs [19].
- pseudouridine (sec.1.3), so far undetected in mRNA, has been proven to transform stop codons into sense codons if the modification is introduced artificially, thereby expanding the protein coding region of mRNAs[20, 21].

Riboswitches provide a gene regulation mechanism in bacteria, which can act either co- or post-transcriptionally [22] and will be discussed in sec.1.2.3.

1.2. RNA function, conformation and dynamics

1.2.1. What makes RNA different from DNA and proteins

At a first glance the only difference from RNA to DNA is that adenosine pairs with uridine in RNA, while it pairs with thymidine in DNA. However, the DNA component thymidine monophosphate (TMP) is synthesized from deoxy-uridine monophosphate (dUMP) by the enzyme thymidylate synthase [23]. This relation, the discovery of first naturally occurring catalytic RNAs three decades ago [24, 25] and other aspects make a primordial RNA world a widely accepted hypothesis: RNA could have acted as the universal biomacromolecular ancestor, being information carrier and catalytically active component at the same time [26].

While RNA can obviously serve as information carrier in a DNA-like manner as mRNA, it is more alike to proteins in terms of structural complexity [27] and is, unlike DNA but like proteins subjected to, e.g., nuclear import and export [28] and can even be edited base-specifically [29, 30]. Proteins are biopolymers consisting of 20 canonic proteinogenic amino acids that can form three basic structural domains: Small side-chains prefer β sheets [31], larger side-chains prefer α helices [32] and the amino acid proline breaks helices into unstructured loops [33]. RNA on the other hand can access a regime of complex tertiary structure, which is blocked to DNA, since it carries an additional 2'-OH moiety at the sugar. This moiety organizes RNA into a different helix form than DNA and provides an additional hydrogen bond donor and acceptor, thereby creating the basis for numerous complex tertiary structural motives [27, 34]. For RNA conformational dynamics are as important for functionality as they are for proteins [35], and, as with proteins, RNA conformation and function are tuned by site-specific modifications of individual monomers in the chain [14].

1.2.2. tRNA conformation, modification and function

A particularly interesting RNA to study conformational dynamics and the influence of base modifications is tRNA (transfer RNA). Following the model of yeast Phenylalanine tRNA (tRNA^{Phe}), the primary structure of canonical tRNAs folds

into a cloverleaf like shape, thereby forming the structural features of the acceptor stem, the D stem loop (DSL or D arm) and the T stem loop (TSL or T arm) and the Anticodon stem loop (ASL) [36, 37]. This 2D structure (Fig.1.2a) is able to form an additional level of tertiary interactions (Fig.1.2b) that result in a three dimensional fold resembling the letter “L” (inset in Fig.1.2b). Here the D arm (orange) and T arm (blue) fold onto each other, resulting in the elbow of the L, while acceptor stem and anticodon stem loop form the two arms. The fate of tRNA is to become aminoacylated with its cognate amino acid at the CCA-end (1), to form a ternary complex with an elongation factor protein (2) and hybridize to its cognate codon on mRNA in the ribosome (3), thereby enabling the synthesis of a protein with a given sequence via ribosomal catalysis (4) [38]. Now tRNAs differ in sequence and in the amino acid they are able to transfer on one hand (although up to six isoaccepting tRNAs exist [38]), but have to adopt a similar conformation to function in the ribosome on the other hand, while each tRNA should, ideally, only be accepted for its cognate mRNA codon sequence.

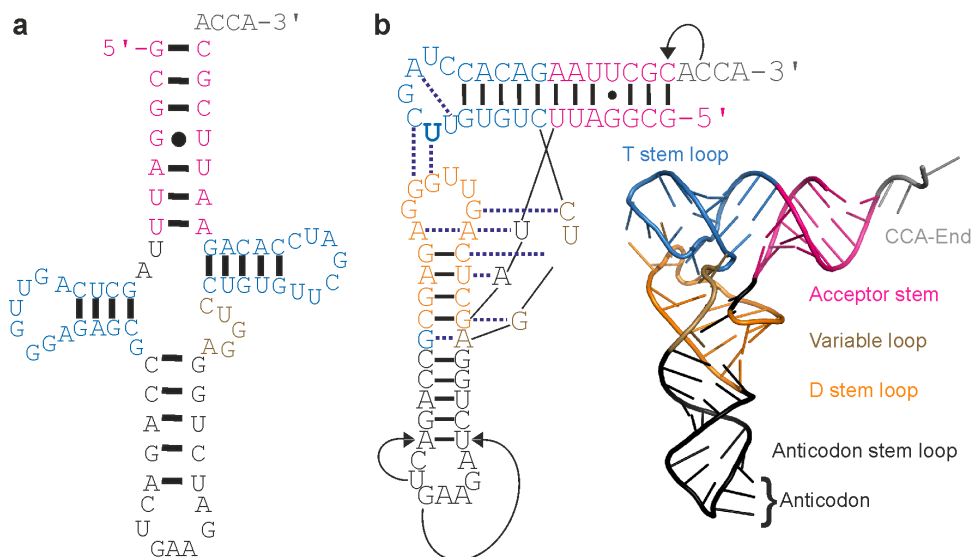


Figure 1.2.: Structure of yeast tRNA^{Phe} [36]: Secondary (a), secondary with tertiary interactions and three dimensional crystal structure (PDB ID 1EHZ) (b) and modified bases of the anticodon domain (c), T stem loop (d) and D stem loop (e).

These seemingly contradictory requirements are met by conformational flexibility of tRNA. E.g., the ASL of yeast tRNA^{Phe} differs in conformation, depending on whether the RNA is free in solution, bound to modifying or processing enzymes, to its aminoacylating enzyme or whether the tRNA is acting in translation

1.2 RNA function, conformation and dynamics

in the ribosome [35]. As tRNA is a ~75mer build of only four different nucleotide monomers, the initial conformational space may seem restricted as compared, e.g., to proteins consisting of 20 canonical amino acids [38]. But in fact more than 150 nucleoside modifications were discovered to date in RNA [13–15] and are thought to sustain, optimize and modulate the functional conformation of the RNA they alter [35]. The majority of these modifications is also incorporated into tRNA [14, 39] where an especially high modification density is achieved, as the example of yeast tRNA^{Phe} shows [36, 40] (see Fig.1.3).

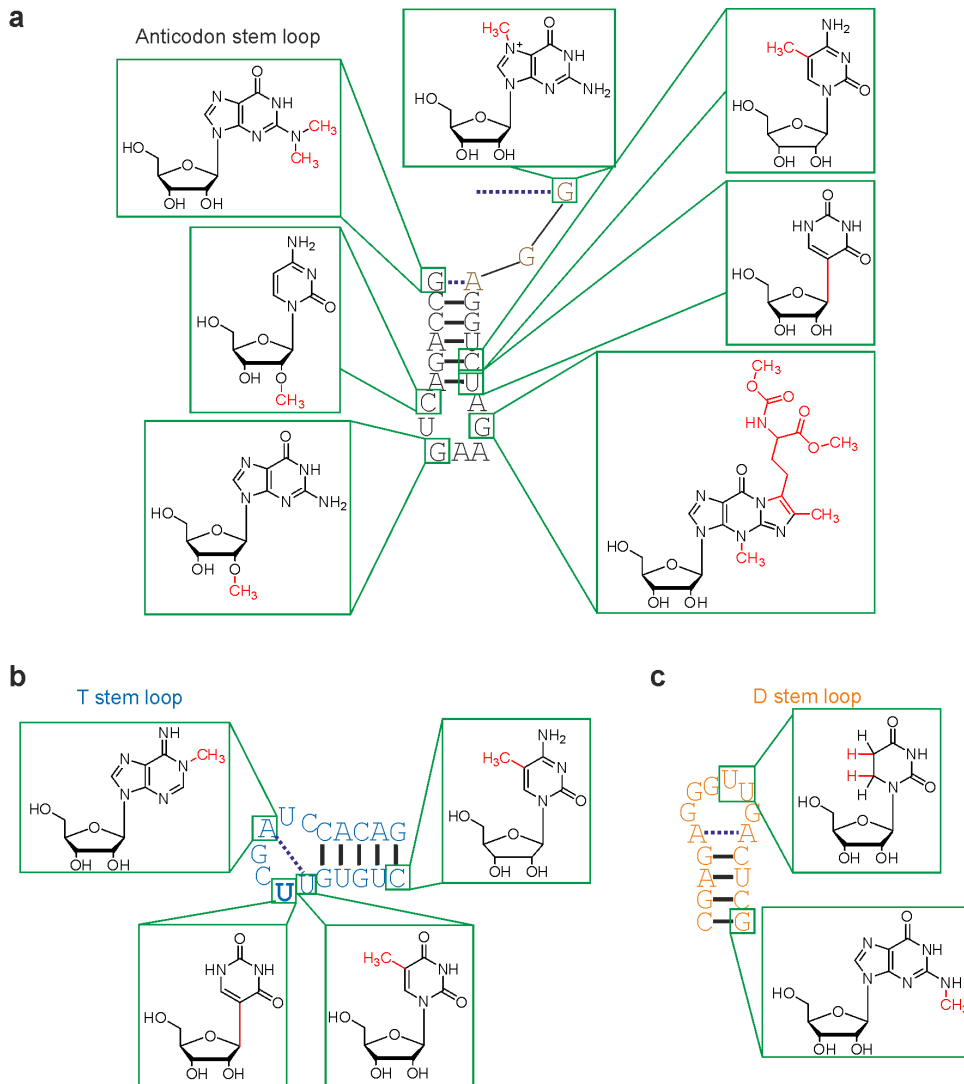


Figure 1.3.: Modified nucleosides of yeast tRNA^{Phe} [36]. Chemical differences to canonical nucleosides are depicted in red. For clarity divided into ASL (a), TSL (b) and DSL (c).

One would expect the ASL to be the most heavily modified part, as it contains the most specific function. Surprisingly this is not true over all tRNAs, because the D- and the T-arm contain the bulk of the modifications, resulting in a stable 3D structure, which is well protected against degradation [39]. This leads to a half life of several days instead of minutes for less structured RNAs. In fact correct core modification is mandatory for a tRNA to take part in translation: Only a structurally stable transcribed tRNA receives the terminal CCA, essential for aminoacylation, by action of the CCA-adding enzyme [41], while unstable, hypo-modified tRNAs are marked for degradation by CCA-CCA addition [42].

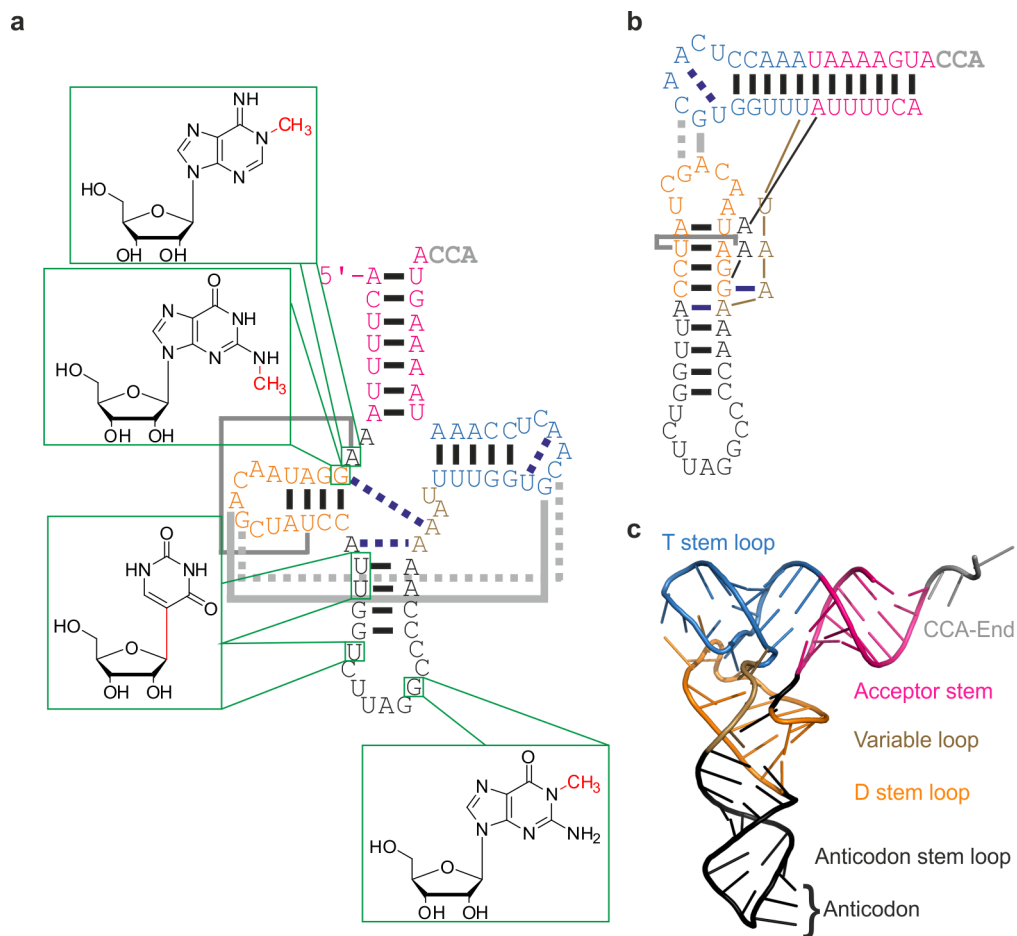


Figure 1.4.: Structure [43] and nucleoside modifications [14] of human mitochondrial tRNA^{Leu(CUN)}. Secondary cloverleaf conformation with tertiary interactions as thick lines and nucleoside modifications (a), pseudo-tertiary structure (b) and 3D structure of canonical tRNA [36] (c).

1.2 RNA function, conformation and dynamics

Besides yeast tRNA^{Phe} this work investigates human mitochondrial (hmt) tRNA^{Lys} and tRNA^{Leu(CUN)}. Matching the hypothesized endosymbiotic origin of the organelle [44], the mitochondrial genome contains only a minimal set of tRNAs that show varying extends of degeneration compared to the canonical secondary and tertiary tRNA structure given in Fig.1.2 [43]. Although the modification level of mammalian mitochondrial tRNAs is low in general and they are less stable in structure due to a high A-U content [43], some mitochondrial tRNAs still contain most of the tertiary interactions that are applied by canonical tRNAs to adopt the canonical L shape, like tRNA^{Leu(CUN)} (see Fig.1.4).

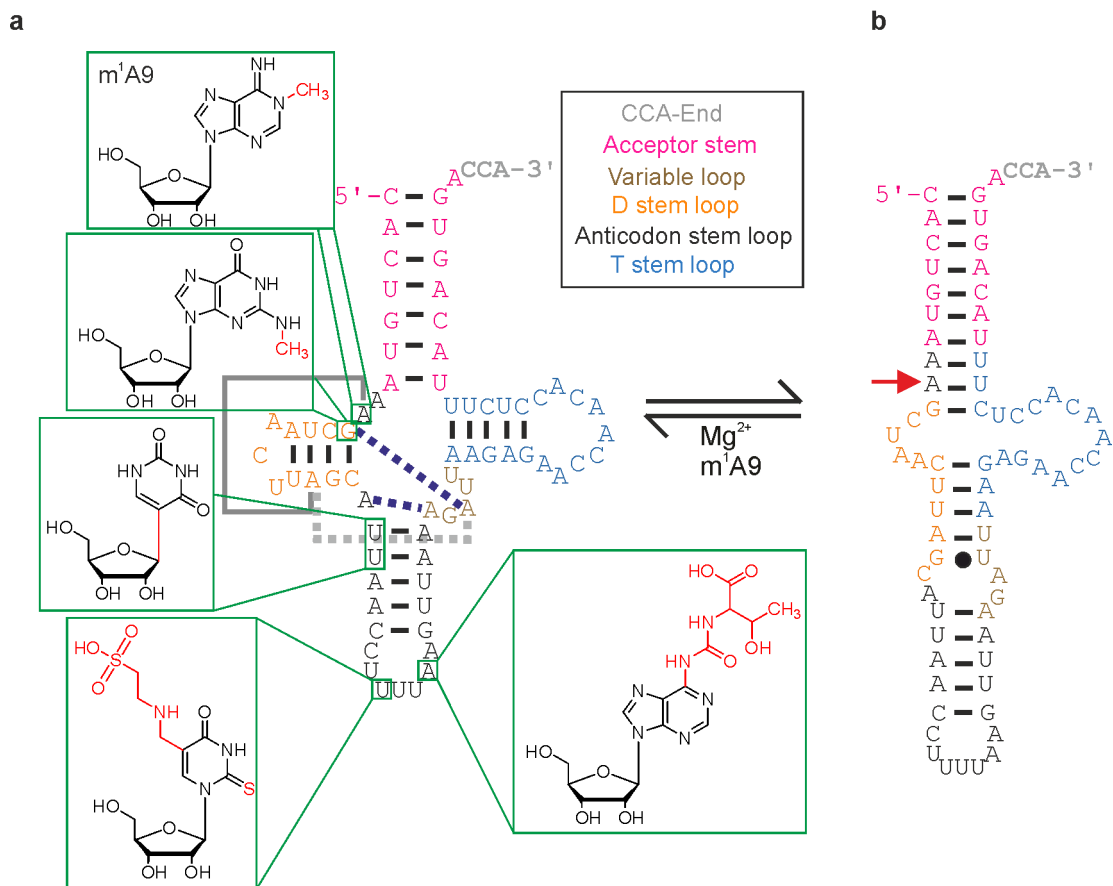


Figure 1.5.: a Secondary structure, tertiary interactions and nucleoside modifications of hmt tRNA^{Lys} [45]. The conformation native to unmodified tRNA is the extended hairpin given in b [45], while Mg²⁺ [46] and the m¹A9 modification [46, 47] (marked by a red arrow in b) promote the canonical cloverleaf conformation.

In contrast, human mitochondrial tRNA^{Lys} lacks any canonical interactions between D arm and T arm (Fig. 1.5a) and the unmodified tRNA prefers an extended

hairpin conformation instead of the canonical cloverleaf [45]. Already the introduction of a single modification, m^1A at position 9 (marked with a red arrow in Fig. 1.5b), leads to a significant fraction with a cloverleaf fold [47], rendering the tRNA a particularly descriptive example for the possible structural importance of nucleoside modifications.

1.2.3. RNA conformation in riboswitches

The development of the SELEX (Systematic Evolution of Ligands by EXponential Enrichment) method in 1990, allowed the identification of artificial nucleic acid aptamers for almost any ligand [48, 49]. The concept of RNA aptamers was established in nature only one decade later: In 2002 Winkler, Nahvi and Breaker discovered an element located in the untranslated region of bacterial mRNA capable of gene regulation upon binding of thiamine [50]. Depending on whether the ligand is bound or not, these mRNA elements, present in bacteria in general, function as a conformational switch that either aborts transcription or prevents translation and were thus termed riboswitches [51]. To date a large variety of ligands was discovered that either activate or deactivate the gene according to the type of riboswitch [22].

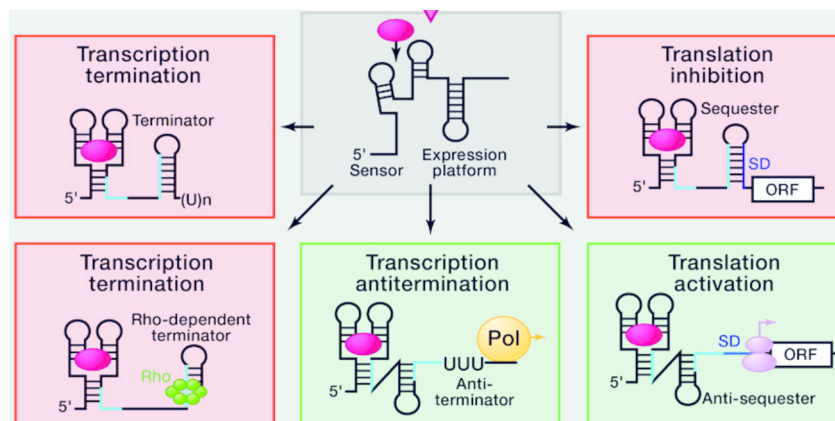


Figure 1.6.: Schematic representation of the types of riboswitches (figure adopted from [22]). Binding of a purple ligand to the aptamer domain (sensor) indicated by two stem loops stabilizes the binding competent conformation that includes a structural change in the expression platform. Depending on the type of switch this can result in transcription termination (red) by a rho-dependent or rho-independent terminator or ligand binding can resolve a terminator, thereby activating transcription (green). Translation can be equally either inhibited (red) by sequestering of the ribosome binding site (Shine-Dalgarno sequence, SD) or it can be activated by making the SD accessible (green).

To fulfill their task, riboswitches are composed of two parts: An aptamer domain senses the regulatory need by specific ligand binding, resulting in conformational adjustment of a second component, the so called expression platform [22]. As is shown in Fig.1.6, the expression platform can serve as the actual genetic switch by several different mechanisms.

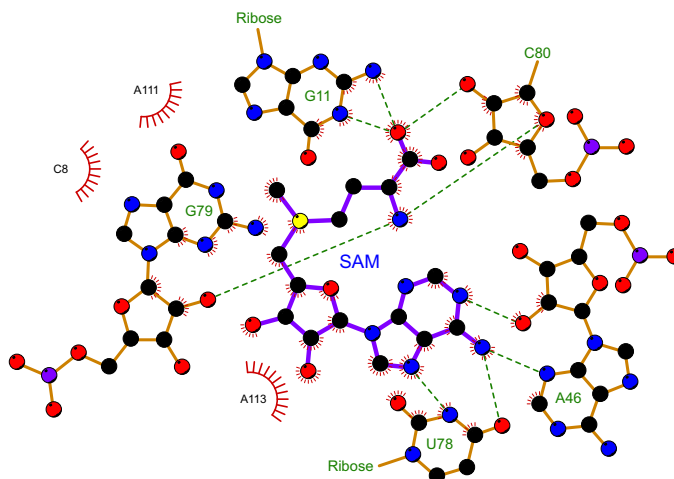


Figure 1.7.: Ligand binding of the SAM I riboswitch aptamer domain in a 2D projection of the cocrystal structure [52] generated by LigPlot⁺ [53]. Hydrogen bonds are depicted as green dashed lines, nucleotides surrounded by 'red eyelashes' are involved in stacking interaction with the ligand, shown in blue. Atoms are represented as spheres: Black corresponds to carbon, blue to nitrogen, red to oxygen, purple to phosphate and yellow to sulfur.

Although a wide span of riboswitches have been characterized recently on the single molecule level [54–60], this characterization was restricted to the ligand binding aptamer domain alone. However, omitting the expression platform removes the actuator and reduces the switch to a mere sensor (Fig.1.6), that is always capable of ligand binding. The difference for metabolite binding of the whole riboswitch vs. the pure aptamer is well characterized for the *Bacillus subtilis* SAM-I riboswitch: The RNA binds S-Adenosyl methionine with 200 nM affinity, if the expression platform is included [61], while the affinity of different aptamer domains varies from 4-20 nM [52, 55, 61–63]. The high affinity of the aptamer domain for SAM can be attributed to numerous hydrogen bonds and stacking interactions formed in the interaction (see Fig.1.7).

1.3. Pseudouridine

1.3.1. General aspects

As the previous section shows, structure and conformational dynamics are an important feature of any RNA and especially tRNAs are densely modified to fine-tune this feature [13–15]. The longest known [64] and most abundant modification [65] is pseudouridine (Ψ): The C-C-glycosidic isomer of uridine (U) is generated by enzymes called pseudouridine synthases. As is evident from Fig.1.8, Ψ and U share the same Watson-Crick face (red), but the former possesses an additional hydrogen bond donor with the NH1-imino-proton (orange). The actual advantage of pseudouridinylation is still mysterious and mostly addressed as stabilization by “additional hydrogen bonds and base stacking” [66].

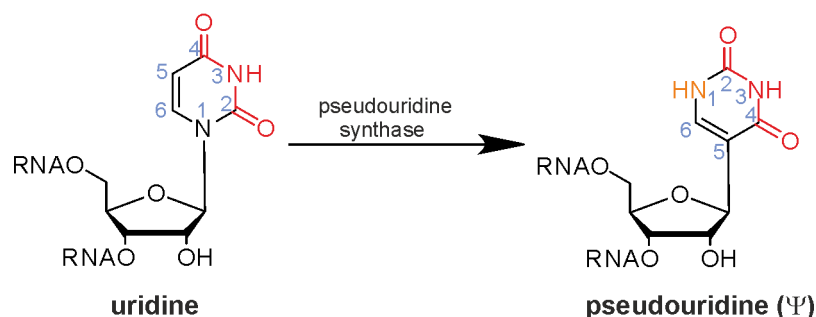


Figure 1.8.: The formation of pseudouridine (Ψ) by pseudouridine synthases. The isomerization is also indicated by the different arrangement of atom numbers in the pyrimidine ring for Ψ vs. U. Note that both nucleosides share the same Watson-Crick face (depicted in red), but the N1 of Ψ is no more involved in the glycosidic bond and represents an additional hydrogen bond donor marked in orange.

Evidence accumulates, that the main structurally stabilizing effects of Ψ do indeed involve the NH1 imino proton: NMR revealed the NH1 of Ψ -A base pairs to be located in the major groove, while being protected from chemical exchange with solvent water [67–70], an effect attributed to water hydrogen bonds bridging the Ψ NH1 to nearby phosphate oxygen atoms [71]. The resulting enhanced rigidity of the RNA backbone may have been interpreted previously as ‘improved base stacking’. Several reviews provide insight into the various proteins involved in pseudouridine formation and into the modification’s distribution over all kinds of RNAs [72–75].

1.3.2. Occurrence in tRNA

Fig.1.9 summarizes the pseudouridine sites over all tRNAs of the respective indicated organisms. Although most possible occurrences cluster in the anticodon loop, pseudouridine sites are distributed over the whole tRNA sequence, especially in the case of eukaryotic tRNAs.

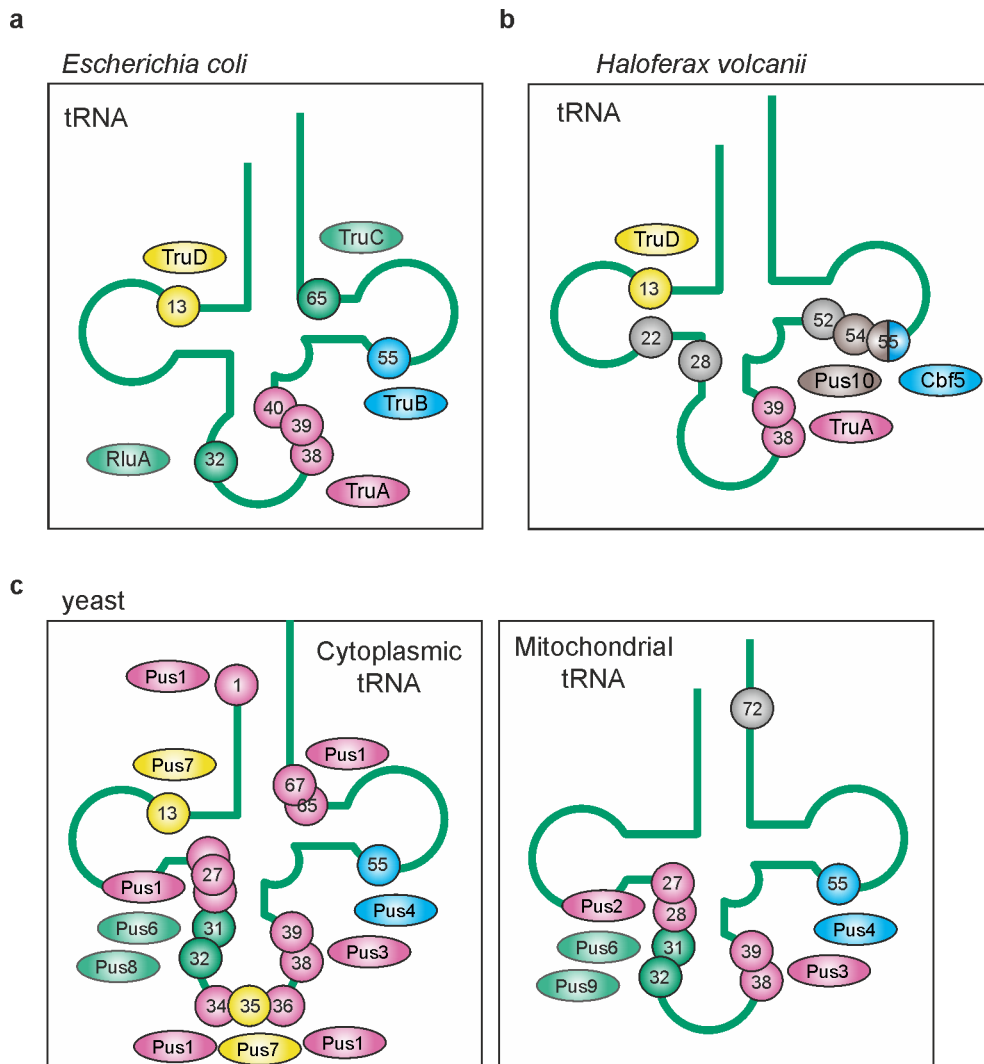


Figure 1.9.: Pseudouridine distribution in tRNAs. **a** Eubacterium *Escherichia coli*, **b** archaeon *Haloferax volcanii*, **c** eukaryote yeast (*Saccharomyces cerevisiae*). Modified from [75].

As Fig.1.9 shows, Ψ at position 55 in the TSL, generated by TruB in eubacteria [76], is especially conserved. It is assumed that Ψ 55, contained in nearly all cytosolic tRNAs [14], enhances the tertiary interaction between the D loop and the T loop ([77], position 55 is depicted in bold in Fig.1.2).

1.3.3. Effects of 5-fluoropyrimidines on RNA and DNA

Studies on the mechanism of enzymatically catalyzed reactions greatly profit from inhibitors that resemble reaction intermediates or are converted into such intermediates by the enzyme: Irreversible stalling of the reaction in a covalent complex of enzyme and inhibitor can provide valuable insight in the underlying chemistry [78].

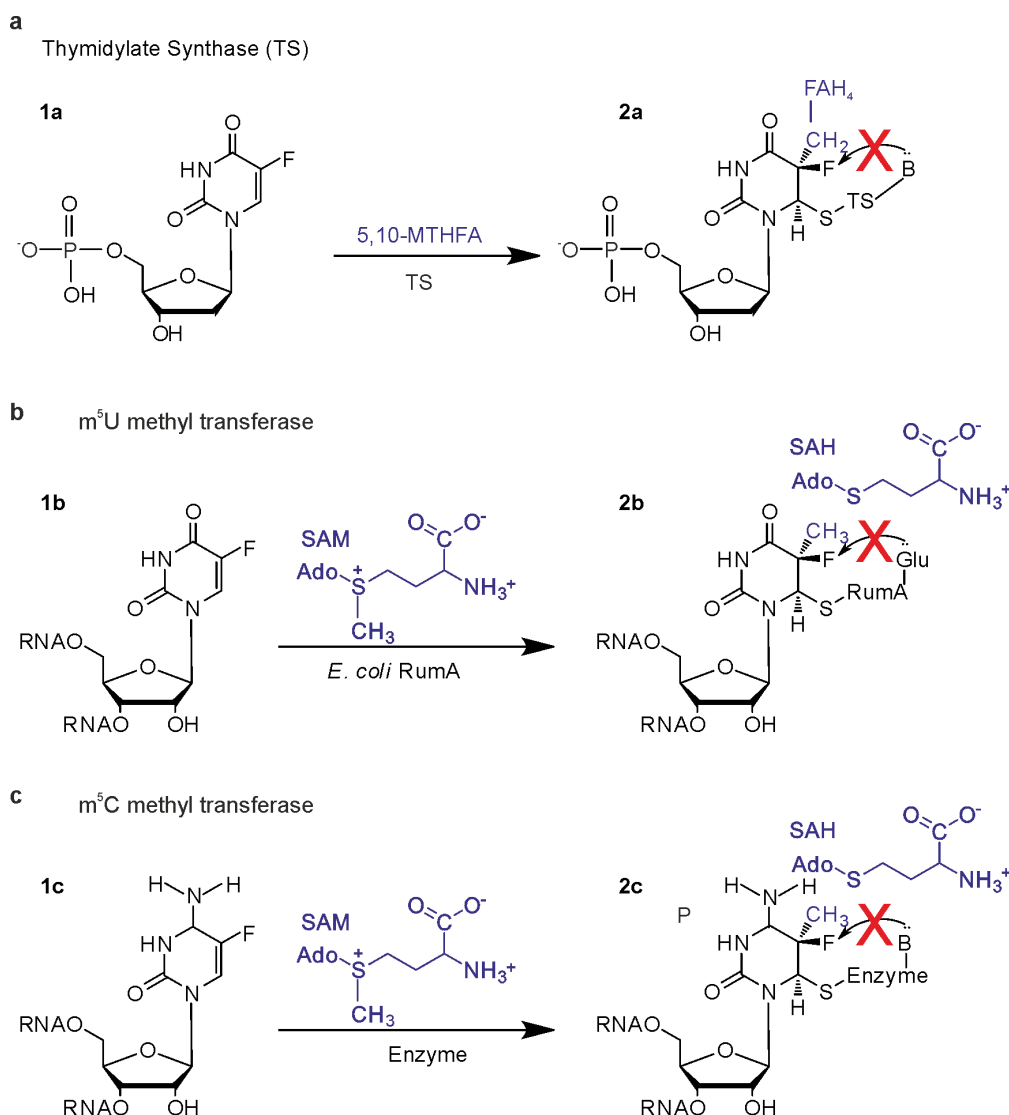


Figure 1.10.: Inhibition mechanism of 5-fluoropyrimidines on thymidylate synthesis [79] (a) and methyl group transfer [80–82] (b+c). Note that the mechanism of inhibition shown in c is similar for m⁵C methyl transferases acting on DNA [83].

The anti-cancer drug 5-fluorouracil (5FUra) [84] is such a valuable mechanistic inhibitor of nucleic acid modification enzymes: The drug can be converted to dUMP (Fig.1.10 **1a**) and act as a covalent inhibitor of thymidylate synthase (TS), allowing elucidation of the enzyme's mechanism (Fig.1.10 **a**) [23]. In addition 5-fluorouridine (5FU) incorporated into RNA proved to be a catalytic suicide inhibitor for RNA m⁵U methyl transferases (Fig.1.10 **b**), allowing again insight into the enzymatic mechanism [81, 85, 86]. The cytidine analog of 5FU, 5-fluorocytidine (5FC), was equally helpful for mechanistic investigations on m⁵dC DNA methyltransferases [80, 87–89] and m⁵C RNA methyltransferases [90, 91]. Remarkably and in contrast to 5FU, the compound displays high toxicity only in fungi and bacteria and not, e.g., in humans, as only the former are able to efficiently deaminate 5FC to 5FU [92, 93].

Until now it is not clear, whether TS inhibition is the main therapeutic mode of action of 5FUra [84], as more and more evidence suggests predominance of a RNA based mode of action [94–96]. Since the most abundant modified nucleoside in RNA, pseudouridine (Ψ), is equally derived from U, RNA related toxicity of 5FU may also include a yet unclear mode of Ψ synthase inhibition, as will be addressed in the next section.

1.3.4. 5-Fluorouridine in the investigation of pseudouridine synthases

Already early studies of Ψ synthases [97–99] reported, supposedly non-covalent, inhibition of these enzymes by 5FU-containing RNA. Based on the action of the drug on the modification enzymes discussed above, 5FU was ultimately proposed to act as covalent suicide inhibitor of Ψ synthases [100, 101]. As Ψ is formally generated by a transglycosylase reaction, i.e. cleavage of the glycosidic bond followed by isomerization and reattachment, the nucleophilic attack of the essential aspartate residue [73, 102] could target either the C1' of the ribose (acylal mechanism, Fig. 1.11a) or for the C5 of the uracil in a Michael addition (Fig. 1.11b), similar to the mechanisms discussed above [101].

Surprisingly, cocrystals of 5FU-RNA with Ψ synthases did not contain the expected covalent suicide adduct of enzyme and RNA, but a hydrated and rearranged product of 5FU conversion, 5S-6R-6-hydroxy-5-fluoro-pseudouridine

(Fig. 1.11c) [76, 103–107]. Together with several reports on SDS PAGE stable complexes of 5FU-RNA with Ψ synthases [101, 104, 107, 108], these findings seemed to support the Michael addition mechanism, as the hydroxy group could result from hydrolysis of an ester bond between enzyme and base. However, complex disruption studies consistently showed for several enzymes, that the hydroxyl group resulted from nucleophilic attack of water and not from ester hydrolysis [108–110].

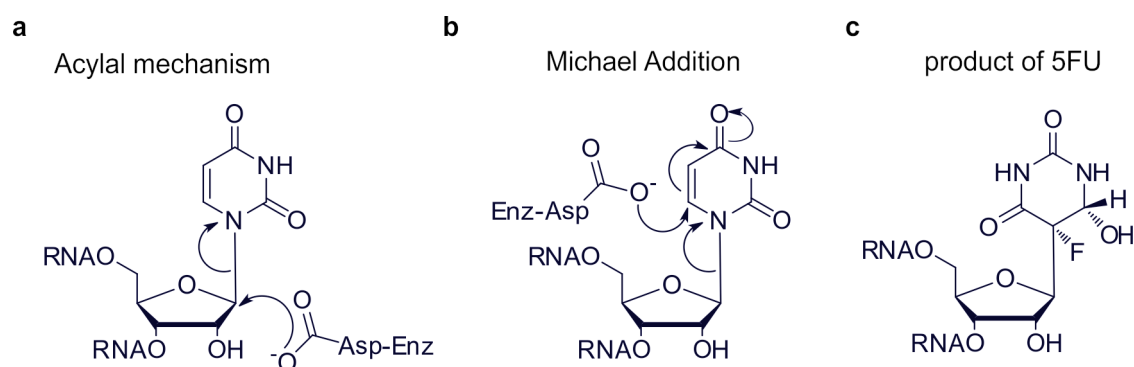


Figure 1.11.: Mechanisms proposed for pseudouridine synthases: Nucleophilic attack on C1' (a) or on C6 of the base (b). The mechanistic probe 5FU is converted into the rearranged and hydrated compound shown in c.

With this discovery both mechanisms were again equally compatible with literature, as both could result in compound **2** given in Fig. 1.12. With U-RNA the last step could formally be imin enamin tautomerism (rather: abstraction of R=H by a base and simultaneous protonation of the nitrogen by another base) to generate pseudouridine (compound **3**), while nucleophilic attack of water in case of 5FU would generate 5S-6R-6-hydroxy-5-fluoro-pseudouridine (compound **4**). In a recently published cocrystal structure of Ψ synthase RluB with 5FU-containing RNA, nucleophilic attack on compound **2** was not launched by water but by a non-essential tyrosine [105, 111] of the enzyme, generating a covalent ether bond between RNA and enzyme (compound **6**). Although, eventually, the long sought after structure of a covalent 5FU-RNA Ψ synthase complex was solved, it did not turn out to be a catalytic suicide complex in the classical sense: Instead of stalling the reaction it was an alternative final product.

Miracco and Mueller recently performed an extensive NMR study on the products of 5FU-RNA turnover by *E. coli* TruB [112], a rare event in the RNA field due to the high material consumption of such experiments. To render matters

1.3 Pseudouridine

even more complicated, TruB generated two products that were isomerized at the C1' of the ribose: 75% of the product was in the usual ribo form (compound 4), and 25% was in the arabino form (compound 5). This surprising generation of anomers was and still is a strong indicator for a mechanism involving attack at C1' (Fig.1.11a). Since an equivalent anomerization was so far not reported for the generation of pseudouridine (Fig.1.12, compound 3), the study resulted in the proposal of a third 'glycal' mechanism to account for the different products of U and 5FU turnover.

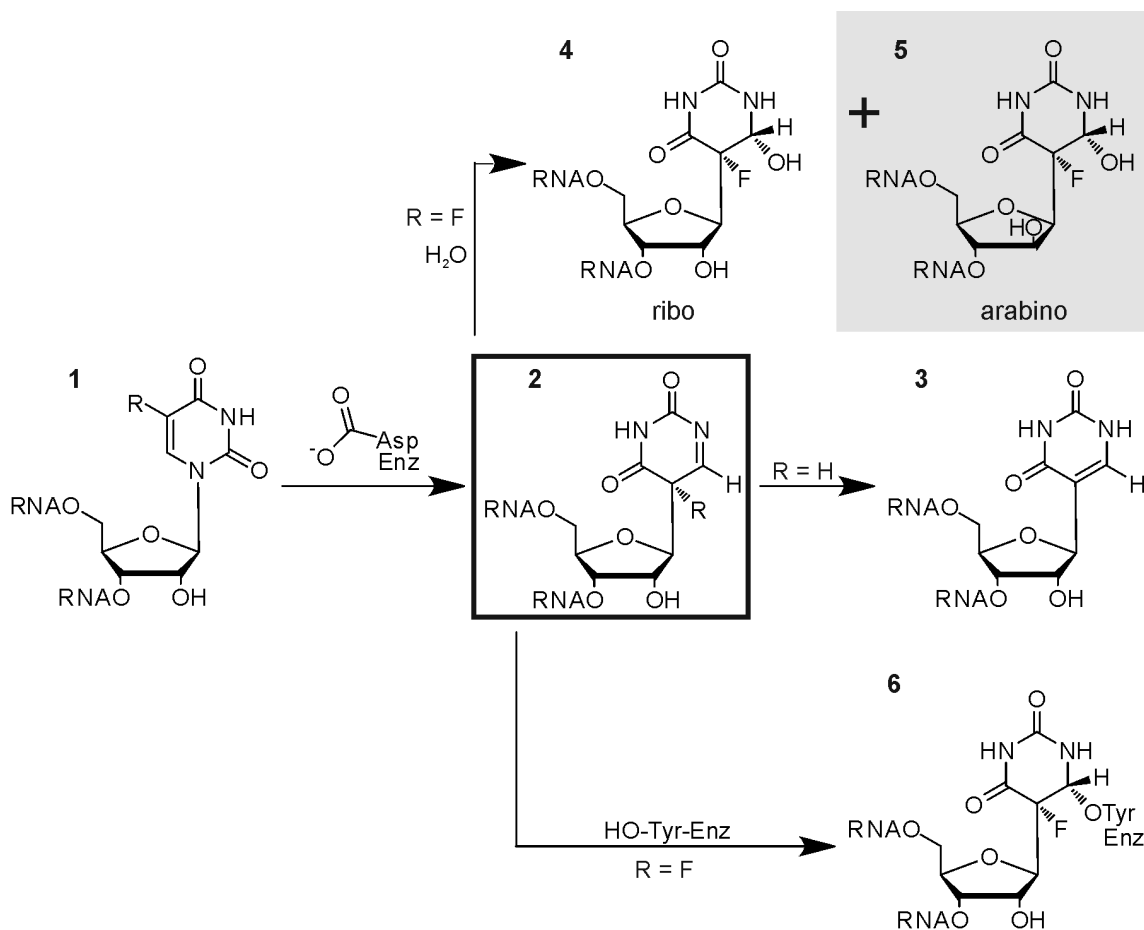


Figure 1.12.: Products generated from conversion of compound 2 in the presumed last step of Ψ formation [113]. Note that gray-shaded compound 5 [112] has to be generated by different route.

All in all, the use of 5FU in investigations of Ψ formation brought confusing results so far: Some enzymes, such as *E. coli* TruA [100, 101, 110] and RluA [108], seem to be strongly inhibited by 5FU-RNA and do form a SDS-stable complex. *E. coli* TruB contradicts this trend: The enzyme is only modestly inhibited by

5FU-RNA and does not form a SDS stable complex [108]. Still all three enzymes convert 5FU into compound **4**, as does TruB of *Thermotoga maritima*, which again forms an SDS stable complex [104]. Although *E. coli* TruB was reported to generate anomers from 5FU [112], equivalent products were neither contained in the respective cocrystal [76], nor reported in other crystallographic studies [103–105, 107, 114]. In general studies of Ψ synthases suffer from total failure of the mutagenesis approach usually applied to identify catalytic amino acid residues, that in turn allow conclusions on the mechanism: Only the catalytic aspartate proved essential, while mutating other residues usually results only in a modest decrease of activity [102, 115, 116]. Recently the conserved basic active site arginine R181 of *E. coli* TruB proved to be important for catalysis, but inability to assign a specific role in chemistry prevented mechanistic insight [117].

1.4. Sensitivity of cyanines towards their biomolecular environment

1.4.1. Protein induced fluorescence enhancement of cyanines

In contrast to other dyes, cyanines are almost unaffected by amino acid related quenching [118]. However, already in early experiments involving cyanine dyes as protein labels, an increase of fluorescence lifetime, as well as bathochromic spectral shifts have been observed [119, 120]. In single molecule experiments fluorescence showed strong dependence on the dye label positions: Quantum yields of 31–48% were obtained, depending on which of the protein's cysteine residues was used for dye attachment [121]. This implies highly specific dye interactions with a given protein environment, that in turn specifically influence the quantum yield.

While similar bathochromic spectral shifts can be caused by dissolving free dye in less polar solvents [120, 122, 123], an increase of fluorescence lifetime is facilitated by increasing solvent viscosity [120, 123, 124]. In accordance with this principle, the ability of a Cy3 nucleic acid label to sense protein proximity is attributed to protein induced enhancement of the dye environment's local viscosity [125].

1.4 Sensitivity of cyanines towards their biomolecular environment

It is established that the protein/viscosity induced fluorescence lifetime increase of cyanine dyes is caused by a reduced isomerization rate to a non-fluorescent *cis*-form, the main non-radiative decay route of cyanines (see Fig. 1.13a) [122–124].

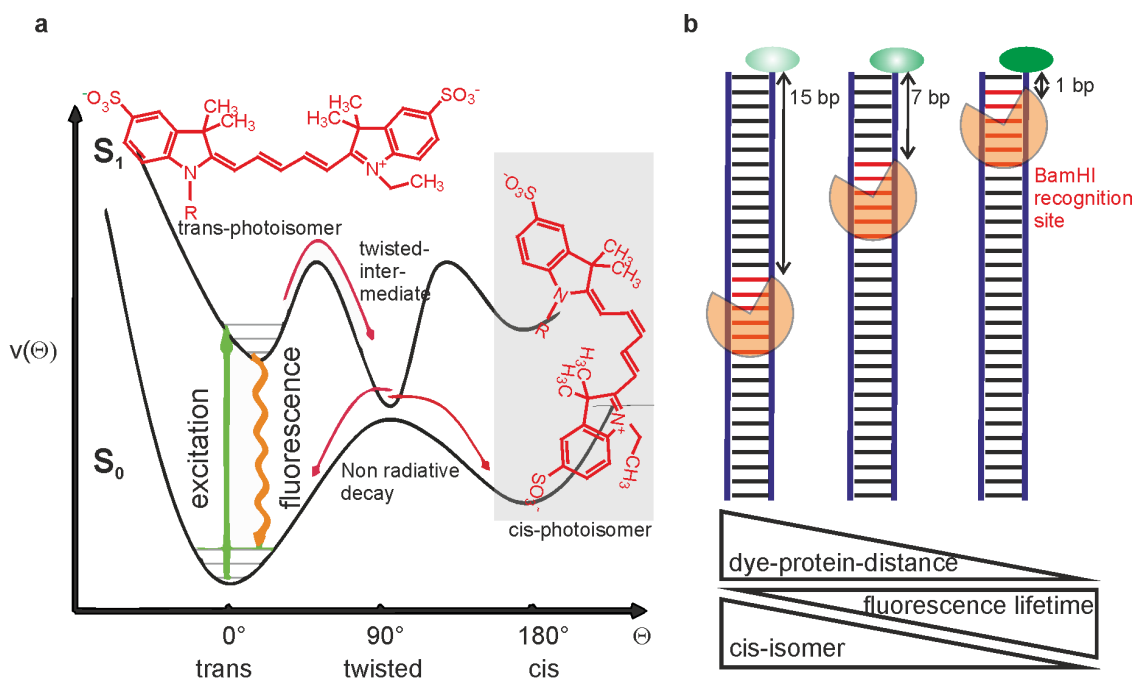


Figure 1.13.: Protein influence on spectroscopic properties of cyanine dyes. **a** Energy diagram of the photophysics of the cyanine Cy5: If the dye is flexible enough to form a twisted intermediate, photoisomerization may result in a non-fluorescent *cis*-isomer [124] (figure modified from [126]). **b** BamHI binding does not influence a Cy3 label 15 base pairs (green ellipsoid) away, but the dye's fluorescence lifetime increases the nearer the protein gets (inspired by [125]).

The so called 'protein induced fluorescence enhancement' (PIFE) inherent to cyanine dyes found wide application in experiments on nucleic acid motor proteins, as reviewed in [125]. In such experiments the nucleic acid substrate was labeled, usually with the particularly responsive cyanine Cy3, resulting in a 'typical' intensity increase of 2-2.5-fold upon protein binding [125]. This effect proved strongly distance dependent in single molecule experiments: For a label distance of 1-10 base pairs from the protein recognition site, the increase decayed from 2.6-fold to 1.3-fold, indicating a narrow sensitivity range of 0-4 nm [127]. Still the underlying physical effects await further clarification: Only a connection to the above mentioned *cis-trans*-isomerization is strongly suggested, since the non-isomerizable cyanine dye Cy3B does not show any PIFE [127]. Neither the nature

and specificity of dye protein interactions resulting in PIFE, nor their possible dependence on amino acid sequence were addressed to this date [125].

1.4.2. Interaction of cyanine fluorophores with nucleic acids

Environmental sensitivity of cyanines is better understood for dye nucleic acid interactions than for proteins. Sulfo-cyanines Cy3 and Cy5, which are used in this work, stack on a DNA helix if they are attached to the 5' end, an effect which is relatively independent of whether a long or a short tether is used for dye attachment [128–131].

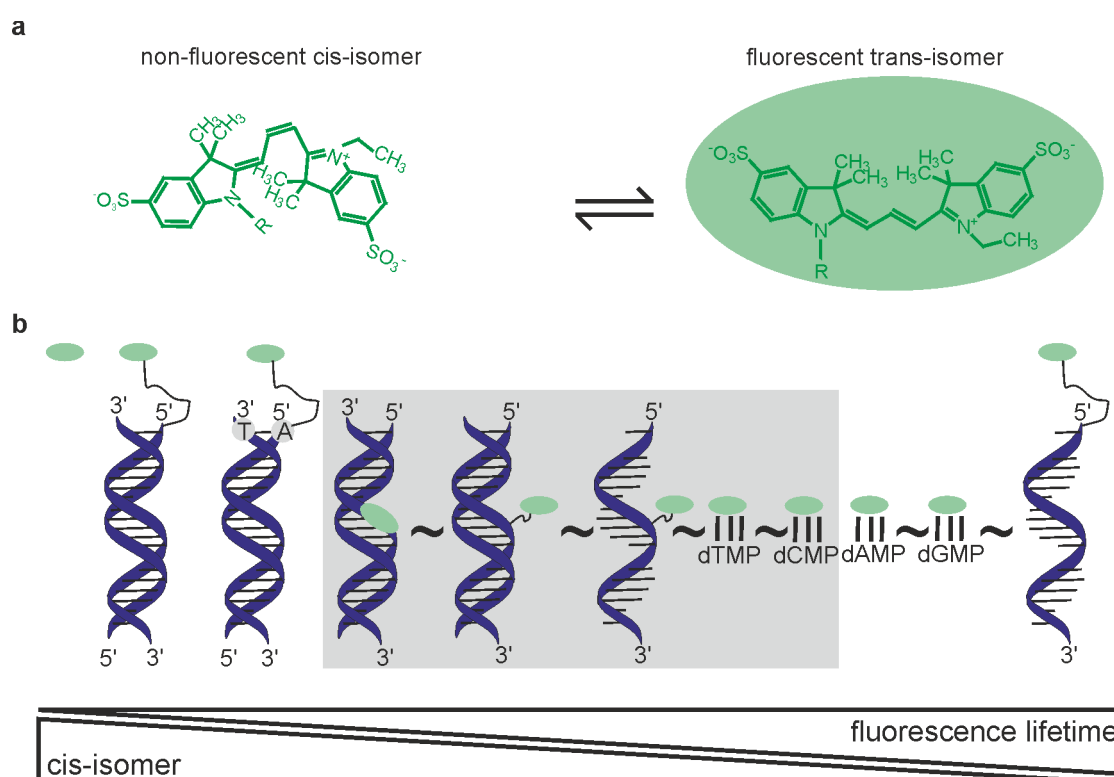


Figure 1.14.: Influence of single nucleotides or DNA attachment on the fluorescence lifetime of Cy3. **a** Isomerization to the non-fluorescent cis-form results in a short fluorescence lifetime and low quantum yield of the free dye [124]. **b** Cy3 interaction with free monomeric dNTPs (indicated by vertical lines) at >80 mM concentration results in enhanced fluorescent lifetime by reducing cis-isomerization, while purines have a significantly larger effect [132]. Interaction of a Cy3 label with DNA is highly dynamic, but also specific for the label environment [133–135]. Note that Cy3 incorporated into the DNA backbone is doubly linked but is, surprisingly, still capable of cis-isomerization, resulting in an intermediate fluorescence lifetime [136].

This interaction results in an increase of fluorescence lifetime by reduced cis-isomerization [123], while interactions are dynamic in nature [133, 137]. In fact the fluorescence lifetime of Cy3 is sensitive to the exact form of dye attachment or the presence of free dNTP, as is summarized in Fig.1.14. Note that the existence of more than two (long and short) lifetime components is not included for clarity.

The fluorescence of single stranded 5'-Cy3-labeled DNA exhibits a highly complex sequence dependency: Sensitivity to a single base pair change (or removal) exists, purines increase fluorescence lifetime, while highly rigid sequences decrease fluorescence lifetime [134]. Remarkably, cyanine dyes attached to the 3' end of a 16mer RNA helix via a 3-Carbon-linker approach free rotation, at least in MD and Monte Carlo simulations [138].

Obviously, even the simple model systems presented above, mostly consisting of structurally limited DNA, show a range of complex, in part cooperative and in part pleiotropic, effects on the fluorescence of the Cy3 label. Studies on RNAs of more complex structure that are internally labeled at the base are lacking however, although they would be highly relevant for this work.

1.5. Theory of Microscale Thermophoresis

1.5.1. General Theory

In 1856 Carl Ludwig discovered that the salinity of an aqueous solution changes site-specifically if one applies a temperature gradient [139]. This coupling between heat flow and mass flow is known as Soret effect and movement of molecules in a temperature gradient is termed thermophoresis [140]. Now, almost 200 years later, it is established [141], that thermophoresis is a linear drift response. The velocity of this drift depends on the nature of the particle under investigation and the strength of the temperature gradient ∇T :

$$v = -D_T \nabla T \tag{1.1}$$

with v describing the particle's drift velocity and D_T being the thermophoretic

diffusion coefficient. Typical thermophoresis experiments apply temperature gradients of only 1-3K, rendering the temperature dependence of the Einstein relation insufficient to fully account for the effect [140]. Rather, thermophoretic diffusion counteracts Brownian diffusion until a steady state is reached, where the thermophoretic flux j_{TP} and the counteracting Brownian motion j_D balance each other. For low analyte concentrations this can be described as

$$j = j_{TP} + j_D = -cD_T\nabla T - D\nabla c = 0 \quad (1.2)$$

here D is the Brownian diffusion coefficient and ∇c is the concentration gradient generated by thermophoresis. Conversion and integration results in a description of the change of an initial concentration c_0 caused by thermophoresis:

$$\frac{c}{c_0} = \exp(-S_T\Delta T) \quad (1.3)$$

The Soret coefficient $S_T = \frac{D_T}{D}$ describes both direction and magnitude of thermophoretic diffusion that are specific to a certain analyte: Usually the analyte is depleted by thermophoresis, but accumulation is equally possible [140]. For small temperature gradients and small concentrations as they are applied in the Nanotemper measurements of this work, Eq.1.3 is valid [140]. In a microscale thermophoresis experiment the equation describes the concentration change achieved at the balancing point of Brownian and thermophoretic diffusion for a temperature difference ΔT [141]. Under these conditions, the Soret coefficient S_T and therewith the magnitude, as well as the direction of thermophoresis is influenced by several properties of analyte, buffer and experimental conditions [141]:

(1) Surface area, (2) hydration entropy, (3) effective charge, (4) debye length (inversely proportional to ion concentration/ionic strength), (5) temperature (inverse proportionality)

One should be aware that changing the above mentioned properties can influence the Soret coefficient independently of actual analyte properties. For nucleic acids the influence of ionic strength is of special interest, as structure of nucleic acids changes with ion concentration [142]. However, influence of ionic strength on thermophoresis of nucleic acids is not fully understood at present [143].

1.5.2. Experimental Implementation

Thermophoresis measurements usually appear in this work as shown in Fig.1.15.

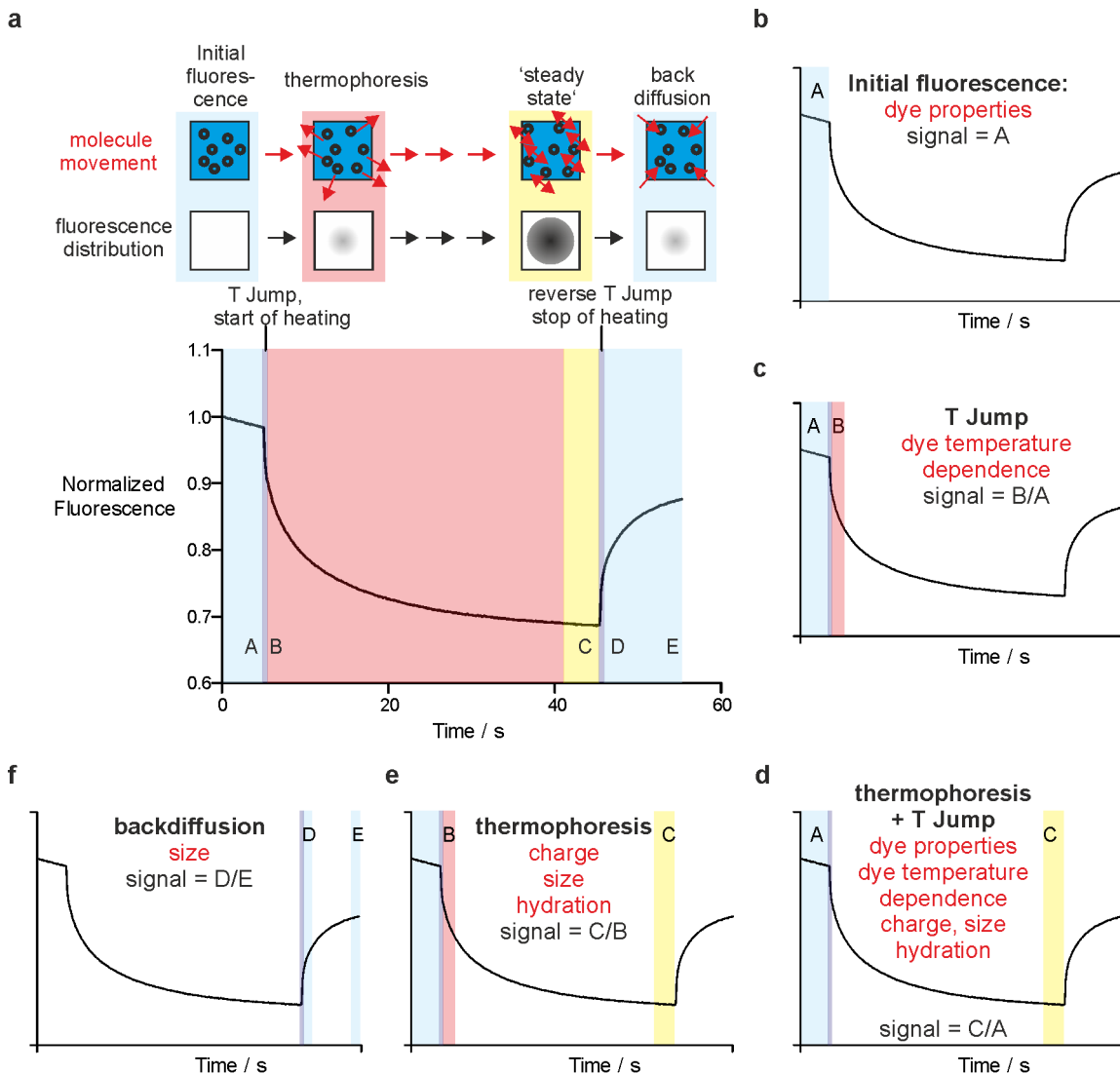


Figure 1.15.: Readout and analysis of MST titrations. **a** In the beginning the initial fluorescence is recorded (light blue left), which decreases slightly over time due to bleaching of the fluorophore. After activation of the IR laser, a very fast decline in fluorescence can be observed, which is termed T Jump (dark blue left) and is caused by a decrease in fluorophore quantum yield with rising temperature. Subsequent to this jump typically a slow decrease of fluorescence, caused by thermophoretic depletion of the labeled molecules, follows (red), until thermophoresis is balanced by Brownian motion ('steady state', yellow). Stop of heating results in a reverse T Jump and an eventual reversion of thermophoretic depletion by Brownian diffusion (backdiffusion, light blue right). **b-f** Several signals can be extracted from MST curves that are potentially sensitive to binding in a titration series. The signals differ in their physical background, with 'thermophoresis' being the usual readout.

Each measurement starts with the recording of initial, thermophoresis-free fluorescence (first 5 seconds in Fig.1.15a). At a time point specified by the user (usually 3-5 s) an IR laser starts to heat the observation volume with an intensity specified by the user ('start of heating' in Fig.1.15a). The first ~0.5-1s following are dominated by strong effects directly related to heating of the solution. This phase is termed temperature jump (T jump), since it is (usually) characterized by a fast and pronounced decrease in fluorescence intensity. Due to the elevated temperature thermal relaxation pathways are favored, which results in a reduced quantum yield of the fluorescent dye [140]. In consequence, thermophoresis curves only conform to Eq.1.3 after the T jump: In the example in Fig.1.15a analyte concentration and therewith fluorescence signal decrease exponentially (seconds 5-~41 in Fig.1.15a), until the steady state implied by Eq.1.2 is established at ~45 s (yellow range in Fig.1.15a).

At a user-specified time point the IR laser is switched off and an inverse T jump occurs due to cooling, followed by a backdiffusion phase (seconds ~50-55 in Fig.1.15a). The actual readout of one thermophoresis curve is a single fluorescence intensity value that is determined as a ratio. As is shown in Fig.1.15b-f, this ration can be determined from different phases of a thermophoresis curve, which differ in the nature of their sensitivity to binding [140]:

- changes of the dye's local environment by binding can render initial fluorescence sensitive to binding (Fig.1.15b)
- T jump is only responsive to binding, if the temperature response of the dye is changed by the interaction of interest (Fig.1.15c)
- thermophoresis depends on size, charge and hydration (Fig.1.15e)
- backdiffusion (Fig.1.15f) can only reflect larger changes in hydrodynamic radius, as they are caused by association of macromolecules or by extensive conformational changes

Due to these differential sensitivities, comparison of different thermophoretic readouts can allow conclusions on the monitored interactions that go beyond mere affinity analysis [140]. However, a comprehensive interpretation of the additional information content inherent in microscale thermophoresis data is just beginning.

2. Goal of this Work

About ~150 RNA modifications are known to date and their number can be expected to increase in future [13–15]. At least m⁶A [11] and m⁵C [17–19, 144] are implied in epigenetic mechanisms, while evidence accumulates suggesting an epigenetic importance of pseudouridine [20, 21]. The chemical sophistication of some modifications even implies a role in sensing and transducing the metabolic state of the cell [145], a strategy generally applied by bacterial mRNAs [22].

Even in times when research focusses on the complex regulatory networks of epigenetics long-standing foundations are far from being fully understood: The highest modification density is inherent in tRNA [14], an RNA investigated for a long time. However, even here modifications seem to underlie complex, in part pleiotropic and partly cooperative mutual influences [146]. One would expect modification enzymes to be the best sensor to address the need for a given modification, but substrate enzyme interaction remains quite enigmatic for tRNA in particular: Cocrystals of enzyme and RNA, if available at all, are mostly limited to small parts of the whole tRNA, for technical reasons (e.g. [76, 147]). Such minimal substrates are also widely used in turnover studies [148–151]. This restricts knowledge on how a whole tRNA molecule is recognized by modification enzymes mostly to docking models [76, 147, 149, 152–154], although the few available full cocrystals imply significant alterations in tRNA conformation upon protein binding [155, 156].

This work seeks to improve the understanding of enzyme tRNA recognition and of RNA conformation by connecting three techniques so far highly underrated in RNA research: **(1)** The environmental sensitivity of cyanine dyes, so far only applied to nucleic acid motor proteins and to DNA models [123, 125], **(2)** advanced spectroscopy to profit most from this sensitivity and **(3)** fluorescence based microscale thermophoresis, which is sensitive to changes in hydration, charge and size which could be induced by protein binding and/or conformational changes

in the RNA [140].

In the first section of this thesis investigates the applicability of microscale thermophoresis (MST) towards enzyme interaction with tRNAs that are labeled with cyanines at different positions. These studies are complemented by MST studies on tRNA conformation. In a brief excursion conformation of tRNA and tRNA ribosome interaction are investigated by single molecule FRET. A particular focus lies on interaction of pseudouridine synthase TruB with U55- and 5FU55-tRNA: A comprehensive characterization of this interaction is sorely needed, as more and more evidence accumulates that 5FU may not be the hoped for mechanistic covalent suicide inhibitor of the enzyme [108, 110]. Instead, it seems to be turned over by the enzyme, but by a different chemical mechanism than for the reaction of U [112]. These recent discoveries render the enzymatic mechanism of pseudouridine formation as enigmatic as ever already ~60 years post its discovery [64].

3. MST on RNA

3.1. Evaluation of RNA protein interactions

3.1.1. MST detects binding of many tRNA modifying enzymes

To test the general suitability of Microscale Thermophoresis (MST, see sec.1.5) for RNA-protein interactions, a yeast tRNA^{Phe} construct carrying the fluorescent labels Cy3 at G3 in the acceptor stem and Cy5 at U33 in the anticodon loop was generated by splinted ligation techniques [157, 158] (Fig.3.1). Five different modification enzymes were tested independently for tRNA affinity in MST titrations (Fig.3.1), with the highest concentration being in the double digit μM range.

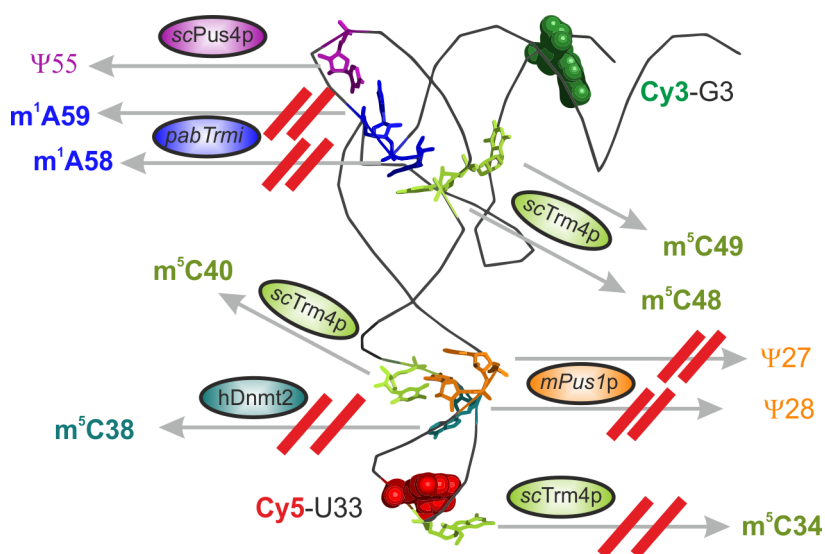


Figure 3.1.: Yeast tRNA^{Phe} in gray ribbon representation (PDB ID 1EHZ), fluorophore labeled bases depicted as spheres: Cy3 green, Cy5 red. Possible substrate sites of the enzymes used in this screen represented as color coded, full chemical structures [153, 159–161]. Crossed reaction arrows depict positions with non-substrate bases or the wrong recognition elements for pabTrmi, [162].

As is evident from Fig.3.1, the screen comprised of three different enzyme classes from two domains of life: m¹A methyl transferase Trmi from the Archaeon *Pyrococcus abyssi* (pab), pseudouridine synthase Pus4p and m⁵C methyl transferase Trm4p from the lower eukaryotic fungi yeast or *Saccharomyces cerevisiae* (sc) and two enzymes of two higher eukaryotes: Pseudouridine synthase Pus1p from *Mus musculus* (m) and m⁵C methyl transferase Dnmt2 from *Homo sapiens* (h).

RNA in constant concentration was titrated with increasing amount of protein and, following 30 min incubation at room temperature, subjected to MST experiments performed by Cy5 excitation and detection. Thermophoresis curves resulting from these experiments are shown in Fig.3.2.

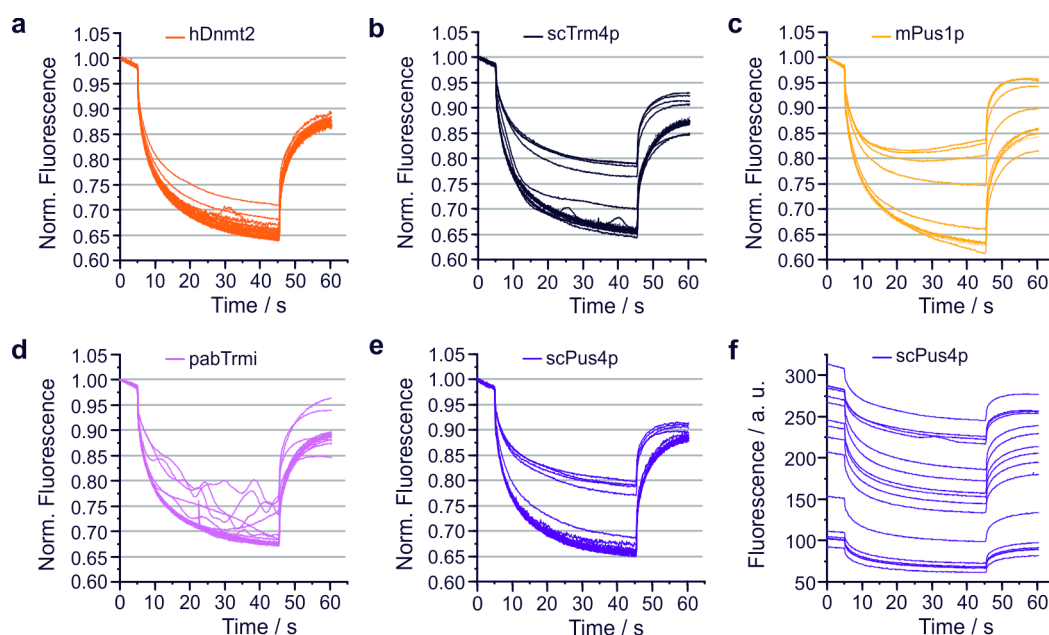


Figure 3.2.: MST Traces of the protein screen. Normalized curves are given for titration of yeast tRNA^{Phe} with hDnmt2 (a), scTrm4p (b), mPus1p (c), pabTrmi (d), scPus4p (e) and a representative example of unnormalized data (from scPus4p) (f). The increase of protein concentration is suggested by a wedge.

For all proteins investigated an increase of protein concentration coincides with a decrease in thermophoresis depletion (meaning normalized fluorescence, see Fig.3.2a-e). The curves of scPus4p, scTrm4p and mPus1p (Fig.3.2b, c, e) show two saturation phases at similar intensity levels, separated by a more or less steep transition: High thermophoresis depletion (= fluorescence decrease) for unbound and mostly unbound tRNA and low thermophoresis depletion for high degrees of protein binding. The experiments for pabTrmi (Fig.3.2d) and hDnmt2 (Fig.3.2a)

3.1 Evaluation of RNA protein interactions

diverge from this trend: The pabTrmi traces show prominent fluctuations that may indicate severe aggregation of the homo-tetrameric protein [163]. To unambiguously identify aggregation as cause for the fluctuations, experiments with fresh, gelfiltrated protein preparations would be needed. The Dnmt2 titration differs concerning the range of thermophoresis: All tritration sets achieve thermophoresis of ~ 0.8 for the highest protein concentration, except hDnmt2, where the highest protein concentration yields a thermophoretic decrease to $0.7\times$ of the initial fluorescence.

Fig.3.2f shows unnormalized MST curves of scPus4p that are representative in their trend for all experiments: Absolute fluorescence intensity increases with increasing protein concentration and thus with protein binding. Fig.3.3 shows the increase of the fluorescence intensity of the highest protein concentration normalized to the fluorescence intensity of RNA alone (100%) for all five enzymes investigated. This intensity increase can be observed in absence of thermophoresis effects (meaning at a temperature gradient of zero) in the beginning of each measurement (seconds 0-5 in Fig.3.2f). For all enzymes investigated the protein-related intensity increase ranges from 175-345% of the RNA only intensity. A weak correlation is evident in such that two enzymes modifying the ASL, where the Cy5 label is located, namely mPus1p and scTrm4p (Fig.3.1), cause the largest fluorescence increase upon binding.

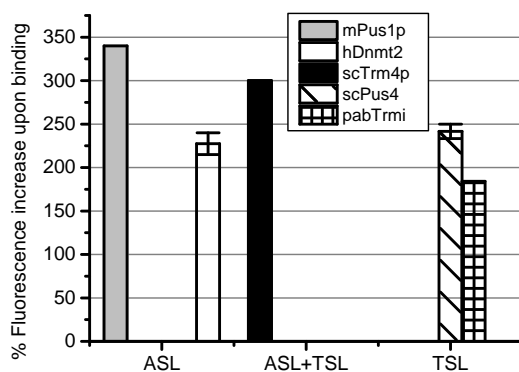


Figure 3.3.: Percental increase in fluorescence of the U33-Cy5 label (located in the anticodon loop) upon protein binding, compared to RNA only intensity. Enzymes were grouped according to their site of action. Error bars represent the SD of a duplicate measurement in the same experiment.

This effect, termed 'protein induced fluorescence enhancement' (PIFE), enabled the use of the related cyanine Cy3 as sensor for protein proximity, as was reviewed recently in [125]. For Cy5 similar effects are caused by non covalent [120], as well as covalent [124] binding of proteins.

The weak nature of the correlation visible in Fig.3.3 may be accounted for by the different amino acid sequence and structure of the proteins investigated: These differences should result in qualities of dye-protein interaction that are unique for a given protein as is, in consequence, the PIFE. Matching to the simplified 'proximity hypothesis', pabTrmi, the enzyme with the most distant modification site (see Fig.3.1), causes the lowest intensity increase. The, in comparison to mPus1p and scTrm4p, small effect of hDnmt2, acting on ASL residue 38 (Fig.3.1), may be explained by incomplete binding evident from the raw data in Fig.3.2e.

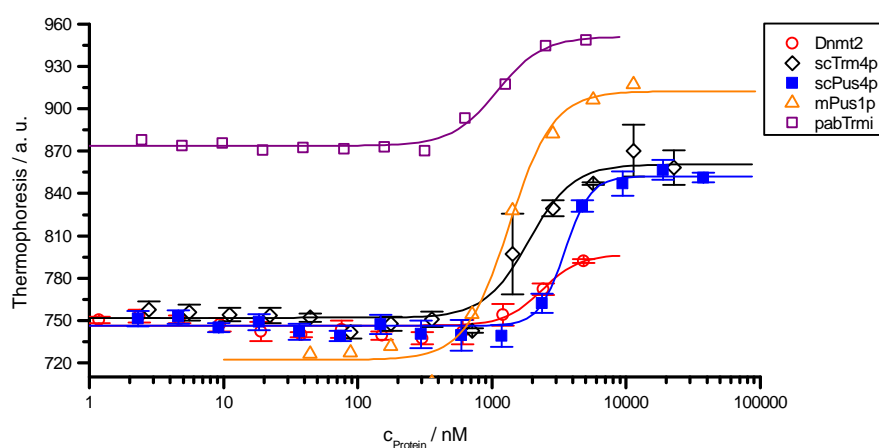


Figure 3.4.: Enzyme tRNA binding isotherms as determined by MST. Note that for pabTrmi the back diffusion regime is shown, generating a large y-offset compared to the other curves. Sets with error bars were measured in duplicate during the same experiment. Fits to the Hill equation are shown by solid lines.

Analyzing, plotting and fitting the raw data of Fig.3.2 for the 'MST regime' (see sec.1.5) results in the titration curves shown in Fig.3.4. Other ways to analyze thermophoresis curves, as they are described in sec.1.5, were equally suitable, as is discussed in sec.A.1.1. Note that for pabTrmi (Fig.3.2d and purple open squares in Fig.3.4) the back diffusion regime had to be analyzed to minimize the impact of protein aggregation on analysis (see sec.1.5 for elaboration on this analysis). Presumably due to this different analysis, the pabTrmi titration curve

3.1 Evaluation of RNA protein interactions

possesses a high y-offset compared to the other titration curves. For the other four enzymes the y-offset and the y-range from no binding (RNA only) to nearly full binding differs due to a different magnitude of thermophoresis effects. Solid lines represent fits to the Hill equation, that were applied since a fit to a simpler binding model did not converge:

$$Fraction\ bound = \frac{1}{1 + K_d / ([C_{Protein}]^n)} \quad (3.1)$$

The Hill coefficient n describes the sigmoidicity of the curve, which is visible from plots as the steepness of the transition from RNA only to nearly fully bound signal. Traditionally, n is interpreted as an estimate for the number of ligand binding sites in a protein, a procedure that is only valid for positive cooperativity [164]. The fits yielded Hill coefficients $2 < n < 5$, see Tab.3.1. The highest value, $n = 4.44$, was obtained for the oldest preparation, scPus4p (see Tab.3.1 and Fig.3.4) yielding an apparent EC50 of 3439 ± 149 nM. RNA contaminating the protein preparation, evident from $A_{260} / A_{280} = 1.48$, is assumed to contribute to this apparent deviation from a 1:1 binding model. However, due to a lack of protein RNA cocrystal structures for all cases, a 1:1 binding remains to be proven. Even crystals of the RNA free protein, lending some support to a 1:1 binding model, are only available for pabTrmi [163], the human homolog of mPus1p [154] and hDnmt2[165].

Table 3.1.: Results of a screen for protein binding using microscale thermophoresis. EC50 values and Hill coefficients n were determined from fits to the Hill equation. Errors are standard errors of the fit, while underlined values were determined twice in the same experiment. For pabTrmi values in parenthesis result from a fit to the backdiffusion regime.

Protein	age / y	modification	yeast tRNA ^{Phe} substrate?	ref.	EC50 / nM	n
scTrm4p	5	m ⁵ C34, 40, 48, 49	bad substrate	[160]	1880± <u>108</u>	2.63±0.151
scPus4p	7	Ψ55	yes	[161]	3439± <u>149</u>	4.44±0.20
mPus1p	6	Ψ27+28	scPus1p binds	[159, 166]	1410±71	3±0.151
hDnmt2	4	m ⁵ C38	no	[153]	2350± <u>195</u>	3.23±0.268
pabTrmi	5	m ¹ A58+59	no	[162]	662 (1087)	31.1 (2.57)

As is evident from Tab.3.1, affinity of the tRNA modification enzymes investigated does not reflect, whether the tRNA is substrate or not: All enzymes investigated show μM affinities. E.g., the homo tetrameric enzyme pabTrmi methylates

either A58 or A59, requiring an additional A 5' of the modification site [163]. Although this sequence prerequisite disqualifies yeast tRNA^{Phe} as a substrate, the RNA is bound with the highest affinity determined. Although the Dnmt2 titration curve determined here lacks saturation the determined affinity falls within a previously reported range of $K_d \sim 1 - 6 \mu\text{M}$ [153].

Although all protein preparations used were of advanced age, all enzymes investigated were found to bind yeast tRNA^{Phe} with reasonable affinity, independent of whether they treat the tRNA as substrate or not. The results demonstrate a universal applicability of MST in RNA-protein interaction studies (1), that MST is fast in assessing protein aggregation (2), an expected low binding specificity of tRNA modifications enzymes (3), the suitability of protein induced fluorescence enhancement (PIFE) typical for cyanine dyes [125] as a fast screen for interactions (4) and, presumably, an improvement of the MST signal by PIFE (5).

3.1.2. Influence of dye labels on tRNA upon TruB binding

The tRNA recognition mechanism of Ψ synthase TruB of *Thermotoga maritima* is unknown to date. Mutagenesis studies established size and shape of the tRNA T stem loop (TSL) as main recognition element, rendering the isolated TSL an equally good substrate as whole tRNA [148]. In consequence several available cocrystal structures contain only this minimal substrate [76, 103–105, 167], restricting information on TruB-tRNA recognition to a docking model resulting from such a minimal substrate cocrystal (Fig.3.5) [76].

To probe for tRNA-enzymes interactions involved in TruB-tRNA recognition, the fluorescence labels Cy3 and Cy5 were distributed over the tRNA surface by splinted ligation techniques [157, 158]¹ (sec.7.2.1). Fig.3.5 shows the label distribution: Cy3 in the acceptor stem at G3 and U7 or in the D loop at U17, Cy5 either at U33 in the anticodon loop or at C49 at the 5' edge of the TSL minimal substrate. In an attempt to trap a covalent intermediate of tRNA-enzyme interaction, the putative covalent inhibitor of Ψ synthases, 5-fluorouridine (sec.1.3.4), was placed en lieu of the canonical uridine at substrate site 55. For comparison two constructs were also investigated as U55 variant lacking the assumed inhibitory properties.

¹Yeast tRNA^{Phe} constructs were in part synthesized by Roman Teimer [168].

3.1 Evaluation of RNA protein interactions

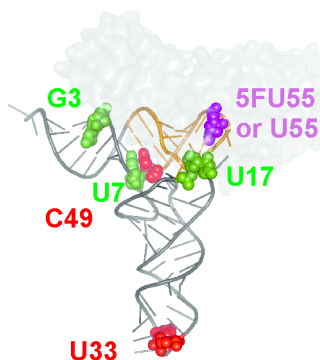


Figure 3.5.: Docking model of *E. coli* TruB (gray surface) to yeast tRNA^{Phe} (dark gray cartoon) [76]. The enzyme's minimal substrate is shown in orange, the substrate position U55 (or 5FU55) is shown as purple sphere and the used dye labeling positions are depicted as either green (Cy3) or red (Cy5) spheres.

Enzyme-RNA interaction was assessed by MST titration experiments of tRNA with protein, protein binding was already visible from raw MST data (Fig.3.6).

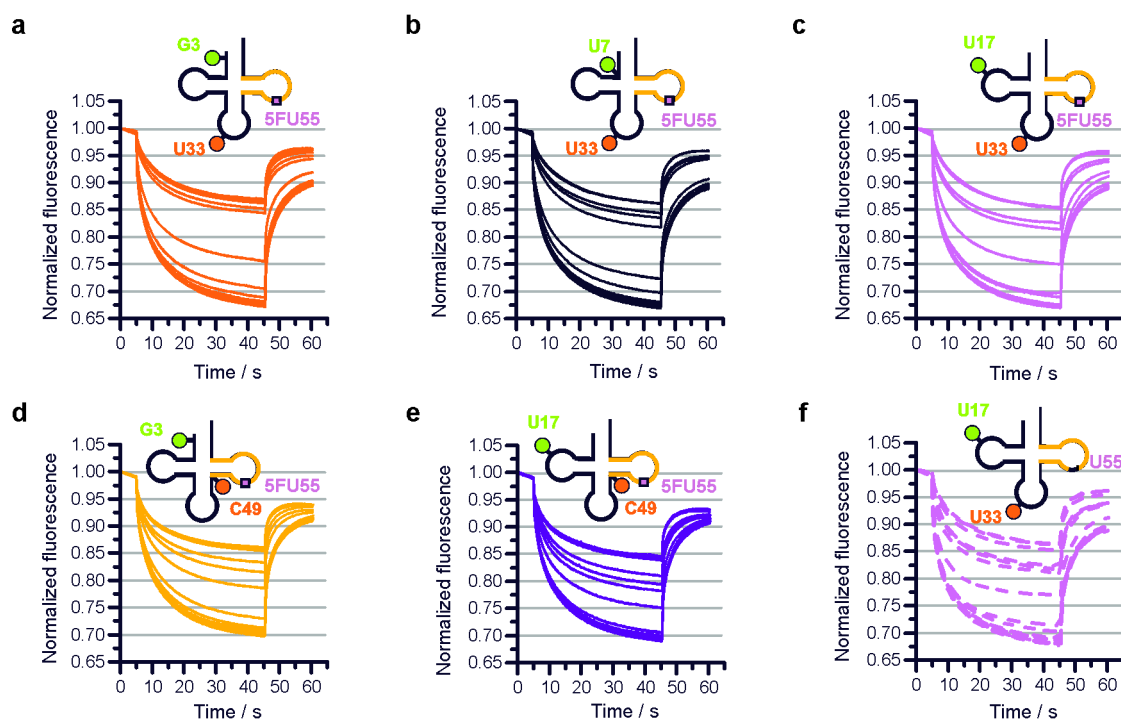


Figure 3.6.: Normalized thermophoresis curves of tRNA-TruB interaction. The dye combinations are indicated by small cartoons with Cy5@C49 located at the edge of the enzyme's minimal substrate shown in orange. Note that panel **f** represents the U55-variant of **c** and that U17-C49-U55 showed similar traces as the 5FU55 counterpart (see appendix).

The pronounced smoothness of the MST curves, compared to curves of other proteins in this work, is attributed to superior sample homogeneity achieved by the use of gel filtration (sec.7.3). In addition the protein is assumed to be less prone to aggregation due to its thermostability [169]. The position of the Cy5 label causes the most striking difference in the raw data: Curves with U33 are mostly located in either the low binding regime ($\sim 0.65\text{--}0.75$) or the high binding regime ($\sim 0.85\text{--}0.9$) and do not reach a similar end value for all curves in the back-diffusion regime (Fig. 3.6a-c+f). In contrast curve sets representing a label at C49 do not show a gap between 0.75 and 0.85 and all reach similar end values in the backdiffusion regime (Fig. 3.6d+e).

Titration curves resulting from analysis of the 'MST regime' (see sec.1.5) in the raw MST data of Fig.3.6 are shown in Fig.3.7a for Cy5-U33 constructs and in Fig.3.7b for Cy5-C49 constructs. Other ways to analyze thermophoresis curves, as they are described in sec. 1.5, are equally suitable, as is discussed in sec. A.1.2.3. All curves given in Fig. 3.7 yield reasonable fits to a 1:1 binding model with affinities depending mainly on the position of the Cy5 label: The U33 label shows a slightly higher affinity than the C49 label. Surprisingly a comparison of 5FU55- and U55-tRNA variants does not confirm the suspected tight, probably covalent, interaction of 5FU55-tRNA with TruB.

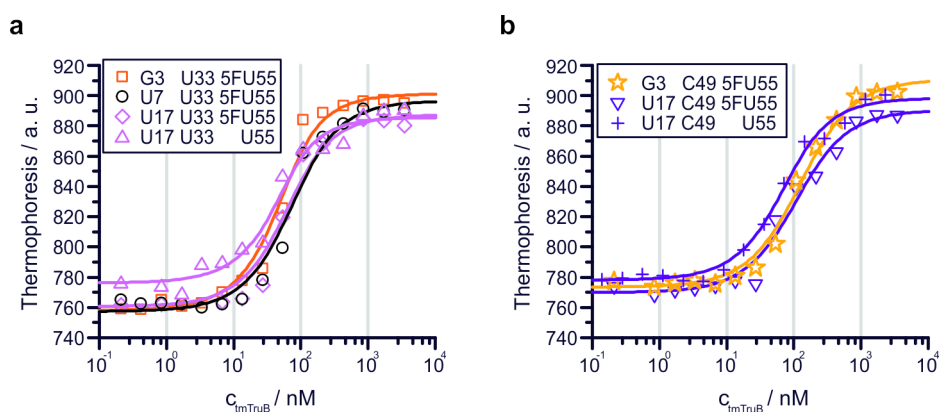


Figure 3.7.: MST titration curves of tRNA TruB interaction. Constructs are sorted by Cy5 labeling site: Either at U33 (a) or C49 (b). Solid lines represent fits to a 1:1 binding model.

Fig.3.8a shows the K_d 's resulting from the fits in Fig.3.7 spanning a range of 20-100 nM. The 2-5x weaker binding of the C49 label 5FU55 variant, compared to the U33 label, reflects the C49 label's location in the enzyme's minimal substrate [148] (Fig.3.5). In contrast positioning of the Cy3 dye, as well as position dependent

3.1 Evaluation of RNA protein interactions

labeling-chemistry (see Appendix), seem to have only minor influence on enzyme affinity.

The 'Protein Induced Fluorescence Enhancement' (PIFE) typical for Cyanine dyes (sec.1.4.1), an effect already observed in this work for other tRNA modification enzymes in sec.3.1.1, was equally observable for the tRNA-TruB interaction. Fig.3.8 **b** shows the percental increase of Cy5 fluorescence for >90% TruB binding compared to the RNA only intensity.

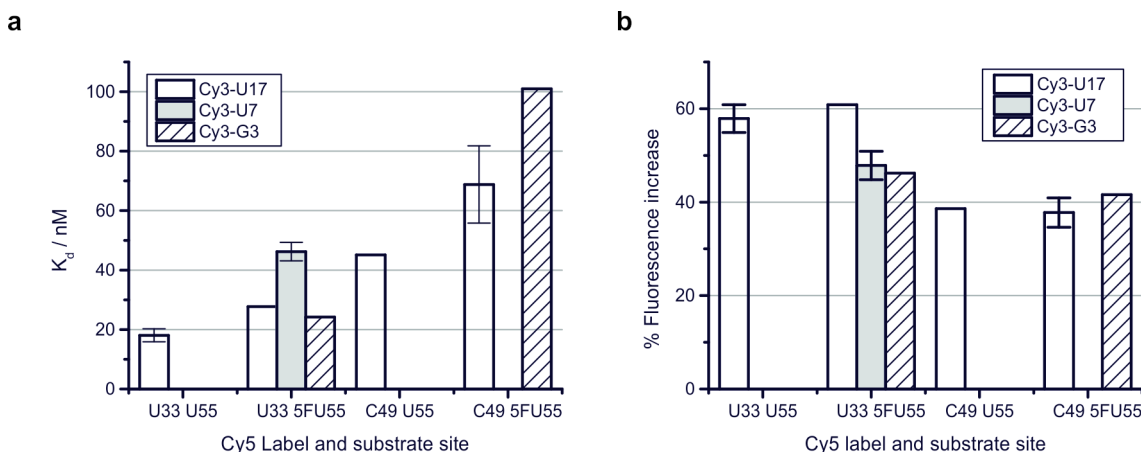


Figure 3.8.: Results of MST titration of various yeast tRNA^{Phe} FRET constructs with TruB. Error bars represent the SD of duplicates. **a** Dissociation constants resulting from fitting a 1:1 binding model to MST data. Values are grouped for Cy5 label position and substrate site. **b** Relative increase of Cy5 fluorescence for >90% binding compared to the RNA only fluorescence intensity.

For all constructs the intensity increase spans a range of ~40-60%. The observed fluorescence increase of the C49 label is 0.2-0.3x lower than for the U33 label. Two scenarios would explain this difference in responsiveness: Either the U33 label interacts with TruB to a higher extent than the C49 label, or TruB binding induces a change in the tRNA's conformation that enhances fluorescence of the U33 label. Increased dye-protein interaction for the U33 over the C49 label is improbable for two reasons: The docking model shown in Fig.3.5 does not imply any interaction of TruB with U33 and the positively charged, tRNA-binding competent surface of TruB [76, 103] does not seem to allow TruB to bind the tRNA in another orientation than suggested by the docking model. In consequence it seems unlikely that the enzyme could interact with substrate position in the T loop and the anticodon loop, containing the U33 label, at once.

However an unlikely event tends to come with unusual features: Provided the TruB bound tRNA is significantly distorted, the enzyme could interact with U33 and U55/5FU55 at once. Such a conformational distortion is, e.g., evident in the so called 'lambda tRNA' bound to the tRNA modification enzyme archaeosine tRNA-guanine transglycosylase [155]. The enzyme modifies G15 in the D loop and thus shares a feature with TruB: To gain access to their substrate site both enzymes have to dislodge D stem loop and T stem loop by disrupting tertiary interactions. A docking model suggests that TruB and archaeosine tRNA-guanine transglycosylase could simultaneously bind to the same tRNA molecule [155]. Yeast tRNA^{Phe} is indeed capable to adopt lambda RNA conformation by extending the anticodon stem with base pairs of D stem and variable loop. Details of lambda RNA and the possible impact of tRNA labeling on TruB action, U55 vs. 5FU55, as well as the enzyme's influence on the dye labels spectroscopic properties are investigated in more detail in chapter 4.

In summary MST showed that TruB binds five differently dye labeled tRNA, two of which were tested as 5FU55 and U55 variants, with similar affinity (up to five-fold). Neither a significant inhibitory effect of 5FU55 over U55, nor an effect of the Cy3 labels on enzyme binding could be detected. The Cy5 labels do influence enzyme tRNA interaction with Cy5-U33 labeled tRNA possessing a slightly higher affinity.

3.1.3. MST to evaluate binding mode of Mouse Ψ synthase I

The Pus1p family of Ψ synthases is of particular scientific interest: A mutation in the human PUS1 gene causes 'Myopathy and Sideroblastic Anemia' (MLASA) [170, 171], and modification by Pus1p is involved in nuclear receptor signaling [172–174]. Pus1 enzymes are extremely versatile concerning their substrate positions and they act on various different types of RNAs [173, 175–177]. How the enzymes recognizes different substrate positions, situated in different structural contexts, is poorly understood to date. For tRNA as substrate, a mutagenesis approach coupled to the determination of enzymatic turnover by the human homolog hPus1p allowed the identification of a minimal substrate [178]. This minimal substrate contains tRNA nucleotides 26-65 (blue/yellow in Fig.3.9).

3.1 Evaluation of RNA protein interactions

To shed light onto the tRNA binding mode of mouse Pus1p [159], a novel probing strategy for tRNA enzyme contacts had to be developed. A library of human mitochondrial tRNA^{Leu(CUN)} FRET constructs carrying 5FU at substrate position 27 was generated in a so-called dye walk: Using an established ligation system [179], Cy3 and Cy5 dyes were ‘walked’ along the secondary structure by attaching them to a modified uridine at different positions (Fig.3.9). Three positions for each dye enabled eight dual labeled constructs (Fig.3.9, U66 and U54 share the same ligation fragment, preventing the 9th construct).

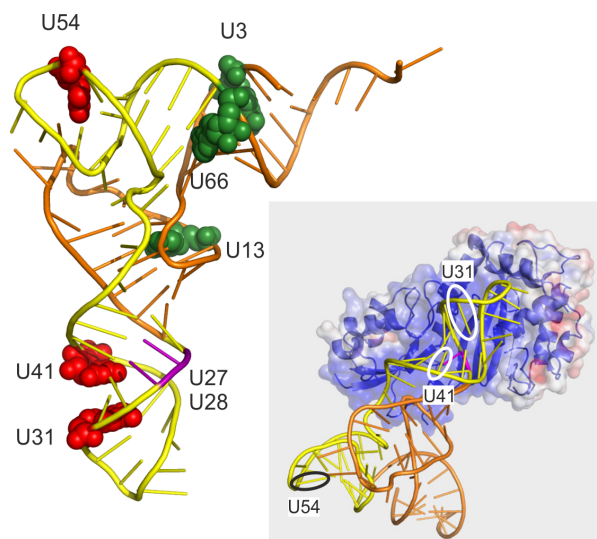


Figure 3.9.: Tertiary structure of the tRNA^{Leu(CUN)} constructs: The hPus1p minimal substrate [178] is shown in yellow, substrate positions 27 and 28 in purple, dye labeling positions are indicated as green (Cy3) or red (Cy5) spheres (model PDB ID 1EHZ). Inset: Docking of yeast tRNA^{Phe} (orange) into apo-hPus1p (Fig. modified from [154]). The minimal substrate of hPus1p is depicted in yellow, the substrate position 27 is marked purple, Cy5 labeling positions are indicated by ellipsoids.

Fig.3.9 shows that the minimal substrate contains all three Cy5 labels, while the Cy3 labels are one (U66) to 23 (U13) nucleotides distant. The labels could interfere with Pus1p binding either by direct contact or by altering the tRNA structure. To gain insight into possible interference of the dye labels with protein binding that could in turn provide evidence concerning the enzyme’s tRNA recognition mechanism, tRNAs were titrated with mouse Pus1p enzyme and MST curves, shown in Fig.3.10, were recorded in standard settings for each titration point.

The U31 label (Fig.3.10a-c) exhibits a lower apparent thermophoresis depletion, than the positionally similar U41 label (Fig.3.10d-f). Poor data quality precludes

a more detailed investigation of this effect. No other clear trend for a given label or a given label combination is eminent from the raw data. For yet unknown reasons, the thermophoresis response of the U3-U31 construct, depicted in Fig. 3.10a, is particularly low. All curves show fluctuations that indicate sample aggregation, except U13-U54 and U3-U54. Curves of U3-U54 are noisy due to a low overall fluorescence intensity. Fig. 3.11 shows analyzed data of the 'MST regime' (see sec. 1.5) from Fig. 3.10 fitted to a 1:1 binding model. Any other analysis described in sec. 1.5 was also responsive to protein binding, as discussed in sec. A.1.3.

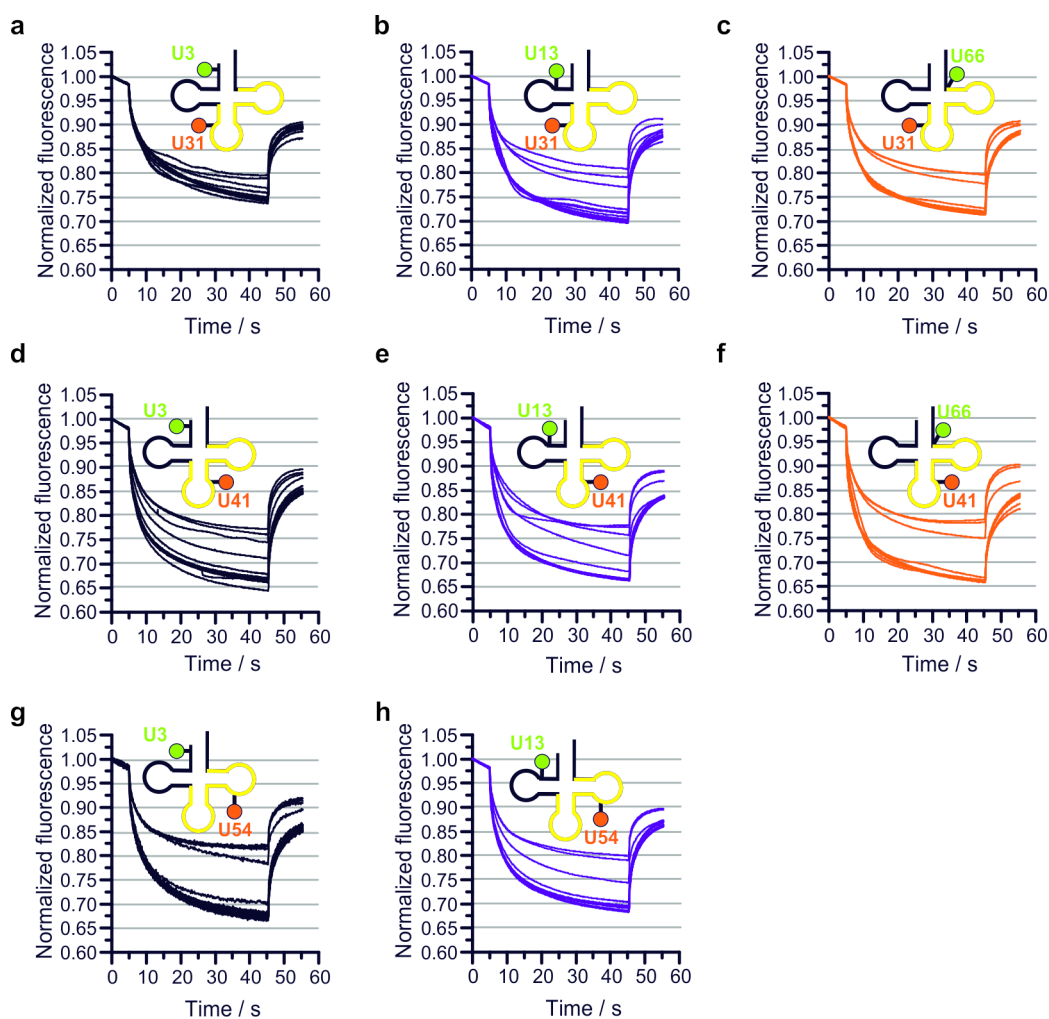


Figure 3.10.: Normalized MST curves of titrations with mPus1p. A tRNA secondary structure cartoon indicated the label positions for each graph: green Cy3, red Cy5, the minimal substrate of human Pus1p is indicated in yellow. Note that all graphs contain 16 curves, but that most curves superimpose in the regime of high thermophoresis depletion (low protein binding, low normalized fluorescence). Measurements were performed by N. Vickneswaran.

3.1 Evaluation of RNA protein interactions

All fits depicted in Fig.3.11 have in common that the saturation binding regime lacks any experimental data, rendering them very rough approximations of the actual binding affinities. The baseline for low protein concentrations lies between 760 and ~810 a. u., depending on the construct (Fig.3.11). A significantly higher affinity of U3-U54-tRNA compared to U13-U54 is implied by the data in Fig.3.11c. Without saturation binding data, this difference from one Cy3 label variant to the other is neither reliable, nor is it observed for other Cy5 labels (Fig.3.11a+b).

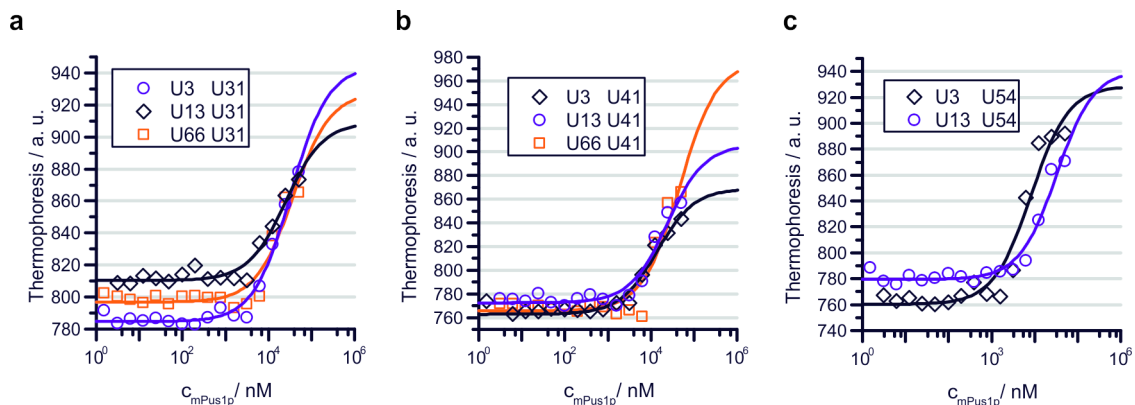


Figure 3.11.: MST titration curves of tRNA^{Leu(CUN)} mPus1p interaction fitted to a 1:1 binding model. Cy5 at: **a** U31, **b** U41, **c** U54.

Fig.3.12 shows that mPus1p binding of all constructs occurs with affinities from ~10 to 50 μ M and causes a protein-related increase in fluorescence intensity peaking at ~30-45% for the highest enzyme concentration (Fig.3.12b).

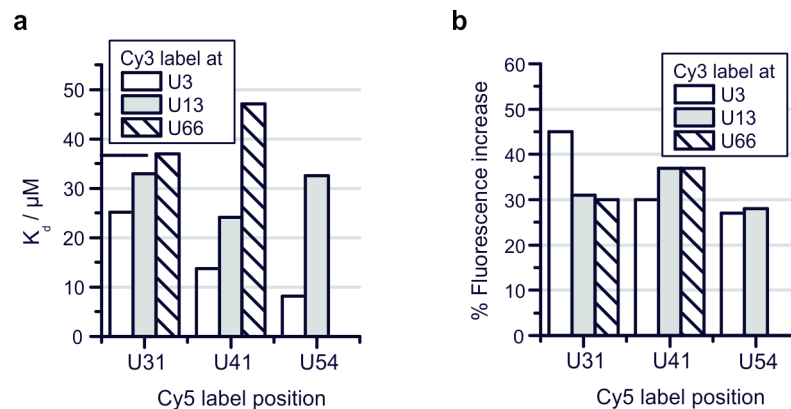


Figure 3.12.: Results from MST titrations of tRNA^{Leu(CUN)} constructs with mPus1p. **a** Affinities determined by fitting MST data to a 1:1 binding model. Error bars represent the SD of duplicates. The various Cy3 label variants are grouped for the Cy5 label used for detection. **b** Percentage of increase in Cy5 fluorescence intensity from zero to the highest protein concentration, determined from thermophoresis-free fluorescence.

The lack of saturation binding precludes extensive discussion of label related differences in binding affinity: The detectable fivefold difference in affinity lies within the uncertainty of fitting unsaturated binding curves. Previously reported affinities of homologous Pus1 enzymes indicate up to 10^4 x stronger binding [116, 154, 166, 178]. Binding affinities of mPus1p for tRNA determined here are also significantly weaker than the values determined for binding by TruB (sec.3.1.2). This decrease in affinity is in part expected to be caused by protein aggregation. However, constructs labeled at U54 show no aggregation related fluctuations (Fig.3.10g+h) but fail to reach a higher degree of binding (Fig.3.11c). It is therefore possible that the high age (6 years) rendered a part of the enzyme preparation incapable of tRNA binding without causing the protein to aggregate. In lack of a fresh, homogenous mPus1p preparation for comparison, this remains speculation.

Interpretation of the PIFE effect is principally possible even in lack of full binding, but does not provide meaningful conclusions: If protein proximity would be the only factor promoting PIFE, Cy5 labels at U31 and U41 should be more responsive to protein binding, than the U54 label (Fig.3.9). However, the data in Fig.3.12b does not show any consistent trend supporting such a hypothesis.

In summary a dye walk on human mitochondrial tRNA^{Leu(CUN)} generated eight tRNA constructs, that were all responsive to mPus1p binding in MST experiments and as assessed by an intensity increase in fluorescence of the observed Cy5 label. However, due to lack of saturation binding, no clear conclusion can be drawn based on these results. A fresh preparation of mPus1p purified to homogeneity by gel filtration should result in affinities that are in better agreement with literature. Future experiments should include turnover assays, either for the second substrate position U28 or for U27, requiring new ligations.

3.2. MST to evaluate conformation of hmt tRNA^{Lys}

The unmodified transcript of human mitochondrial (hmt) tRNA^{Lys} (KWT) resides in a structural equilibrium between an extended hairpin conformation and the canonical cloverleaf, while the non-canonical conformation predominates [45]. Misfolding can be reverted by introducing modification m¹A9 native to this tRNA [47] or, more efficiently, by exchanging A50-U64 *vs.* G50-C64 (KE mutant), thereby

destabilizing the extended hairpin while stabilizing the cloverleaf [45] (Fig.3.13).

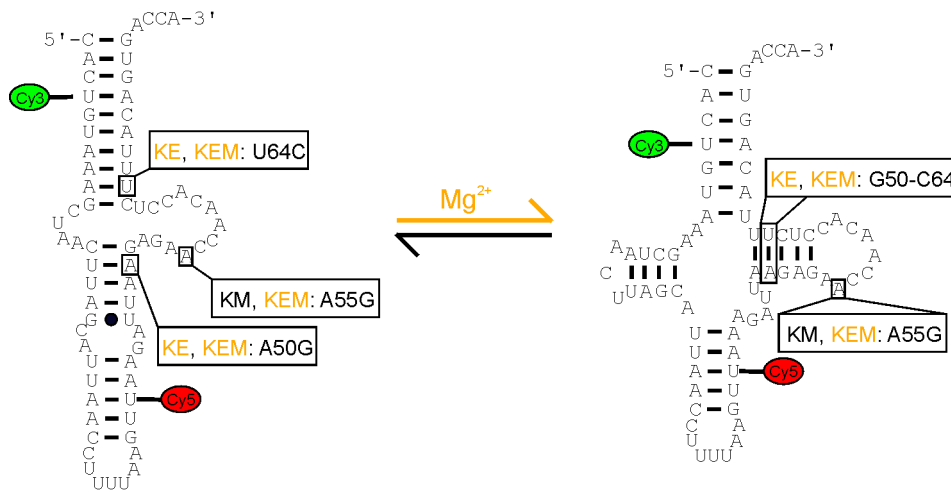


Figure 3.13.: Secondary structures of fluorescently labeled human mitochondrial tRNA^{Lys} mutants. Conformational equilibrium between extended hairpin (left) and canonical cloverleaf form (right) is shown, while cloverleaf promoting factors are depicted in orange.

Aminoacylation experiments support this model: While KWT is aminoacylated very poorly, the KE mutant reaches ~60% of the level reached by native tRNA^{Lys} [180]. A native pathological MERRF mutant A55G (KM) is not hampered in aminoacylation, while the unmodified, combined mutant KEM is charged to only the level of KE [180]. Structural probing [180] and methylation assays [181] imply a shared tertiary structure for unmodified KE and KEM. A folding energy landscape derived from smFRET experiments showed that cloverleaf folding of KWT increases with increasing Mg²⁺ [46, 158]. KM is less responsive to Mg²⁺ (presumably due to a less stable tertiary structure) and KE, as well as KEM, undergo very little Mg²⁺ induced structural change (since they possess cloverleaf conformation already) [182].

To explore the power of MST in distinguishing tRNA conformations, fluorescently labeled variants of KWT, KE, KM and KEM (Cy3 at U4 and Cy5 at U41, see Fig.3.13) were generated by splinted ligation² and subjected to two MST titrations with Mg²⁺: Once at 40% IR (MST) laser power with $0 \leq c(\text{Mg}^{2+}) \leq 400$ mM and once at 80% IR laser power and $0 \leq c(\text{Mg}^{2+}) \leq 1800$ mM. Normalized MST curves of these experiments are given in Fig.3.14.

²Hmt tRNA^{Lys} constructs were synthesized by Benjamin Hofmann [181].

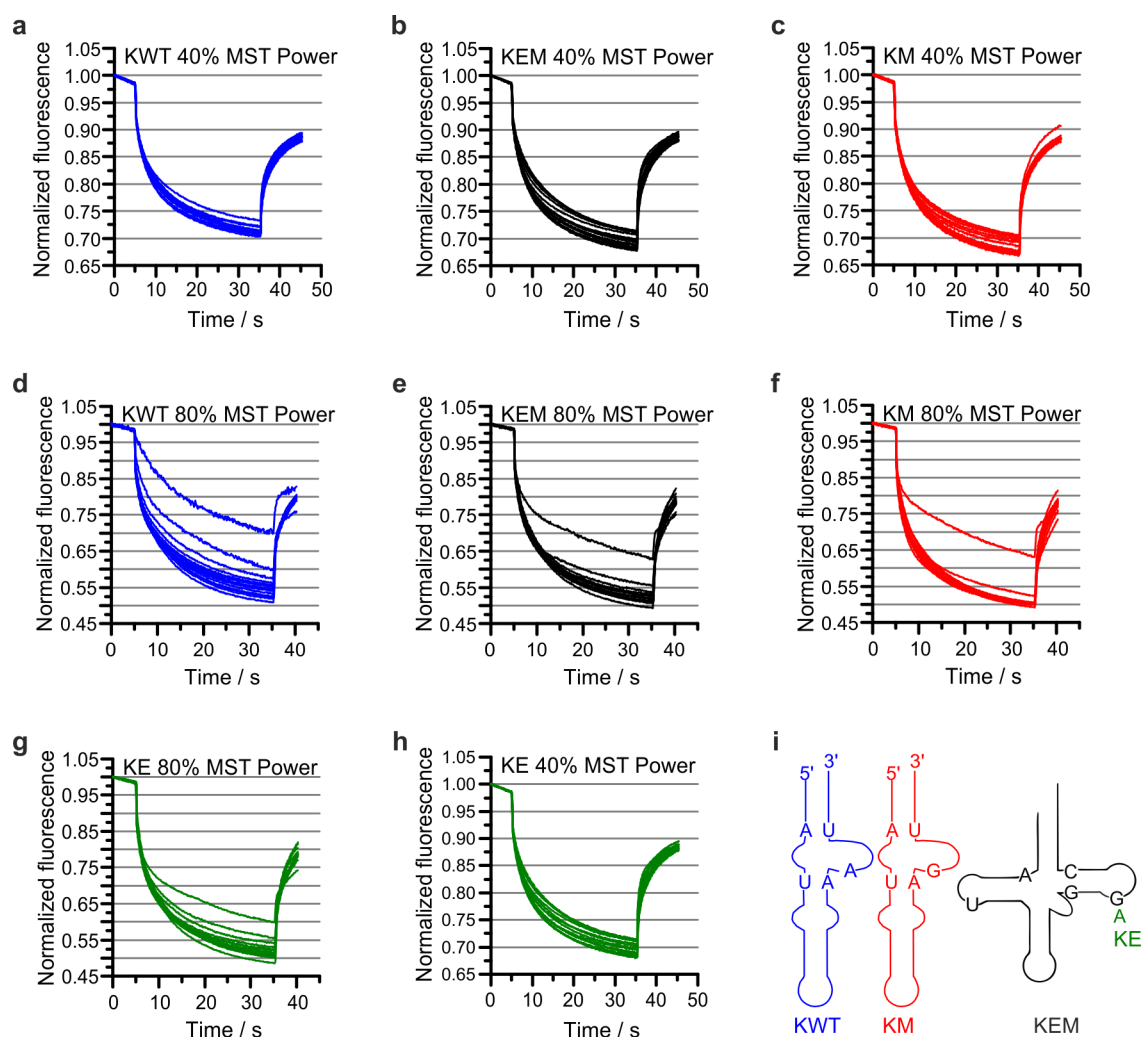


Figure 3.14.: Normalized MST curves of tRNA^{Lys} Mg²⁺ titrations at medium salt concentration and medium IR (MST) laser power **a-c+h** and at high salt concentrations and high IR (MST) laser power **d-f+g**. Assumed secondary structures of these constructs are indicated as cartoons in panel **i**. Note that KE was omitted for clarity, as the only difference to KEM is A55 instead of G55. Native A55 presumably results in a more compact tertiary structure.

At medium MST power (Fig. 3.14a-d) all constructs show only ~5% deviation over all curves with a maximal thermophoresis depletion of ~67.5%. KWT (Fig. 3.14a) shows thermophoresis accumulation with increasing Mg²⁺, that is lower in magnitude than the depletion of the other constructs. At 80% MST power the maximum thermophoresis depletion reaches ~47.5% and thermophoresis depletion is reduced again at high salt concentrations.

Fig. 3.15 shows the titration curves resulting from the raw data given in Fig. 3.14. The plots conform to literature in such that KE and KEM show similar response

3.2 MST to evaluate conformation of hmt tRNA^{Lys}

to increasing Mg²⁺ concentration, while the response of KWT is different and KM represents a third case, at least for up to 400 mM Mg²⁺ and medium IR laser power (Fig.3.15 a).

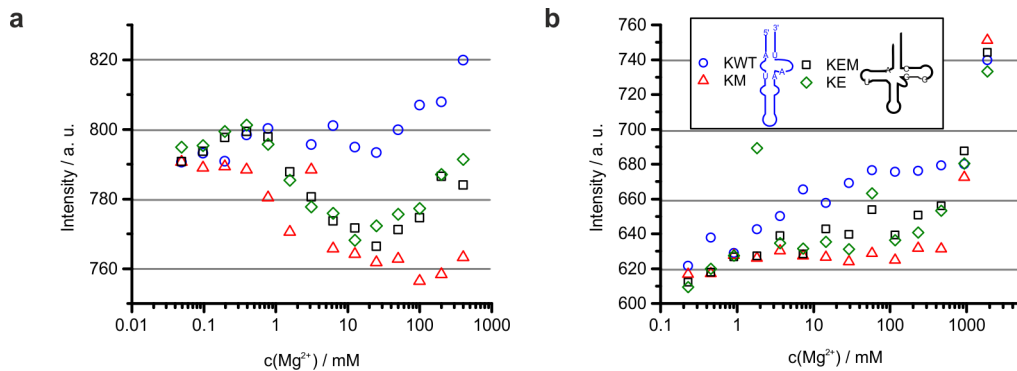


Figure 3.15.: MST titration of tRNA^{Lys} mutants with MgCl₂. Titration series of all constructs in one run were performed at 40% IR laser power (a) and, in a second experiment, at 80% IR laser power (b). The legend shown in b is equally valid for a.

All samples show equal thermophoresis in absence of Mg²⁺ in both experiments and start to deviate near physiological Mg²⁺ concentrations at ~1-3 mM. For low salt concentrations and low laser power (Fig.3.15a) thermophoresis depletion increases from ~3 mM Mg²⁺ on for KE, KEM and KM until ~50 mM. From ~50 mM on magnitude of thermophoretic depletion decreases again for both cloverleaf mutants (KE and KEM), while thermophoresis of KM remains constant in the high depletion regime. KWT differs from this behavior in showing a decrease and not an increase of thermophoresis depletion from 3 mM Mg²⁺ on (note that such a decrease of depletion leads, of course, to a higher fluorescence signal).

In the high-salt, high laser power experiment (Fig.3.15b) all constructs show a decrease in thermophoretic depletion from ~0-3 mM Mg²⁺. At this threshold sample behavior deviates again: KWT, as in the other experiment, shows an ongoing decrease in thermophoretic depletion with rising salt concentration. In contrast, thermophoresis of the other constructs is similar and remains constant with increasing Mg²⁺. The cloverleaf mutant KEM and KE differ from KM only in showing a steeper decrease in thermophoresis depletion from ~50 mM on. In contrast to the low laser power low salt experiment, thermophoresis values coincide again at high salt concentrations (Fig.3.15b).

A model allowing full interpretation of the data is not available due to the complexity of the experiments:

- Thermophoresis depends on the hydrodynamic radius, which, for tRNA, was found to vary significantly with ionic strength, from 5.7 nm-3.4 nm [183, 184] at zero MgCl_2 to ~ 2.5 nm at 15 mM MgCl_2 [183].
- As a diffusion-based response, thermophoresis is viscosity-dependent and viscosity increases about two-fold from 0-2 M Mg^{2+} [185].
- Thermophoresis possesses an ionic component which depends on the ionic strength of the buffer [141, 143, 186].
- Analyzing an unresolved ensemble of multiple structures is challenging.

However, the data implies that different conformational ensembles of the same tRNA can be distinguished by thermophoresis. Obtained results are supported by the above discussed literature in such, that the cloverleaf mutants behave similar, while the wild type and the MERRF mutant represent cases of their own. These preliminary results can form the basis for future MST experiments on constructs of tRNA^{Lys} that carry their native nucleoside modifications to different extents. Such an analysis should complement single molecule FRET studies of Kobitski et al. [46, 158] by including two so far uninvestigated nucleoside modifications 5-taurinomethyl-2-thiouridine (taum⁵s²U, [187]) at the wobble position 34 and a threonylcarbamoyladenine (t⁶A, [45]) at position 37. Conformational effects of these modifications are implied by recent studies showing significant influence of antidocon stem loop modifications on the innate flexibility of tRNA [35, 39].

3.3. MST of a SAM binding riboswitch

Riboswitches are a particularly interesting type of RNA, since they possess at least two different conformations that form a dynamic equilibrium: One conformation that is able to bind with high affinity to a specific ligand and one conformation that is not capable of binding [22]. In presence of ligand the binding competent conformation is highly favored, and the resulting ordering allows crystallization studies [22]. Binding of SAM to the *B. subtilis* SAM-I riboswitch, introduced in sec.1.2.3, should generate a large MST signal, since the binding competent and the binding incompetent conformations differ in secondary and tertiary structure (Fig.3.16). In detail, the antiterminator helix is disrupted in favor of the terminator helix, meaning the hybridization of the nucleotides shown in bold in Fig.3.16a changes into the hybridization depicted in Fig.3.16c, thereby allowing formation of the binding pocket [188].

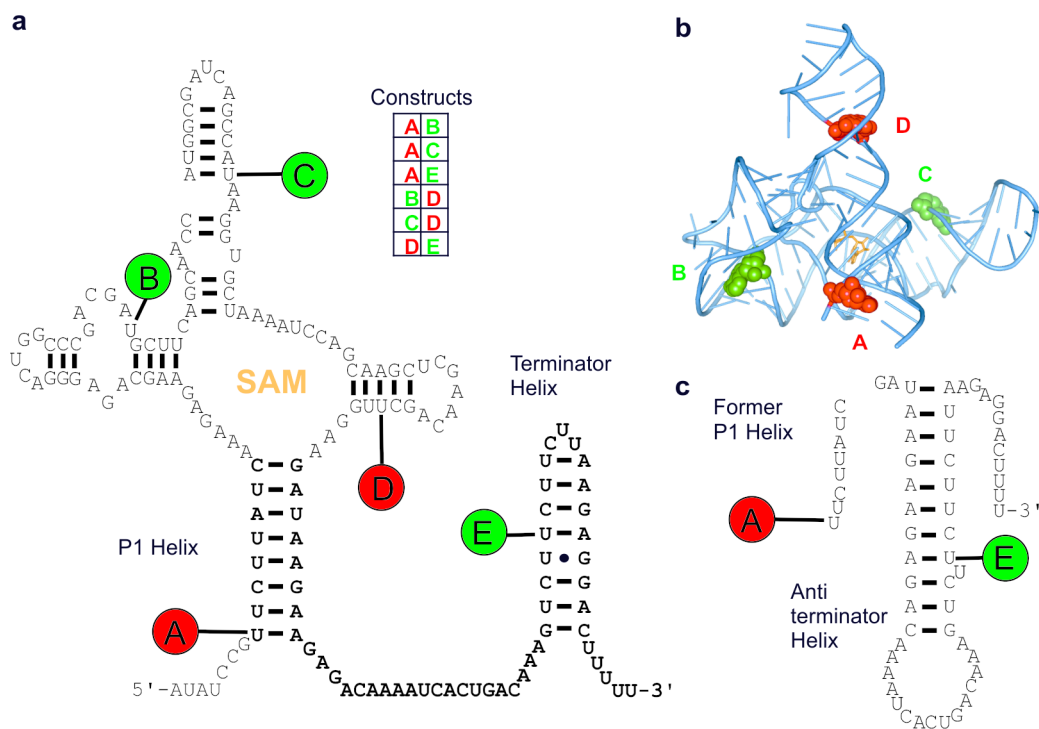


Figure 3.16.: Structure of SAM-I riboswitch constructs. **a** Secondary structure of the SAM bound form, hybridization specific for this structure bold [61]. **b** Crystal structure of SAM bound aptamer domain [52], lacking the expression platform and therewith label E. Bases at label positions colored green (Cy3) or red (Cy5), bound SAM orange. **c** In the putative SAM free secondary structure the terminator helix hybridizes with the 3' part of the (former) P1 helix, forming the antiterminator helix [188].

As depicted in Fig.3.16, the fluorescent labels Cy3 and Cy5 were distributed over all five helices of the riboswitch (using splinted ligation techniques³), yielding five label positions. The six resulting differently Cy3-Cy5 labeled riboswitch variants were expected to differ in affinity for SAM, since labels A-D are distributed around the binding pocket and the E label is located at the helix functioning as switch between binding competent and binding incompetent conformations (Fig.3.16). MST titrations with SAM were applied to test for the assumed existence of a conformation-related MST signal and, if confirmed, to assess the suitability of such a signal for SAM affinity determination that could reveal possible label interference with ligand binding.

Fig.3.17 shows MST curves resulting from SAM titrations of all six constructs. Only two of the six constructs show a clear response (~10% of the normalized signal) to rising SAM concentration: The AB and the CD construct (Fig.3.17a+e). The total thermophoresis depletion is significantly higher for constructs carrying the detected label Cy5 at position A (Fig.3.17a-c) compared to the D labeled counterparts (Fig.3.17d-e).

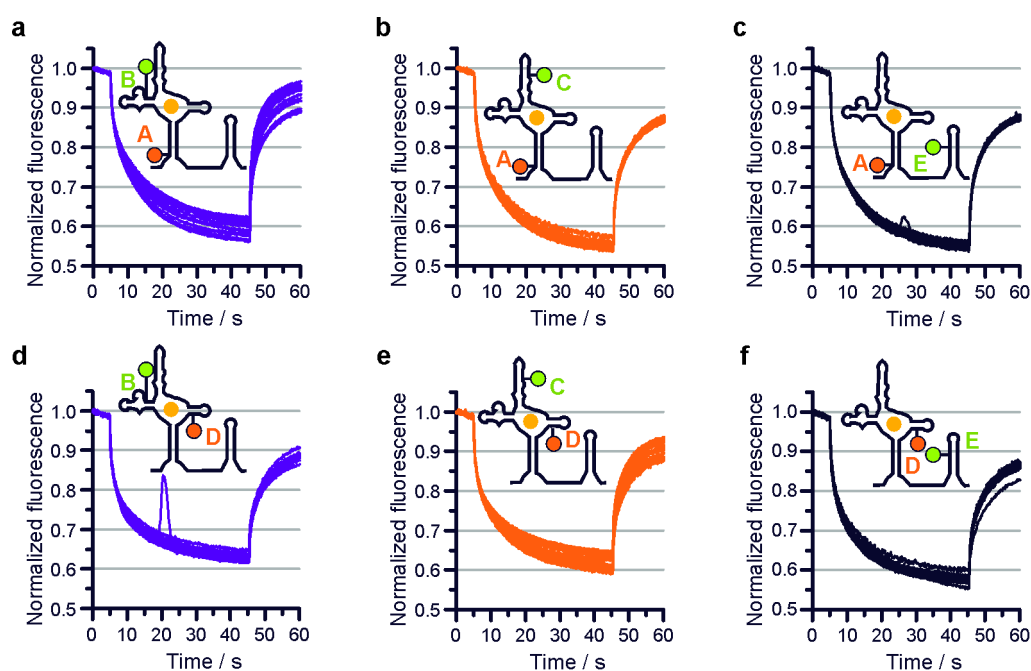


Figure 3.17.: Normalized MST curves of SAM titrations. Fluorescence of the directly excited Cy5 label was detected. The cartoon represents the secondary structure of the binding competent conformation with SAM as orange sphere, label positions are indicated as either red (Cy5) or green (Cy3) spheres.

³Ligations were performed by A. Samanta [189].

3.3 MST of a SAM binding riboswitch

In addition two curves of two different constructs show single aggregate events (Fig.3.17c+d). Since no change in fluorescence intensity was caused by SAM binding (data not shown), dye RNA interactions (if any) are expected to be similar in the SAM bound and the SAM free structures of the SAM-I riboswitch.

The data was analyzed for the 'MST regime' (sec.1.5) to obtain data points for the titration curves given in Fig.3.18, that showed SAM binding for variants AB with $K_d = 44.2$ nM, similar to the native riboswitch [61], and CD with $K_d = 1$ nM, similar to the aptamer domain [52, 55, 61–63]. The titration curves of all other constructs fluctuate around flat lines. For unknown reasons the titration curves shown in Fig.3.18a possess a different y-axis offset than the curves of Fig.3.18b and the flat lines of the ED and the BD construct of Fig.3.18b differ from each other in offset.

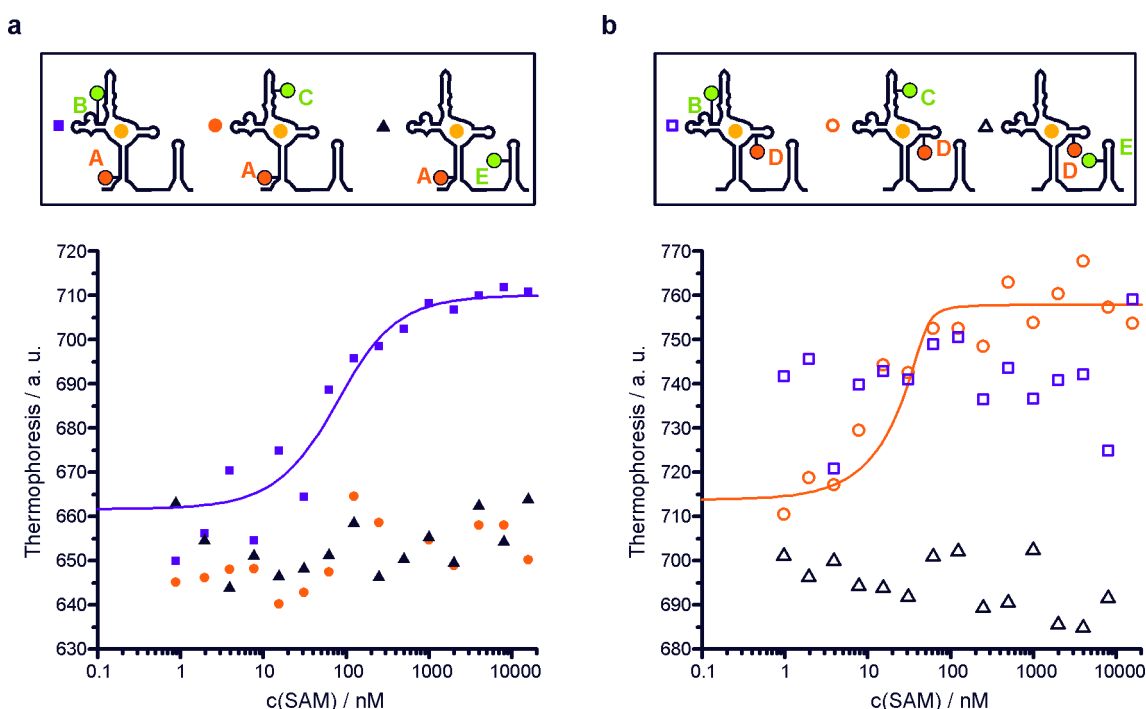


Figure 3.18.: MST titration curves from SAM SAM-I riboswitch interaction (direct detection via Cy5), fits to a 1:1 binding model as solid lines. Constructs with Cy5 at position A (**a**) and Constructs with Cy5 at position D (**b**). Note that the 16 μ M data point of ED is sacrificed to scaling.

In addition to the 'MST regime', the AB construct was also responsive in T jump, MST+T jump and backdiffusion, while the CD construct was only responsive in MST+T jump and backdiffusion and not in the T jump alone (data not shown). In both cases backdiffusion analysis yielded a K_d value that, for yet unknown

reasons, surpassed the result of other analyses by several orders of magnitude.

Conclusions from the MST assays are summarized in Fig.3.19a for constructs carrying the Cy3 E label and in Fig.3.19b for the other constructs.

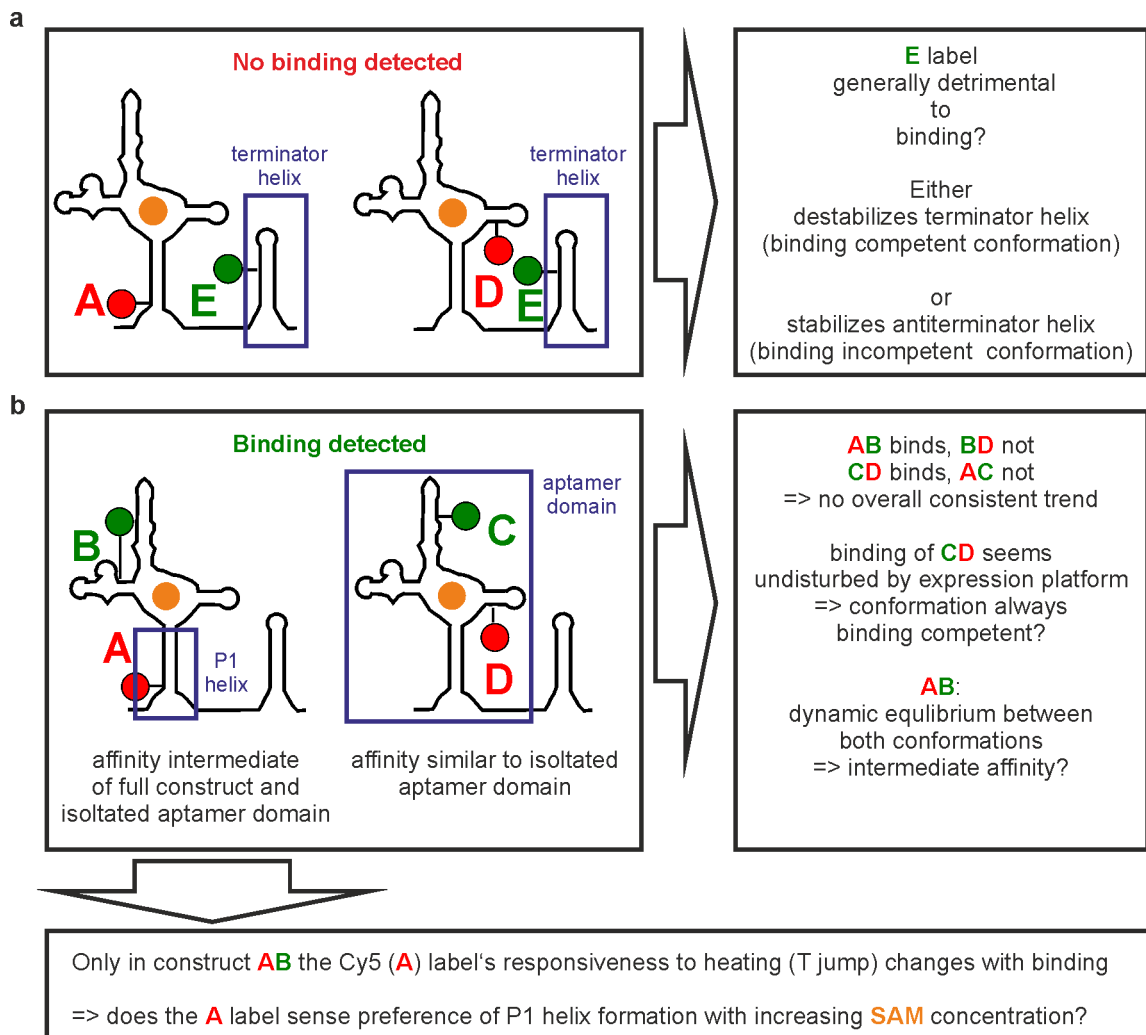


Figure 3.19.: Conclusions from MST titration on SAM-I riboswitch interaction. **a** Constructs with Cy3 at position E. **b** Constructs AB and CD (binding detectable) as well as AC and CD (no binding detectable).

In the simplest hypothesis one label position should consistently favor or disfavor SAM binding by shifting the conformational equilibrium either towards the conformation capable of binding (Fig.3.19) or towards the conformation incapable of binding (Fig.3.16c). That this is not the case for all constructs not containing the E label, implies an isolated, different case for every label combination. However, the data at hand does not provide further insight into possible pleiotropic

or cooperative effects of the various label combinations, that could explain such isolated cases. The possibility that some constructs do bind SAM but binding is not detectable by MST is rather unlikely due to at least two reasons: (1) the significant conformational difference between the conformation that is capable of SAM binding and the conformation that is not capable of binding should result in characteristic thermophoretic behavior for both cases and (2) for the two constructs that showed binding, a signal could be obtained from multiple readouts, which confirms point (1).

Concerning the various possible readouts of a thermophoresis experiment (see Fig. 1.15) it is particularly remarkable, that the two constructs showing SAM binding differed in responsiveness of MST curve parameters. The CD construct lacks the responsiveness in the T jump that is detectable for the AB construct. A responsiveness of the T jump to SAM binding implies a different temperature sensitivity of the Cy5 label at position A in absence and in presence of SAM, as changes in the T jump reflect changes in the local dye environment that influence the dye's temperature sensitivity (see sec. 1.5 and [140]). While the unresponsive D label is located in the middle of a helix occurring in both conformations, the P1 helix harboring the A label is disrupted in favor of the antiterminator helix in absence of SAM (Fig. 3.16a). This structural difference might explain the T jump response of the A label. That both constructs were responsive to SAM binding in the back-diffusion regime of MST data might be related to significantly different hydrodynamic radii of the SAM bound and the SAM free riboswitch conformations rather than to the presence of the small molecule SAM directly.

In summary, SAM binding by a whole riboswitch construct can be measured using MST, at least for two of the six constructs tested. It is to be expected that the conformational change concomitant with binding generates a higher thermophoresis response than SAM binding alone. Comparison of the two label variants for which SAM binding could be detected, revealed interesting and conclusive differences in the responsiveness of MST readouts: Disruption of the P1 helix seems to influence the temperature jump of the A label, but not of the D label. Protein binding to Cy5 labeled RNA results in a much stronger Thermophoresis response (sec. 3.1), which may in part be caused by a change in the dye's spectroscopic properties, rather than by actual thermophoresis (see sec. 1.4.1).

4. Interaction of TruB with 5FU55-tRNA

4.1. Introduction

The number of known modified nucleosides is surging [13–15], a phenomenon intensified by the relation of modified nucleoside to epigenetics [4, 190, 191]. As direct consequence, possible epigenetic involvement of pseudouridine (Ψ), first modified nucleoside to be discovered [64], termed the 'fifth nucleoside due to being the most abundant [14], is back in focus. Besides Ψ 's manifold functions and locations [146, 192–195], the recent discovery that introduction of Ψ in mRNA induces suppression of stop codons [20, 21] contributes to the renewed interest.

In this situation, almost 50 years after Ψ 's discovery, 26 years after the purification of the first Ψ synthase [97] and almost 15 years after reporting the first enzyme-RNA cocrystal structure [76], it is particularly surprising that the enzymatic mechanism of Ψ formation remains elusive [110, 112, 113].

Use of the anticancer drug 5-fluorouracil (5FU) [84], an inhibitor of thymidylate synthase [196], as a suicide probe enabled mechanistic elucidation of several nucleic acid modification enzymes [23, 81, 90]. Early evidence on 5FU inhibiting Ψ formation [97, 98, 197] culminated in the promotion of 5FU as covalent suicide inhibitor of Ψ synthases [101, 198]. However, cocrystal structures of 5FU-RNA and Ψ synthases failed to contain a covalent suicide adduct [106, 107, 114]. Doubt in suicide action of 5FU is most intense in enzymes of the Pus4 family [76, 98, 103], where family member TruB failed to be inhibited by 5FU-RNA in preliminary kinetic studies [108], restricting the evidence for suicide action to a SDS-stable complex band [104].

To reveal a possible covalent nature of the mysterious gel band, we characterized complex formation of TruB with fluorescence labeled, poor, 5FU55-containing

substrates under various conditions. Surprisingly, substrate quality of the U-variant did not correlate with 5FU55-specific complex and subsequent K_d measurements of the TruB tRNA interaction by exploiting responsiveness of several spectroscopic parameters, as well as, thermophoresis, revealed similar affinity of TruB for U55- and 5FU55-RNA. A consistent picture of non-covalent action of 5FU55 is completed by chase experiments in all methods, confirming reversibility of complexation.

4.2. Gel shift and LC-MS/MS analysis

As initial studies on tRNA-TruB binding were successful using yeast tRNA^{Phe} (see sec.3.1.2), an especially well characterized tRNA [40, 199], we retained this choice of substrate. Substrates were generated as described in sec.7.3: In-vitro transcription supplied unmodified U55-tRNA, while a tRNA carrying 5FU at substrate position 55 was synthesized by splinted ligation (Fig.4.1).

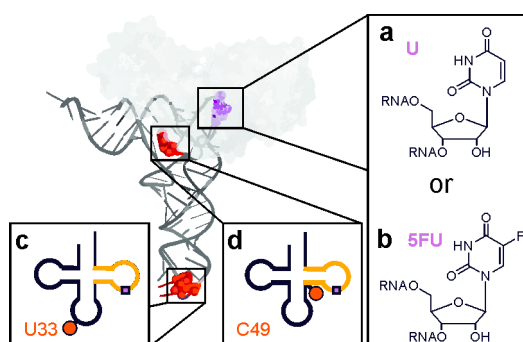


Figure 4.1.: Tertiary (above) and secondary (below) structure representations of the yeast tRNA^{Phe} constructs. Substrate position 55 in purple was either U55 (a) or 5FU55 (b) and the Cy5-label in red was either attached at position U33 (c) or at position C49 (d). The enzyme TruB bound to tRNA as predicted by a docking model [76] is shown in gray.

To generate a complex with *Thermotoga (T.) maritima* TruB, these constructs were incubated with the enzyme in two reactions: Either for 1 h at 70°C, near the enzyme's temperature optimum [200], or for 12 h at 4 °C, as published previously [104]. Following 5 min incubation in SDS buffer at either 25 or 95 °C, samples were analyzed by SDS PAGE (see Fig.4.2). A complex in 40% yield could be detected exclusively for the 5FU variant incubated at 25 °C, heating to 95 °C destroyed the complex.

4.2 Gel shift and LC-MS/MS analysis

Apart from lower concentration (1 vs. 20 μM), the experiment at 12 h and 4 $^{\circ}\text{C}$ reproduces previous work [104]. Phannachet et al. obtained the SDS-stable complex using a 5FU-containing T stem-loop (TSL) minimal substrate (shown in orange in Fig.4.1) and interpreted their finding as a covalent complex resulting from suicide action of 5FU [104]. Obtaining similar complex yields under such different conditions (12 h at 4 $^{\circ}\text{C}$ vs. 1 h at 70 $^{\circ}\text{C}$) motivated us to characterize kinetics of complex formation. Already after 1 minute of incubation in reaction buffer ~30% complex was formed, *vide infra* (Fig.4.3). This result is particularly surprising, as Ψ synthases like yeast Pus1p [166] or *E. coli* TruA, TruB and RluA [201], are remarkably slow in enzymatic turnover and should, in consequence, be equally slow in generation of a covalently trapped catalytic intermediate.

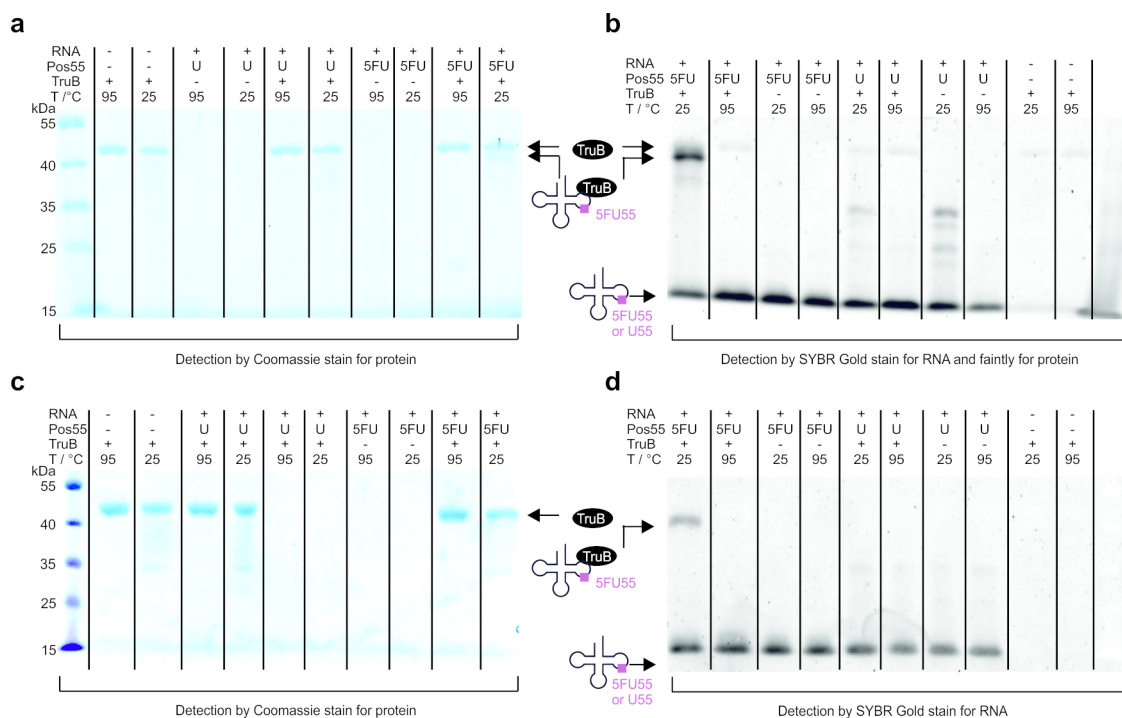


Figure 4.2.: Analysis of SDS-stable complex formation of TruB with unlabeled tRNA. Following incubation at 1 μM concentration at either 1 h and 70 $^{\circ}\text{C}$ (**a+b**) or 12 h and 4 $^{\circ}\text{C}$ (**c+d**), the complex was incubated with 0.5 vol SDS buffer for 5 min either at 25 $^{\circ}\text{C}$ or at 95 $^{\circ}\text{C}$. **a+c** Coomassie stain for protein and **b+d** SYBR Gold stain for RNA. Note that SYBR Gold stains TruB faintly in **b** and that protein marker in **c** is intense due to unrelated staining by stains all and that the complex band in **c** can only be deduced by a less intense protein-only band.

To gain further insight into the nature of the SDS-stable, reportedly covalent, complex, we intended to generate tRNAs that are inferior substrates to TruB: Correlation of U55 substrate turnover with SDS-stable, 5FU55 specific complex yield would indicate a trapped catalytic intermediate. A mutagenesis approach identified nucleotides responsible for the formation of key structural features in the TSL's T-loop (orange in Fig. 4.1) as only elements recognized by TruB [148]. A previous fortuitous finding was that attachment of the fluorescent label Cy5 to C49 at the edge of the TSL, decreases TruB affinity while a label at U33, distant from the modification site in the anticodon loop results in high affinity (sec.3.1.2). Requiring a non-trivial correlation of binding affinity with substrate properties, these labeled tRNAs could provide insight into the nature of the SDS-stable complex.

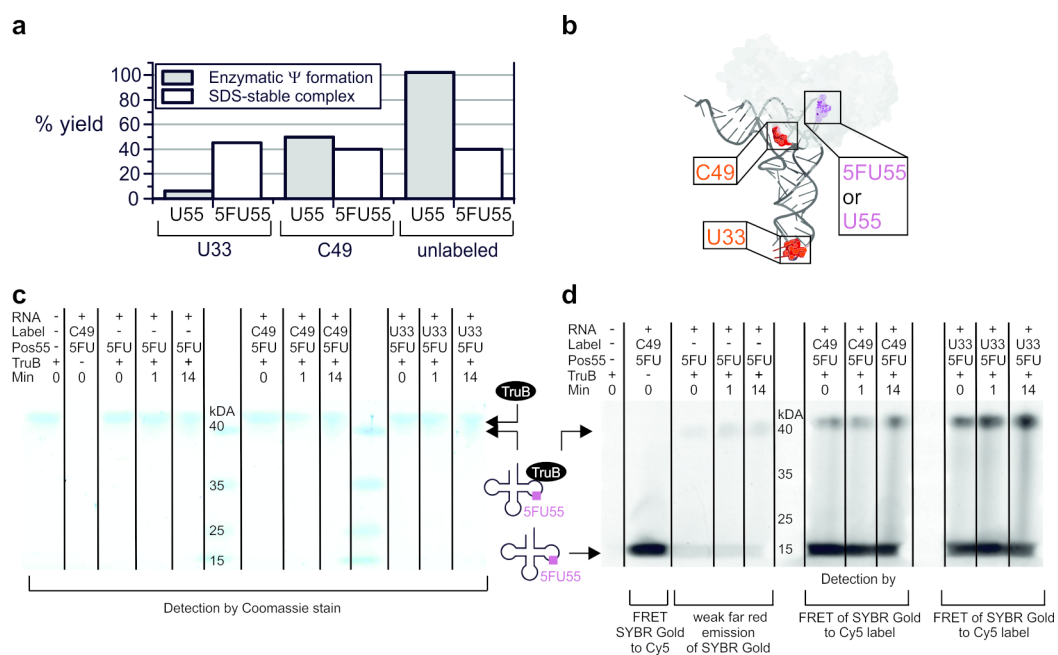


Figure 4.3.: Comparison of the kinetics of SDS stable complex formation with enzymatic turnover for labeled and unlabeled tRNA. **a** Yield of Ψ generation in U55-tRNAs (assessed by LC-MS/MS in duplicate) compared to yield of SDS-stable complex by 5FU tRNAs (data quantified from d). **b** Docking model of yeast tRNA^{Phe} (dark gray) into TruB (shaded gray) with the substrate site as purple and the dye labeled bases as red spheres. **c+d** Kinetics of TruB binding to labeled and unlabeled 5FU55-tRNA analyzed by SDS PAGE. Samples were incubated at 25°C for the time indicated and 5 min in SDS buffer prior to gel loading. Coomassie stain for protein shown in b), SYBR Gold stain for RNA in c) (excitation 488 nm, emission 670BP30). FRET from SYBR Gold to Cy5 generates the stronger signal of labeled tRNAs.

Judging from a docking model of TruB and full tRNA [76] (Fig.4.3b), the enzyme binds solely to the TSL part, and indeed the isolated TSL is an equally good substrate as full tRNA [148]. In consequence, the C49 label was expected to moderately influence enzymatic turnover while a performance comparable to unlabeled tRNA was expected from the U33 label (red dots/spheres in Fig.4.3b). Splinted ligation allowed synthesis of tRNAs in U55 and 5FU55 variants, labeled with Cy5 at U33 or C49, respectively.

Quantification of enzymatic pseudouridine formation by LC-MS/MS showed near quantitative turnover for unlabeled U55-tRNA and interference of the C49 label reducing the yield to ~50% (Fig.4.3a). Totally unexpected was a strong interference of the U33 label causing modification to only ~6%. Interference of a fluorescent label attached remote of the protein binding site (Fig.4.3b), is presumably related to long distance intramolecular rearrangement within the tRNA substrate [202, 203].

The fortuitous discovery that labeling of a tRNA substrate with Cy5 at U33 renders the substrate a negative mutant for TruB opened a new angle on the nature of the SDS-stable complex. As substrate turnover of U55-tRNAs should correlate with formation of allegedly trapped catalytic intermediate for 5FU55-tRNA, labeled RNA impaired in U55-turnover should be equally impaired in 5FU55-complex formation. While the C49 label should significantly reduce the yield of 5FU55-specific complex, the U33 label should almost completely abolish complex formation. However, as shown in Fig.4.3c+d, mixing at 25 °C results in almost instantaneous complexation for all three 5FU55-tRNAs in comparable yield. Thus 5FU55-specific, SDS-stable complexation does not correlate with U55-turnover especially not for U33 tRNA that forms ~7.5x more complex in minutes than Ψ in 1 hour. If low 5FU55-complex yield would result from kinetic inhibition, elongated incubation times and, especially for the thermophilic enzyme investigated, elevated temperature should significantly increase complex formation. However, complex yield was independent of both parameters, at least for C49-5FU55-tRNA (Fig.A.12).

In summary, instantaneous 5FU55-complex formation in similar yields for tRNAs that are either ideal, impaired or basically no substrates as U55 variants, contradicts the hypothesis of the 5FU55-complex as covalent catalytic intermediate and denies the complex any catalytic relevance. Although 5FU55-tRNA forms

a SDS-stable complex with TruB, an equivalent complex was not observable on urea PAGE, be it after an incubation for 10 min at 25 °C (Fig. A.9) or for 12 h at 4 °C (Fig. A.10). In contrast, urea PAGE analysis revealed varied sensitivities of the complex to different denaturing agents: A complex preincubated in SDS remained intact to only ~1%, while preincubation in formamide resulted in intense smearing indicating dissociation of the complex (Fig. A.9). Native PAGE analysis showed similar complex yield for all constructs, while again smearing indicated non covalent complexation (Fig. A.11). Higher resistance against denaturing agents of the 5FU55-tRNA-TruB complex compared to U55-tRNA implied differences in affinity. Consequently, we turned to characterization of the tRNA-TruB complex under equilibrium conditions.

4.3. Microscale thermophoresis

This work established Microscale Thermophoresis (MST) as fast and highly reproducible tool to assess interactions of proteins with fluorescently labeled tRNA (sec.3.1), including the tRNA-TruB interaction. For these highly esteemed qualities, the method was equally applied to the problem at hand: Fig.4.4 shows the primary data of typical TruB titration experiments for all four labeled tRNA variants ($C_{\text{tRNA}} = 50 \text{ nM}$). As noticed elsewhere for dual labeled tRNAs (sec.3.1.2), the thermophoresis curves (Fig.4.4a, c, e and g) differ not for U55 vs. 5FU55 but for the position of the Cy5 label.

In addition, curves resulting from competition of 35 nM labeled tRNAs with an ~100 fold excess (3.3 μM) of unlabeled U55-tRNA are given (Fig.4.4b, d, f, h). Addition of competitor tRNA (chase) results in primary thermophoresis curves similar to those of unbound tRNA over the whole range of protein concentrations, indicating reversibility of TruB binding for U55- as well as 5UF55-tRNA.

Although MST applies thermophoretic separation of bound and unbound components, the small temperature gradients applied keeps the separation from reaching a high degree, thereby preventing significant dissociation of the complex under investigation [140]. In consequence, dissociation constants resulting from MST are not only obtained in buffer conditions considered native but, in general, correspond well to those determined by real equilibrium methods [204, 205]. Additionally, MST allows a fast assessment of protein preparation homogeneity and

4.3 Microscale thermophoresis

reproduces K_d values within a factor of 2 over the course of months (Fig. A.8).

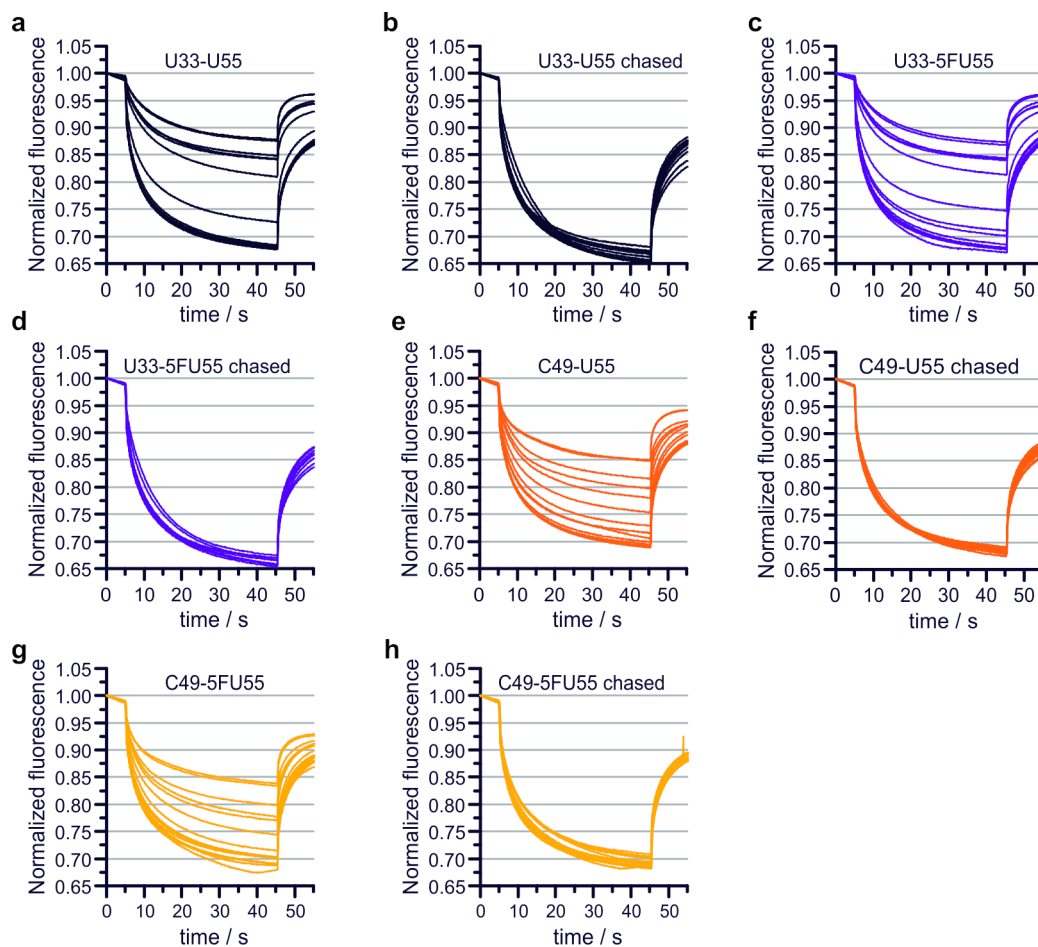


Figure 4.4.: Normalized MST curves for tRNA TruB interaction: Cy5-U33 **a-d**, Cy5-C49 **e-h** and subsequent measurements after addition of unlabeled U55-tRNA in excess (chase).

The above mentioned qualities render MST highly suitable to detect subtle differences in noncovalent interactions as, e.g., U55 vs. 5FU55. In agreement to the primary data (Fig.4.4), MST titrations of a given label (filled symbols in Fig.4.5) are remarkably similar for U55 and 5FU55 variants but differ for the label positions instead: U33 tRNAs (filled squares and circles in Fig.4.5) are bound with higher affinity than the C49 derivatives (filled triangles and diamonds).

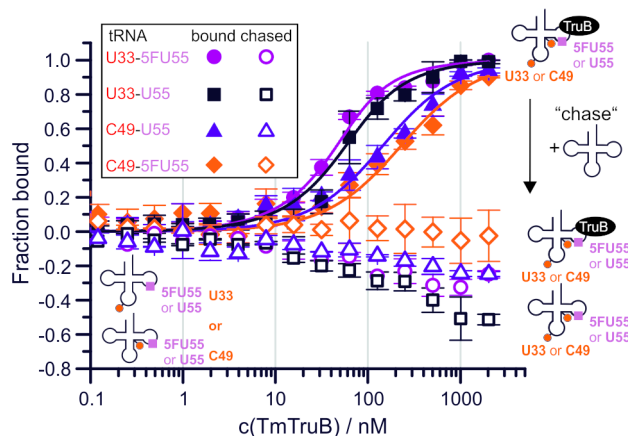


Figure 4.5.: MST titration curves resulting from the raw data of Fig.4.4: TruB binding (filled symbols) fitted to a 1:1 binding model (solid lines). Empty symbols represent the same samples after addition of tRNA^{Phe} in excess (chase). The error bars are standard deviations from triplicate measurements.

Analysis of chase experiments is equally consistent with the raw data (Fig.4.4): Over a wide range of TruB concentrations the signal returns to baseline level, while the signal falls even below the baseline for higher protein concentrations (open squares, circles, diamonds, and triangles in Fig.4.5). As this behavior is evident for U55 and 5FU55-tRNA, complexation is obviously equally reversible in both cases. This unexpected thermophoretic behavior of the chased complex motivated a more detailed analysis of corresponding MST curves. Thermophoresis in a temperature gradient ΔT causes exponential depletion of analyte (i.e. fluorescence signal) with an initial concentration c_0 to concentration c , where thermophoresis is balanced by Brownian diffusion :

$$\frac{c}{c_0} = \exp(-S_T \Delta T) \quad (4.1)$$

4.3 Microscale thermophoresis

with the Soret coefficient $S_T = \frac{D_T}{D}$ [141].

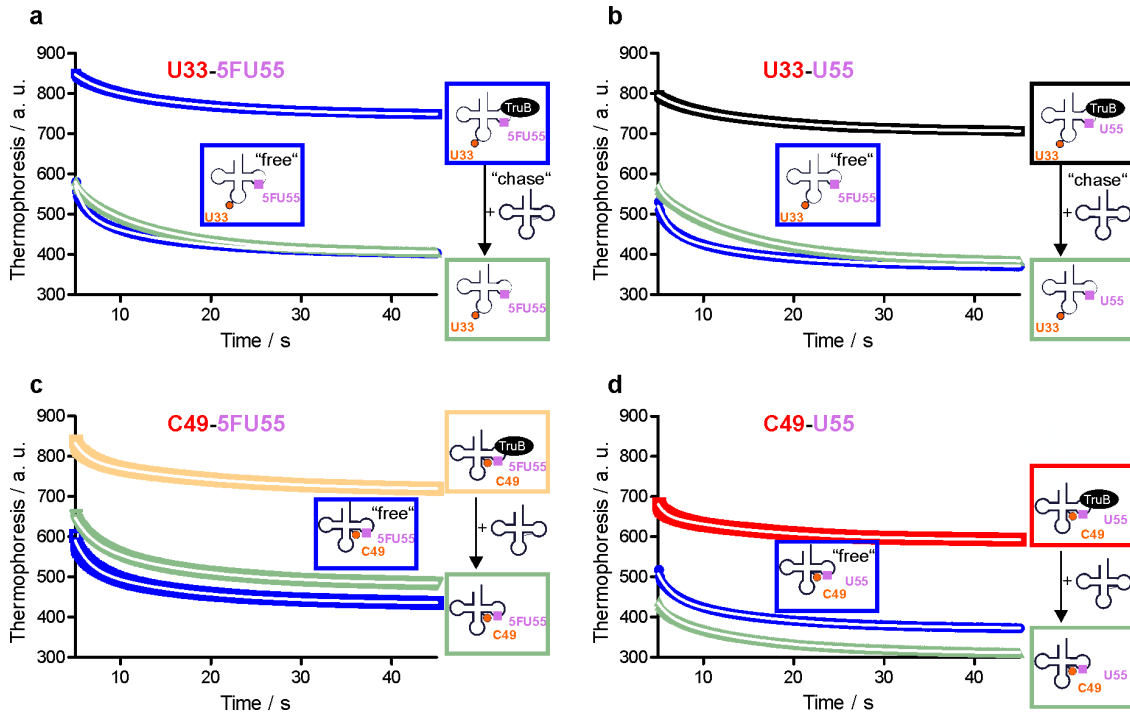


Figure 4.6.: Representative unnormalized MST curves fitted to a two phase exponential decay (white lines). For all constructs the curve with the highest protein concentration with and without competitor U55-tRNA and the protein free curve are shown. Color coding of the protein bound curve corresponds to Fig. 4.4.

An increased fluorescence intensity of the protein bound fraction (PIFE effect, see sec.3.1 and later) implies a decay with at least two phases, for bound and unbound tRNA, respectively. Indeed, unnormalized primary data is well described by a two phase exponential decay (see Fig.4.6). The following simple two phase decay was used for fitting:

$$y = A_1 * e^{-\frac{x}{t_1}} + A_2 * e^{-\frac{x}{t_2}} + y_0 \quad (4.2)$$

Fit parameters, shown in Tab.4.1 on the next page, are in part ambiguous (datasets depicted in red in Tab.4.1).

Table 4.1.: Comparison of thermophoretic properties of free, TruB bound and chased tRNA samples. Parameters were determined from fitting thermophoresis data (shown in Fig. 4.6) to a two phase decay (Eq. 4.2).

RNA state	U33-U55			U33-5FU55		
	free	bound	chased	free	bound	chased
y_0	367	704	381	400	745	402
A_{fast}	539	174	144	698	134	212
A_{slow}	108	111	144	123	107	216
k_{fast}	0.4368	0.4758	0.1	0.4696	0.3331	0.3665
k_{slow}	0.07737	0.08249	0.1	0.08325	0.07491	0.09462
k_{fast}/k_{slow}	~6	~6	1	~6	~5	~4

RNA state	C49-U55			C49-5FU55		
	free	bound	chased	free	bound	chased
y_0	369	590	308	431	713	480
A_{fast}	487	4134	272	539	101	431
A_{slow}	107	94	127	115	627	149
k_{fast}	0.4382	1.020	0.4169	0.4243	0.5578	0.3950
k_{slow}	0.08059	0.08501	0.08273	0.07461	0.06313	0.08036
k_{fast}/k_{slow}	5.437	12.00	5.039	5.687	8.835	4.915

The curves of all chased can indeed be assumed to represent labeled tRNA displaced from the complex, since

$$y_0(\text{free}) \sim y_0(\text{chased}) \neq y_0(\text{bound})$$

but the interpretation of the amplitudes of both components is less clear: For all U33 labeled samples the amplitudes A_{fast} and A_{slow} of the chased sample are, surprisingly, not similar to those of free tRNA but to those of TruB bound tRNA. The decay rates are similar for free, bound and chased U33 tRNAs and for bound and chased samples the respective differences between A_{fast} and A_{slow} are small or even non-existent in case of 'U33-U55 chased'. In contrast the fast component dominates for free tRNA with $A_{fast} \sim 5 - 6x A_{slow}$. Trends for C49 labeled samples are less clear.

However, a general increase in initial fluorescence intensity for the 'bound' sample is evident from Fig.4.6 and from y_0 values given in Tab.4.1. This indicates that protein binding does not only influence thermophoresis, but also the dye's spectroscopic properties.

In summary, it is not clear to which extent the deviation between 'free', 'bound' and 'chased' states stems from thermophoresis or from changes in spectroscopic properties. The implied influence of protein binding on spectroscopic properties, together with preliminary experiments implying spectroscopic shifts¹, motivated a more detailed spectroscopic characterization of tRNA-TruB interaction.

4.4. Spectroscopy of Cy5-tRNA TruB interaction

4.4.1. Spectroscopic change upon TruB binding

Full spectroscopic characterization of tRNA-TruB interaction for both label positions as U55 and 5FU55 variant, respectively, was obtained by quasi-simultaneous determination of time and polarization resolved fluorescence decays, as well as fluorescence excitation and emission spectra. Comparison of measurements in absence to measurements in the presence of an excess of enzyme, revealed all spectroscopic properties to be responsive to enzyme binding (Tab.4.2).

Table 4.2.: Changes in spectroscopic properties upon TruB binding. Shifts in the maximum of excitation $\Delta\lambda_{Ex}^{max}$ or emission $\Delta\lambda_{Em}^{max}$ spectra, fluorescence lifetimes τ_{F_1} and τ_{F_2} .

RNA	spectra		composition multi-fit		lifetimes	
	$\Delta\lambda_{Ex}^{max}$ / nm	$\Delta\lambda_{Em}^{max}$ / nm	A_1	A_2	τ_{F_1} / ns	τ_{F_2} / ns
U33-U55	0	0	0.86	0.14	1.12	2.41
+TruB	8.0	3.0	0.05	0.95		
U33-5FU55	0	0	0.86	0.14	1.16	2.41
+TruB	7.9	3.1	0.14	0.86		
C49-U55	0	0	0.74	0.26	1.12	2.26
+TruB	4.8	2.6	0.08	0.92		
C49-5FU55	0	0	0.69	0.31	1.13	2.23
+TruB	4.5	2.3	0.13	0.87		

Increasing protein concentration resulted in gradual increase of bathochromic shifts observable in excitation, as well as emission spectra (see Fig.4.7 and Fig.A.13), while the shift in excitation surpassed the shift in emission in all cases (Tab.4.2). Furthermore, an increase in protein concentration caused a change in polarization resolved fluorescence lifetimes with . For both label variants a bi-exponential, fast

¹Master Thesis Roman Teimer [168].

fluorescence decay was detected in absence of enzyme, that shifted to the slow decay regime in presence of enzyme (see Tab.4.2 and Fig.4.7). Surprisingly, the U33 label was more responsive in all spectroscopic properties than the C49-label (Tab.4.2). Rotational correlation times also increased with protein concentration and provided additional insight into the different environments of U33 and C49, as detailed in sec.A.2.7.

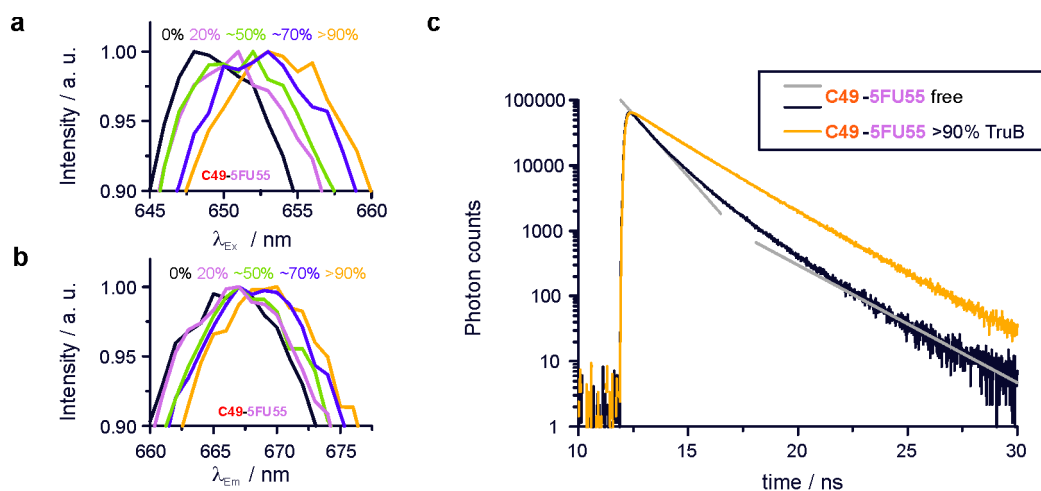


Figure 4.7.: Protein binding (~% binding is given) causes bathochromic shifts of excitation (a, $\lambda_{Em} = 668nm$) and emission spectra (b, $\lambda_{Em} = 647nm$). Fluorescence decay curves (c) differ in absence of TruB and with >90% TruB binding. Grey and black straight lines indicate bi-exponential fast decay (absence of TruB) and bi-exponential slow decay if >90% of tRNA is bound to TruB. Note that the decay curve for >90% TruB binding appears to decay mono-exponentially due to the log-scale of the y-axis!

4.4.2. Spectroscopic titrations

In search for a method to compliment MST, we turned to the above mentioned spectroscopic parameters: Titrating tRNA with protein while monitoring these parameters allowed a determination of dissociation constants. Lifetime and anisotropy were treated simultaneously in a global fit, resulting in a combined titration curve. All resulting 12 curves (three for each of the four constructs), could be fitted to a one-to-one binding model, as shown in Fig.4.8a-d.

For both U55 constructs the titration curves from all three parameters are remarkably similar (see Fig.4.8), while curve sets and therewith the K_d values of both 5FU constructs show variation among the different parameters. Affinity of

4.4 Spectroscopy of Cy5-tRNA TruB interaction

C49-5FU55 tRNA averaged over all three curves ($K_d^{C49-5FU55} = 124.2 \text{ nM}$) is only twofold higher, than the average of C49-U55 tRNA ($K_d^{C49-U55} = 225.8 \text{ nM}$).

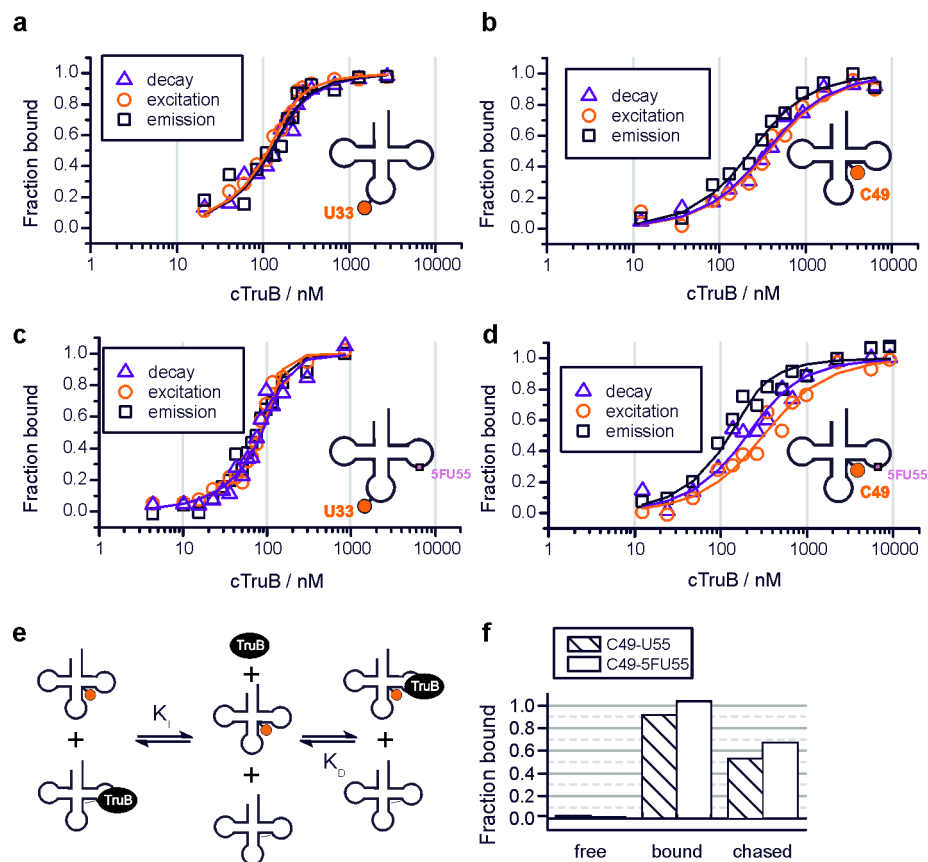


Figure 4.8.: Spectroscopic titration curves of TruB tRNA interaction (ctRNA = 200 nM) for U55 tRNAs a+b and 5FU tRNAs c+d, for all spectroscopic parameters with fits to a 1:1 binding model as solid line. e Schematic representation of the chase experiment. f Chase experiments for C49-tRNA TruB interaction: Averaged values of all spectroscopic parameters in absence of TruB (free), with >90% binding to TruB and after addition of 5.75 μM unlabeled RNA to the complex.

The highest difference between C49-5FU55 and C49-U55, a factor of four, results from comparing affinities determined by bathochromic emission shifts. Higher affinity of 5FU55 vs. U55 is more prominent for the U33 label with eight-fold on average ($K_d^{U33-5FU55} = 3.7 \text{ nM}$, $K_d^{U33-U55} = 30.7 \text{ nM}$) and 14-fold at max, if values from excitation shifts are compared. Indeed, this increased affinity conferred by 5FU55 could be related to our observation of SDS-stability of 5FU55-tRNA TruB complexes and a lower extent of denaturation on urea PAGE compared to U55-tRNA. However, the moderate difference in binding affinity of TruB for 5FU55- vs. U55-tRNA does not justify to interpret the above mentioned complexes as

representing a stable covalent intermediate for 5FU55-tRNA.

To rule out even a trace-amount of covalent 5FU55-complex, chase experiments were performed by adding unlabeled U55-tRNA to preformed complexes, as in the thermophoresis chase experiments (Fig.4.5). In the case of reversible complexation, an excess of unlabeled competitor was supposed to displace the labeled tRNA from a preformed complex (see Fig.4.8e). TruB binding > 95% was achieved by supplementing 200 nM tRNA with 5.23 μ M protein (see Fig.4.8f). Subsequent addition of unlabeled U55-tRNA as competitor in 37x excess over labeled tRNA (5.75 μ M), reduced binding to ~53% for C49-U55 tRNA and to ~67% for C49-5FU55 tRNA (Fig.4.8f).

Thus the single point chase experiment ends up in the error prone steep regime of the titration curves, which together with the absence of a K_d value for unlabeled U55-tRNA, precludes a more detailed analysis of these experiments. Still the chase experiments fit into the results reported above by leaving 14% more C49-5FU55 tRNA bound than C49-U55 tRNA, which is bound by TruB with lower affinity as assessed by the spectroscopic titration curves given in Fig.4.8.

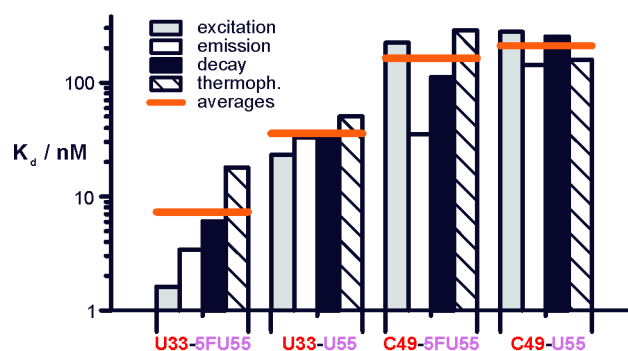


Figure 4.9.: Overview of determined K_d s for the tRNA TruB interaction, which results from a fit to an averaged triplicate measurement in case of thermophoresis. Red bars indicate arithmetic means over the different K_d values for each construct.

An overview on all affinities determined is shown in Fig.4.9, where red lines indicate averages for each construct that point out:

- Tighter binding of U33 vs. C49 tRNA, independent of U55 or 5FU55 variant
- Introduction of 5FU at the target site 55
 - causes a moderate increase in affinity for the C49 label
 - and more substantially so for the U33 label.

4.5. Discussion

4.5.1. Dye label interference with tRNA structure and with TruB turnover

Classical investigations of RNA recognition by proteins apply RNA mutagenesis and assess the effects of these substrate alterations on enzyme binding and turnover. In this concept of 'native' recognition introduction of artificial structures, as e.g. fluorescent dyes, is thought to alienate the interaction in an undesired way and is therefore widely shunned. In contrast to this general opinion, we were able to show that dye labeling can prove advantageous compared to traditional mutagenesis in several ways: By introducing a fluorescent label either outside or at the very edge of a known minimal substrate we tuned substrate quality, compared to the unlabeled substrate, from impaired to almost inactive, while leaving the enzyme recognition site intact.

An unexpected discovery was that a fluorescent label at U33, remote from the substrate site, almost completely abolished pseudouridylation. This low turnover is outstanding for two reasons: Firstly, TruB still binds U33 labeled tRNA with high affinity and secondly, the location of the U33 label is remote of the enzyme's TSL minimal substrate (blue in Fig.4.10a). Due to these two reasons the U33 label can neither sterically interfere with binding, nor is a distorted RNA structure at the binding site implied by the high affinity of the interaction. Instead, the U33 label appears to be in structural cross talk [202, 203] with the target site of TruB and this cross talk presumably interferes with a structural rearrangement of the RNA essential for catalytic turnover.

Fig.4.10a shows the structure of the yeast tRNA^{Phe} constructs applied in this work: Several tertiary interactions (dashed lines) and stacking interactions (curved arrows) stabilize the canonical L-shape of tRNA [36]. Judging from a cocrystal with its T stem loop minimal substrate ([76, 103], Fig.4.10b), TruB forms various interactions with RNA bases (red symbols in Fig.4.10b) that are usually engaged in tertiary interactions between T stem loop (blue in Fig.4.10a+b) and D stem loop (orange in Fig.4.10a) or that are at least shielded from TruB contact by the tertiary structure of tRNA. In consequence, at least a resolution of the interactions between the D arm and the T arm has to follow the initial tRNA binding by TruB.

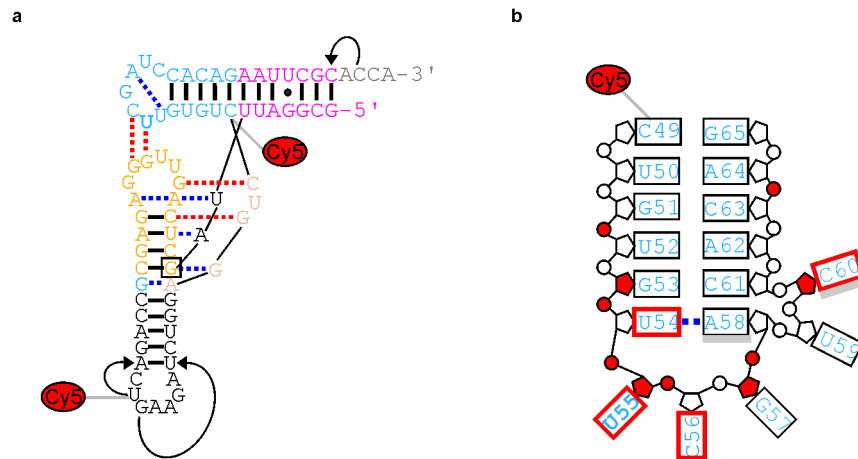


Figure 4.10.: Conformation and TruB interaction of yeast tRNA^{Phe}. **a** Tertiary interactions in tRNA^{Phe} forming the canonical L-shape [36]: Arrows represent stacking, dashed lines hydrogen bonds. TruB substrate positions U55 is represented in bold letters, interactions that are probably disrupted upon enzyme binding are depicted in red. **b** Interactions of TmTruB with the yeast tRNA^{Phe} T stem loop minimal substrate as deduced from the cocrystal structure [103]. Protein contacts at the phosphates, sugars or bases are indicated by red color, stacking of amino acids on RNA bases is indicated as grey bars.

From the present state of knowledge *E. coli* TruB action on full tRNA has to comprise of at least the following steps:

1. An initial binding event, which may already weakly affect base 57 [117].
2. An induced fit process which changes the enzymes structure compared to the RNA free conformation ([76] vs. [103]) and involves detachment of the T arm, a step that may explain the coincidence of tRNA hyperchromicity with TruB binding [201]. A hyperchromic shift in RNA absorption usually results from unstacking of nucleotide bases, caused by the resolution of helices [206]. Thus the hyperchromic shift could be caused by any larger conformational change in the tRNA substrate.
3. Flipping of the bases U55, C56 and G57 into the enzyme's active site [117]. This general feature of Ψ synthases [73] may be part of the previous step, as the rate is similar to the rate of the hyperchromicity event ([201] vs. [117]).
4. Catalysis, the by far slowest step [201].
5. Presumably a change in enzyme structure enabling product release (judging from structural differences of catalytically active vs. inactive enzymes

bound to 5FU-RNA, [76] vs. [207]).

6. There are indications that only turned over RNA is readily released from the enzyme [117]. Still TruB exhibits similar affinities for substrate and product RNAs [117, 201, 208].

Interference of the seemingly remote U33 label with catalytic turnover, but not with binding, implies that catalysis by TruB includes a change in tRNA structure that is by far more substantial than the suggested disruption of D-T-loop interactions. Unfortunately the available cocrystal structures cannot provide insight into the TruB-bound conformation of full tRNA, as they are restricted to TSL minimal substrates [76, 103–105]. Provided that the above stated results can be transferred to the TruB homolog of *Thermogota maritima*, the high affinity of U33 labeled tRNA may be directly related to its catalytic impairment: Failure of substrate turnover may drastically decrease the off-rate of the enzyme tRNA complex. How exactly the U33 label impairs catalysis, whether it interferes, e.g., with the above stated steps 2. or 3., cannot be deduced from present data.

4.5.2. Spectroscopic effects of protein binding

Striking features of the U33 label could be revealed by spectroscopic characterization of the tRNA-TruB interaction: All spectroscopic properties reacted stronger to TruB binding compared to the C49 label, most noteworthy being a ~8 nm bathochromic shift of the excitation maximum (see Tab.4.2). These distinct characteristics imply substantial differences in the TruB interaction with both label variants. The fluorescence of cyanine dyes interacting with proteins and/or nucleic acids is modified by a range of complex mechanisms, preventing allocation of the observed effects to specific causes [123] (see also sec.1.4.1 and sec.1.4.2).

Similar in effect to highly viscous solutions, cyanine dye protein interaction enhances fluorescence (PIFE, see sec.1.4.1) by disfavoring the dye's main non-radiative decay pathway, isomerization to a non-fluorescent cis form [120, 123, 124]. PIFE of the related cyanine Cy3 attached to nucleic acids peaks at 2-2.5 fold [125] at direct contact of protein and dye, while being insensitive for dye protein distances > 3 nm [127].

Our observation of a similar enhancement for Cy5 (see Tab.4.2) is remarkable, as the dye's lower cis-isomerization rate compared to Cy3 [123] was thought to significantly reduce the PIFE. Although the distance sensitivity of the PIFE for Cy5 is unknown, a sufficiently close proximity of TruB to the preferentially affected U33 label is not implied by the docking model (Fig.4.1).

If not related to protein proximity, fluorescence enhancement of the U33 label could be caused by interactions with the RNA it is attached to [123, 135, 136, 138]. Such interactions would be directly related to a substantial conformational change in the tRNA, which was already suggested in the previous section. Cocrytals of modification enzymes with whole tRNAs are quite rare, as is the knowledge concerning conformation of enzyme bound tRNAs. A particularly intriguing example is the so called lambda conformation found in tRNA bound to archaeosine transglycosylase (arcTGT) [155], an enzyme that may be mechanistically related to Ψ synthases, as is discussed later. As is evident from Fig.4.11, yeast tRNA could indeed adopt lambda conformation. Ishitani et al. even hypothesized that arcTGT and TruB could bind tRNA simultaneously [155].

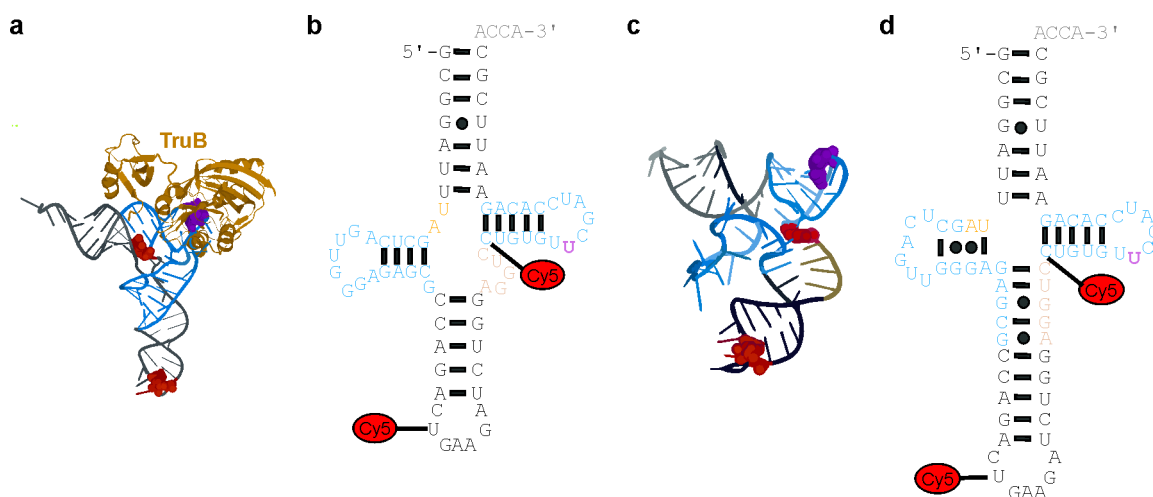


Figure 4.11.: Tertiary (a vs. c) and secondary (b vs. d) structure of yeast tRNA^{Phe} in canonical (a+b) or lambda conformation (c (from [155]) and d). Note that the variable loop, shown in yellow, hybridizes with the 3' part of the D stem loop in lambda conformation (d), thereby extending the anticodon helix (shown in red).

Far less is known concerning bathochromic shifts of excitation and emission in spectra of Cy5, caused by dye-protein interactions [123]. It is especially intriguing that shifts in excitation are larger than shifts in emission. In tendency and

magnitude the bathochromic shifts we observed are reminiscent of effects caused by solvents less polar than water [120], indicating changes of not only the dye's local viscosity but also its local polarity. Changes in all spectroscopic properties as they are conferred by TruB binding (see Tab.4.2) correspond well to effects reported for binding of biotinylated Cy5 to the protein streptavidin [120].

4.5.3. TruB interaction with 5FU55- vs. U55-tRNA

Although it remains to be elucidated how and why the U33- and the C49-label variants are differently affected by TruB binding, both fluorescent labels are superior to mutagenesis: They allow determination of K_d values from multiple parameters in parallel by using different fluorescence based approaches. So far only single parameters were applied, either routinely, as for fluorescence anisotropy [154, 209–211] or rarely fluorescence lifetime or intensity increase [212, 213]. However, to our knowledge, bathochromic shifts were not yet reported as a readout of titration curves and especially the combined application of all four spectroscopic parameters has not been reported until now [211–216].

From Fig.4.9 it is evident that K_d values deviate by a factor of 11 at most (U33-5FU55), while others diverge only by a factor of 2-4x. Comparison of different methods to assess a given RNA-protein interaction easily results in deviations of factor 2-4x, which corresponds to a widely accepted error range [117, 201]. Thus all measurements summarized in Fig.4.9 agree with an only moderately stronger affinity of TruB for 5FU55-tRNA than for U55 substrates.

Enzymatic turnover within one hour varies between the three U55-tRNAs, which is in strong contrast to ~40% SDS stable complex formation within minutes for all three 5FU55-tRNAs (Fig.4.3). Detection of 5FU55-specific complex bands on SDS gels within seconds (Fig.4.3) is absolutely incompatible with the previous interpretation of these bands as a covalent catalytic suicide adduct of 5FU [104], especially since TruB is a slow enzyme [201]. This holds even more true for the U33-5FU55 complex band: A tRNA construct that is basically catalytically inactive as U33-U55 tRNA variant (Fig.4.3a) cannot form substantial amount of catalytic suicide adduct within seconds as 5FU55 variant. Moreover the 5FU55-specific complex proved unstable on urea PAGE (see Fig. A.9, Fig. A.10) and 5FU55-tRNA could successfully be chased from the complex in MST (Fig.4.4, Fig.4.5) and fluorescence experiments (Fig.4.8). However, formation of a covalent suicide adduct

should be irreversible and the said adduct should be resistant to urea. Thus all present results are consistent with a denaturant resistant non covalent interaction of 5FU55-tRNA and TruB.

4.5.4. Comparison with other cases of 5FU inhibition

Covalent suicide adducts of 5-fluoropyrimidines (5FY) have been characterized for several reaction mechanisms all involving methyl group transfer [85, 87, 90, 91, 196]. All mechanisms resemble Ψ formation by involving a nucleophilic attack on the respective 5-fluoropyrimidine, although it is still debated whether Ψ synthases attack the base [113] or the ribose [112] at their target site. In contrast to Ψ synthases, however, all enzymes require a cofactor (either folate/FAD or SAM) and apply a cysteine residue as nucleophile [23, 90, 217, 218], not an aspartate, the residue essential in Ψ formation [73, 102].

Fig. 4.12 compares the knowledge regarding the unambiguously proven covalent complex in the mechanisms of m^5U methyl transferases (Fig. 4.12a) with a suspected similar complex for Ψ synthases (Fig. 4.12b) which should result from a Michael addition of the catalytic Asp to the target uridine [113] (for a full mechanism see introduction). The covalent intermediate **1b** was proposed as late intermediate in the reaction, thereby being analogous to **1a**. However, it is neither clear that the aspartate essential in Ψ formation [73, 102] really acts in a Michael addition, nor was a catalytically essential base identified. Furthermore the Michael addition mechanism [113] and the proposed alternative mechanism for Ψ formation [112] both include compound **3b**, which is not covalently attached to the enzyme, as the last reaction step. In consequence, 5FU would not form a covalent RNA enzyme suicide complex but would be converted into the usually observed hydroxylated product **4b** [76, 103–105, 110, 113] or, for the single report, into a covalent RNA-enzyme complex linked *via* a tyrosine [113].

That the covalent intermediate **1b** could not be observed in cocrystals of enzyme and RNA, was attributed to slow hydrolysis of the covalent adduct or to its destruction by X-rays during measurement [106], presumably resulting in detection of compound **4b**. The recently reported adduct of synthase RluB and compound **4b** is fortuitous, as the tyrosine connecting RNA and enzyme is non-essential for catalysis [105], and not present in the TruD family of Ψ synthases [73]. Therefore the adduct cannot represent a general result of Ψ synthase action on 5FU-RNA.

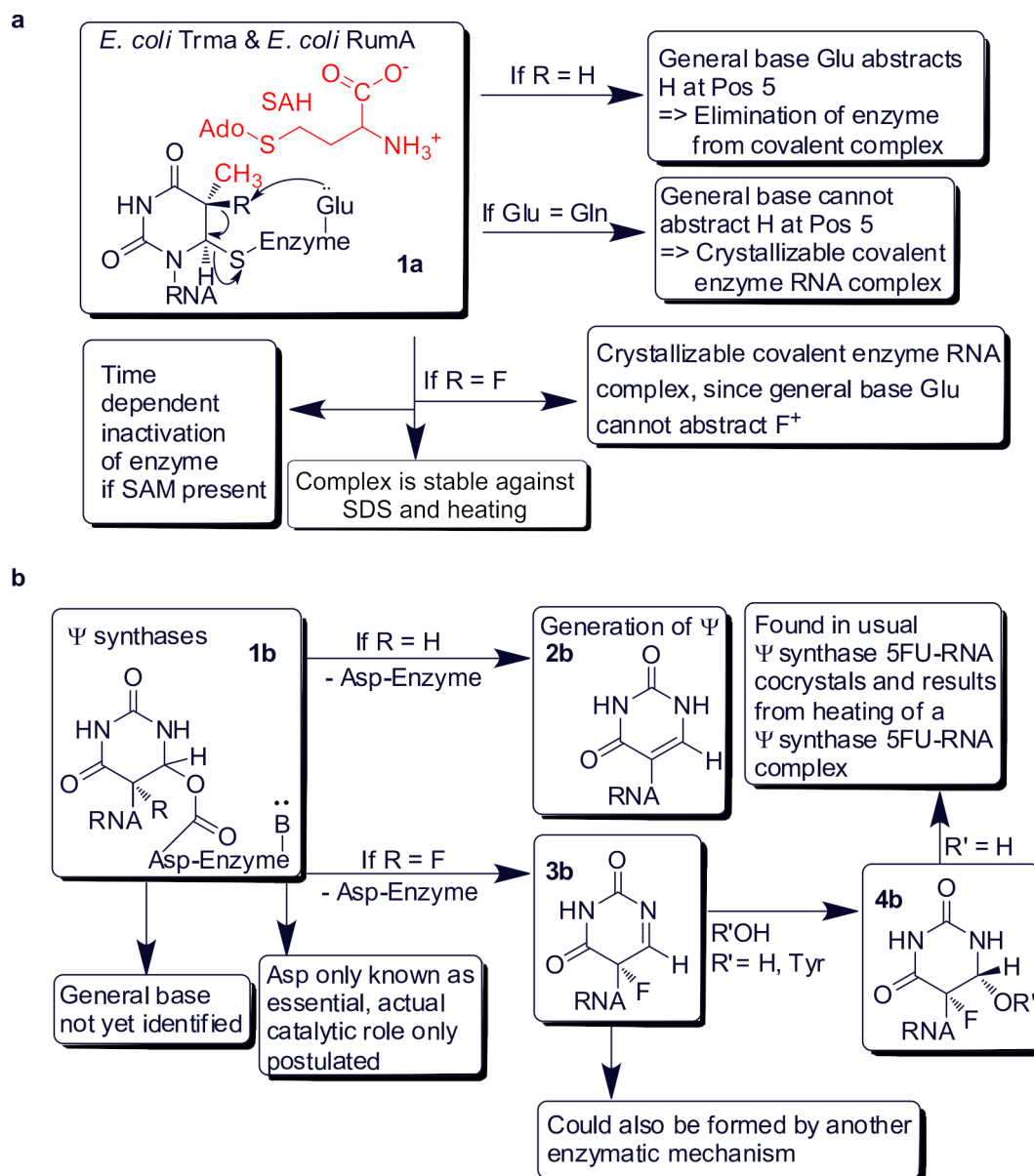


Figure 4.12.: Comparison of 5FU action in m^5U methyl transfer (**a**) and a proposed similar action in Ψ synthesis (**b**). **a** The catalytic thiol of the enzyme attacks U, allowing methyl-group transfer from SAM, thereby generating SAH. Information of 5FU action on m^5U methyl transferases is from [85], RNA cocrystals are from [81] and [82]. **b** Consequences of the proposed Michael addition for Ψ formation [113]. Usual cocrystals contain hydroxylated 4b [76, 103–105, 110, 113], while recently a covalent RNA enzyme complex was reported, containing 4b linked via a tyrosine residue [113].

In line with the differences of Fig. 4.12a vs. b, adducts with methyl group transferring enzymes are generally more stable against denaturation, be it by urea [87, 88] or by heating [86, 87, 90, 91, 218–222]. Furthermore, cocrystal structures of several

covalently trapped intermediates were reported [23, 80, 81, 89, 223, 224]. Cytosine methyltransferases were even reported to form (transient) covalent adducts with non-fluorinated substrates [225, 226]. If the 5FU55-specific complex, observed on SDS gels in the course of this work, is not covalent, as all evidence implies, the mechanism conferring SDS resistance to the complex remains open to debate. Although the mechanism cannot be elucidated to date, it is clear that SDS and fluorine substitution are both involved, as the complex forms only with 5FU55-tRNA (Fig.4.2) and is only stable against SDS denaturation, not against other denaturants (Fig.A.9). Following a comparison of Ψ synthases with other transglycosylation enzymes, effects of SDS (sec.4.5.6) and fluorine (sec.4.5.7) will be discussed.

4.5.5. Comparison with tRNA-guanine transglycosylases

As is apparent from the previous section, Ψ formation differs from other enzymatic mechanism that are inhibited by 5FU: The reaction involves cleavage of the glycosidic bond, applying an aspartate (carboxylate) instead of a cysteine (thiol) as nucleophile Fig.4.12. The enzyme class of tRNA-guanine-transglycosylases (TGTs) utilize an aspartate to catalyze the exchange of guanine against another, hypermodified base in a given RNA sequence [227]. Regarding these intriguing similarities, the mechanism of Ψ formation might be similar to the one of TGTs.

Key steps of bacterial TGT catalysis are shown in Fig.4.13a: Nucleophilic attack of the aspartate on the C1' of the ribose (**1a**) facilitates glycosidic bond cleavage and generates a covalent intermediate of enzyme and RNA [228] (**1b**). In the final step of the reaction the enzyme is released by nucleophilic attack of the hypermodified base 7-aminomethyl-7-deazaguanine (PreQ1), forming **1c**. Addition of an excess of the unreactive 9-deaza-guanine instead of PreQ1 stalled the reaction and enabled crystallization of the trapped covalent intermediate **1d** [229]. Obviously Ψ formation is a transglycosylation reaction, although the base is not exchanged following glycosidic bond cleavage but rather reattached in a different way. In addition to this formal aspect, catalysis by an aspartate implies mechanistic similarities to TGTs. Considerable support for a nucleophilic attack on the C1' of the ribose, as shown in Fig.4.13b, was provided by the work of Miracco and Mueller [112], who were able to prove formation of a minor arabino product in *E. coli* TruB catalysis on 5FU tRNA (compound **2d** in Fig.4.13b).

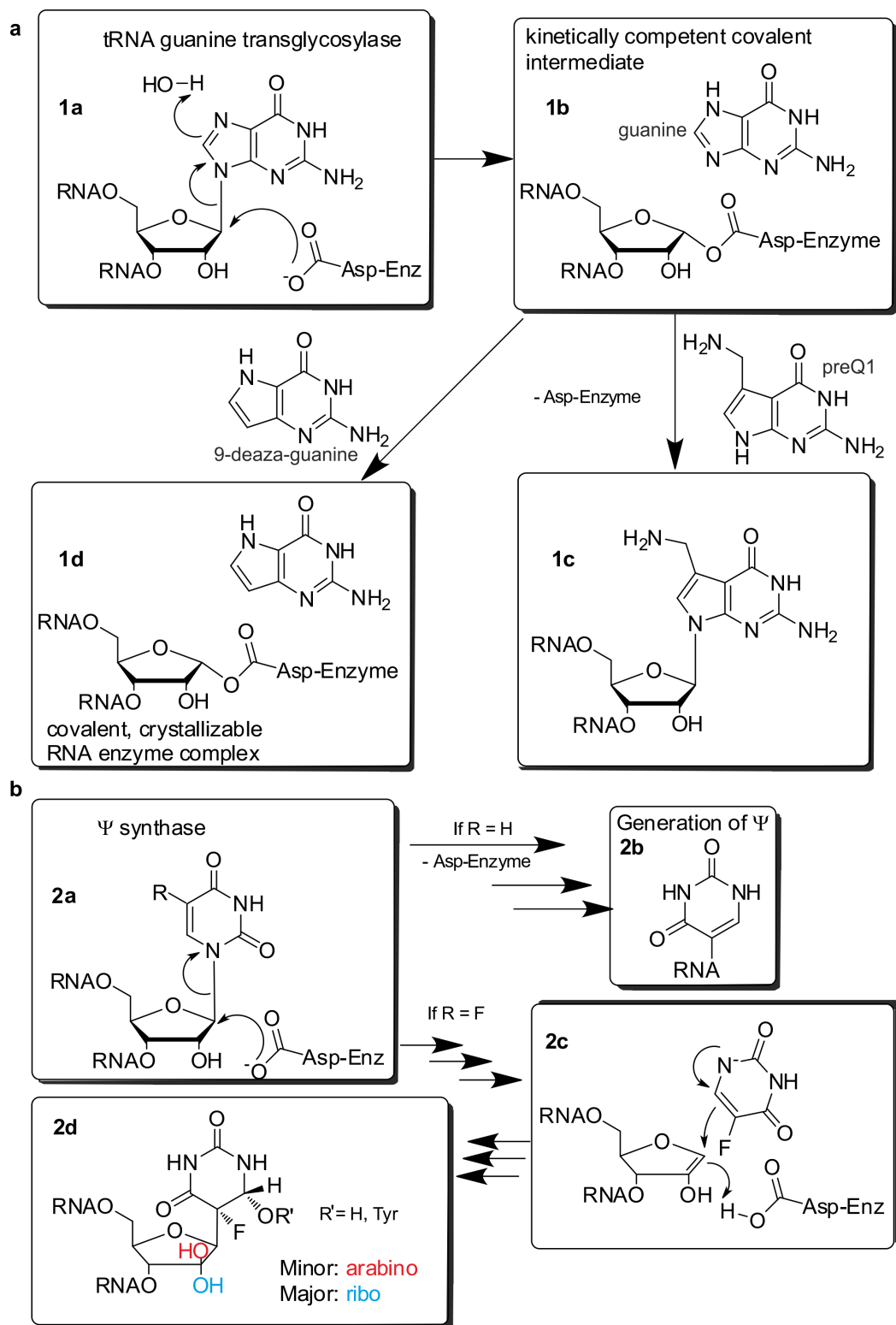


Figure 4.13.: Comparison of tRNA-guanine transglycosylase mechanism [227–229] (**a**) with the glycol mechanism of Ψ formation (**b**, [112]). Note that at least TruB action on 5FU-RNA results in 75% of ribo product and 25% of arabino product (**2d** [112]).

So far, neither biochemical characterizations of other enzymes did evaluate arabinoside formation, nor did any publications on cocrystal structures mention arabinoside/ribose mixtures [76, 103–105]. Partial disorder in a cocrystal of 5FU-RNA Ψ synthase RluA might have been wrongly attributed to only partial occurrence of the long-sought covalent complex [106]: A ribo/arabino-mixture as caused for disorder was not considered at that time, as no previous evidence implied such a mixture.

4.5.6. Effect of SDS on proteins

Protein denaturation by SDS is a complex process, that for micellar levels of SDS, as they are present in the SDS loading dye applied in this work, is thought to be based exclusively on hydrophobic interactions [230]. It is widely accepted that SDS denatures the large majority of proteins and non covalent protein-substrate complexes already at room temperature. Following this reasoning, a Ψ synthase 5FU-tRNA complex surviving such conditions is expected to be covalent in nature [100, 101, 104, 106–110]. That this work showed differential effects of SDS and urea PAGE/formamide on 5FU55-tRNA-TruB complexes (see Fig. 4.2, Fig. 4.3, Fig. A.12 vs. Fig. A.9, Fig. A.10), clearly contradicts a covalent interaction of TruB and 5FU55-tRNA. Rather, these results indicate differences in the interaction of both denaturants with a non-covalent 5FU55-tRNA TruB complex, thereby matching to different protein unfolding pathways caused by charged surfactants (SDS) vs. chemical denaturants (urea/formamide) [231].

To this date only a single attempt to obtain direct proof (using circular dichroism spectroscopy) that the protein in a SDS-stable Ψ synthase 5FU-tRNA complex is indeed denatured was reported and gave ambiguous results [106]. Admittedly, to proof protein denaturation in the case at hand is challenging: Many methods, as e.g. IR or differential scanning calorimetry are unsuitable due to high material consumption and circular dichroism spectroscopy is non-trivial in execution (*vide supra*). Monitoring tryptophan fluorescence [231] is spoiled by its direct dependence on the structural context [232]: *T. maritima* TruB contains four residues in very different structural surroundings, which are expected to complicate interpretation of the protein's denaturation state based on such experiments.

We conclude that, although heating in SDS buffer did not change the migration behavior of TruB (Fig. 4.3), there is, to date no direct proof that incubation in SDS

at 25 °C and 95 °C both result in total protein denaturation and thus prevent any non-covalent interaction with 5FU55-tRNA. The observed bands in SDS-PAGE indeed correspond to a 5FU55-tRNA-protein complex resistant to SDS, but the presented experimental evidence consistently disproves a covalent nature of this complex, since the complex is reversible (Fig.4.5, Fig.4.8) and not stable in urea (Fig.A.9, Fig.A.10). What mechanism exactly confers the remarkable stability to the complex remains to be investigated. As covalent attachment can be ruled out, the conserved fold of Ψ synthases [73] might be responsible, since formation of SDS-stable complexes with 5FU-tRNA could be demonstrated for members of many different Ψ synthase families [100, 101, 104, 106–110] At present pure β sheet proteins serve as model for SDS stability [233], but also stable protein-protein complexes [234–238] and even catalytic activity [239, 240] have been observed in the presence of SDS .

4.5.7. Possible effects of fluorine on TruB binding

To date 25% of all small molecule drugs acting on proteins contain at least one fluorine atom [241], although fluorine-protein interactions are yet ill understood [242]. Possible effects are manifold: Fluorine changes chemical reactivity and ligand properties by electronegativity, size, an ill understood omniphobicity/lipophilicity and by electrostatic interactions [241]. In consequence fluorine has two main points of action: Modulation of basicity/acidity and introduction of electrostatic attractive/repulsive interactions. The overall impact of fluorine substitution on protein binding is difficult to predict [241] and can even result in equal binding affinities of drugs differing in fluorination pattern, achieved by very different but compensating enthalpic and entropic contributions [243].

In the case at hand, yet undefined properties of 5FU55 affect tRNA-TruB interaction already at the initial binding event and confer SDS resistance to the complex formed. Unfortunately, this event is not covered by available cocrystal structures that reflect either conformation post turnover, containing a rearranged and hydrated 5FU [76, 103–105] (Fig.4.14a), or binding of a catalytically inactive D48N mutant [207] (Fig.4.14b). Significantly different active site conformations in the two crystals result in different RNA protein interactions, emphasizing the lack of knowledge on pre-turnover interactions in a catalytically active TruB-5FU55-tRNA complex.

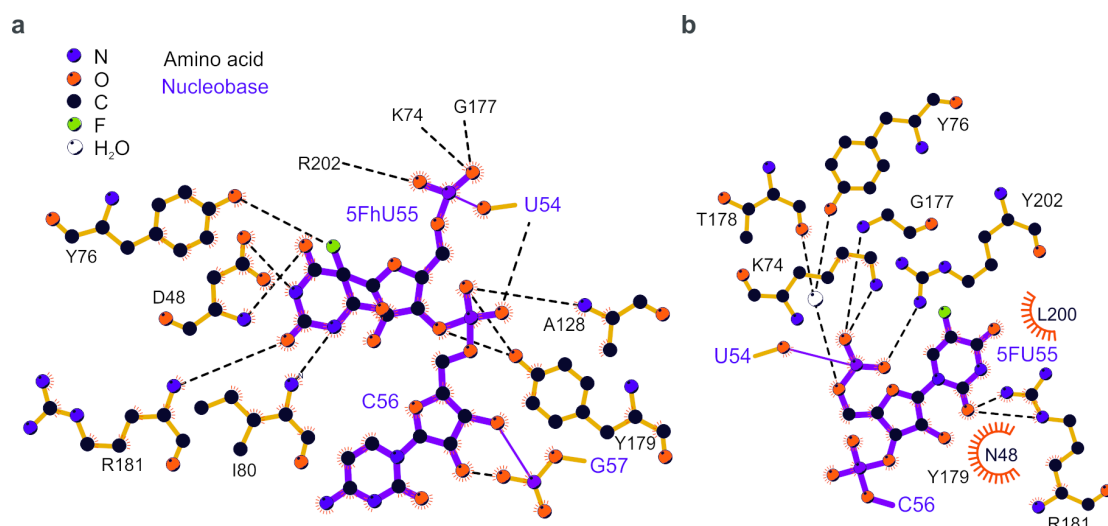


Figure 4.14.: Crystal structures showing structural differences and different protein-RNA interactions in the active site of the wild type (**a**) and a catalytically inactive D48N mutant (**b**) of *E. coli* TruB bound to 5FU RNA. Water cyan, red eyelashes indicate possible hydrophobic interactions and dashed lines possible hydrogen bonds. Structures are from PDB files 1K8W [76] and 1ZL3 [207] respectively, 2D projections were generated using LigPlotPLUS [53].

As in a recent crystal structure of a fluorinated small molecule drug bound to a protein [244], the fluorine in the post-turnover tRNA-TruB complex (green in Fig.4.14a) is in proximity to the hydroxyl group of a tyrosine (Y76), implying hydrogen bonding. However, even for the small molecule case, the nature of a possible fluorine-tyrosine interaction is not clear at present [244].

Although the specific nature of the 5FU55-TruB interaction remains unclear, it can be concluded, that the 5FU55-tRNA TruB complex investigated is SDS resistant due to the presence of 5FU at position 55. Obviously, this resistance originates from more complex effects than a mere increase in affinity: U33-U55-tRNA is bound with higher affinity than C49-5FU55-tRNA, but only the latter complex proved SDS resistant. The lack of evidence for covalent, irreversible inhibition of TruB, 5FU-tRNAs may act as general competitive inhibitors for Ψ synthases. This hypothesis is supported by failure of Pus1 to convert 5FU on a biochemically relevant time scale [179], and by rapid 5FU turnover TruB from *E. coli* [108, 110].

4.6. Conclusion

A complementary set of experiments could demonstrate that the mysterious SDS stable gel band [104], so far taken as clear evidence for a covalent catalytic suicide adduct of Ψ synthase TruB with 5FU-RNA, does neither represent a covalent interaction, nor is the band related to catalysis. In the contrary any relation of SDS-resistance to catalysis is negated by:

- K_d measurements failed to detect a difference in affinity of U55- vs. 5FU55-tRNA large enough to account for a covalent interaction,
- chase experiments unambiguously disproving a covalent interaction by showing reversibility
- and the yields of SDS-resistant 5FU-tRNA-TruB complex not corresponding to yields of catalytic turnover.

These results affect numerous biochemical and biophysical studies where 5FU was applied as an alleged suicide inhibitor in RNA-Pus complexes [98, 101, 103, 104, 106]. The above listed results of the present study do fit into the picture formed by other studies, indicating inhibition of Ψ synthases by 5FU to be weaker in nature than inhibition by the unambiguously proven suicide adducts of 5-fluoropyrimidines and methyltransferring enzymes. In contrast, evidence substantiates that in the case of Ψ synthases, 5FU may share the fate of a potent DNA methyltransferase inhibitor: Inhibition by zebularine was long suspected to be covalent, but proved to be caused by stable, non-covalent binding of DNA methyltransferases to zebularine containing DNA. This strong interaction efficiently removed the enzyme from solution, thereby preventing any catalytic turnover at other, non-zebularine containing substrate sites [245].

The above stated conclusions could only be obtained by a novel and particularly informative approach to RNA-protein interactions consisting of two main phases: (1) Fluorescent dyes instead of classical mutagenesis allowed generation of constructs with variegated turnover efficiency and (2) a full spectroscopic characterization of the RNA-protein interactions, especially by monitoring bathochromic shifts and microscale thermophoresis.

5. Single molecule FRET on tRNAs

5.1. Tolerance of dye positions in ribosome smFRET

5.1.1. Introduction

Frequently, smFRET experiments in biological context are suspected to be spoiled by artifacts: Dye labeling of biological macromolecules is thought to introduce a bias into the biological processes investigated. Investigations of translation, reviewed by Puglisi et al. [246–248], require undoubtedly the most complex smFRET assays: Already the eubacterial ribosome consists of more than 50 individual proteins and RNA strands that sum up to more than 150000 atoms. Furthermore a dye labeled tRNA has to undergo a sequence of (1) aminoacylation, (2) ternary complex formation with EF-Tu protein binding to the acceptor stem and (3) binding of tRNA to the small ribosomal subunit at the anticodon, while the acceptor stem remains bound to EF-Tu, generating the A/T-state [249].

The most frequently used dye labeling procedures target isolated native, fully modified unaminoacylated tRNAs at naturally occurring nucleotide modifications: s^4U8 [250–253], acp^3U47 [250, 251, 253, 254] or D16 and/or D17 [255, 256], all located in the so-called elbow region of tRNA (Fig.5.1A). To assess the performance of artificial tRNA constructs in ribosome FRET, three singly labeled, unmodified yeast tRNA^{Phe} constructs were generated by splinted ligation: A Cy3 variant labeled at C5 of U17, comparable in position to the established D17 label at N4, but differing in linker length, a Cy5 variant labeled by the same strategy at U33 and a variant labeled with Cy5 *via* a 2'-Aminogroup at C49, in contrast to base-labeling in native tRNAs at acp^3U47 (Fig.5.1).

All generated tRNAs, originating from the eukaryote yeast, were subjected to preliminary ribosomal smFRET assays in which all other components originated from the eubacterium *Escherichia coli*. These assays require aminoacylation and

EF-Tu(GTP) ternary complex formation¹. The corresponding donor (Cy3) or acceptor dye (Cy5) was attached to the L11 stalk protein located in the large ribosomal subunit [257].

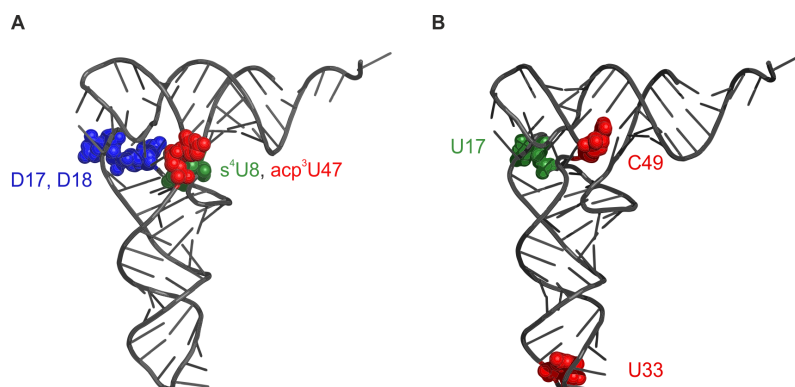


Figure 5.1.: Crystal structure of yeast tRNA^{Phe} with **A** the four dye labeling positions most frequently used in ribosome smFRET experiments and **B** dye labeling positions used in the present study (U17 green for Cy3, U33 and C49 red for Cy5, structure from PDB ID 1EHZ).

5.1.2. Aminoacylation and EF-Tu complexation

Aminoacylation to Phe-tRNA^{Phe} by *E. coli* PheRS proceeded in yields of only 28% and 26% for the constructs labeled at U17 and C49, respectively. In contrast, the U33 label variant was aminoacylated quite well with 60% yield, although the main recognition elements of *E. coli* PheRS, G34, A35 and A36, are in close proximity [258]: By interfering with these contacts, U33 should be the most detrimental label position. The preliminary data at hand does not allow further interpretation of the results. In agreement with a cocrystal, complexation of the aminoacylated tRNAs with EF-Tu of *E. coli* did proceed in good yield [259].

5.1.3. tRNA-Ribosome FRET

Finally, the ternary Phe-tRNA^{Phe}-EF-Tu(GTP) complexes were subjected to preliminary smFRET experiments with ribosomes labeled at the L11 stalk, as in the work of Chen et al. [257]. Proximity of the tRNA to the ribosomal L11 stalk

¹All experiments except construct generation are unpublished results of the group of Prof. Barry Cooperman, University of Pennsylvania, Philadelphia, USA.

5.1 Tolerance of dye positions in ribosome smFRET

protein is required for a FRET signal. In consequence, comparison of the relative abundance of FRET events allows a crude, qualitative assessment of the ribosome's affinity to the respective tRNA. FRET events of the respective constructs were counted and normalized to the event count of D16/D17 labeled tRNAs as reference (Tab.5.1). The C49 label was best tolerated by the ribosome, followed by the U33 label, while the U17 label was, surprisingly, not well tolerated, although being identical in label position to the reference.

Table 5.1.: Preliminary results of smFRET ribosome assays^a of three different singly labeled yeast tRNA^{Phe} constructs compared to Cy3 or Cy5 labels at D16/17 .

Label	% FRET ^b	High E _{FRET}	Low E _{FRET}	Distance to L11 stalk / nm ^c
Cy3@D16/17	100	0.57	0.32	4/3.3
Cy3@U17	9.4	n. d.	n. d.	4
Cy5@D16/17	100	0.61	0.34	4/3.3
Cy5@U33	18.8	0.45	-	6
Cy5@C49	33.8	0.56	-	3.6

^a All experiments were conducted by the Lab of Prof. Barry Cooperman [257].

^b Percentage of FRET events with the L11 stalk, normalized to D16/D17 labeled tRNA.

^c Distance in classical state, determined from crystal structure of Yusupov et al. [260].

A dynamic distribution between two FRET states, as it was reported for D16/D17 labeled tRNAs [257], could not be observed for the other label variants (Tab.5.1). However, transfer efficiencies for labels U33 and C49 reflected the relative distance to the L11 stalk label in being lower than or similar to the D16/17 label, respectively. The FRET efficiency of the U17 label was not determined due to the scarcity of events.

The EF-Tu(GTP)-tRNA^{Phe} ternary complex first contacts the ribosomal A site in the so-called A/T state [249] (Fig.5.2). A tRNA (black) occupies the A site of the small subunit, while still binding to EF-Tu (blue) [261]. Fig.5.2 shows that interactions of the small ribosomal subunit with A site tRNA do concentrate on the anticodon stem loop, involving mRNA (orange) and the ribosomal decoding center [249]. Considering, that it is located just one base 5' of multiple interactions between ribosome and the tRNA anticodon, the U33 label is surprisingly well tolerated. In contrast, neither the U17 label, nor the C49 label are well tolerated, although only the former could contact the ribosome (at H89 of the large ribosomal subunit) [249].

In summary, fluorescent labeling of tRNAs is tolerated unexpectedly well in all

steps required for ribosome-tRNA smFRET experiments. Presumably due to the long linker, the U17 label is inferior in performance to the D17 label at the same position. The U33 label shows the greatest potential, especially to monitor tRNA mRNA interactions, although being located in the heat spot of ribosome-tRNA interaction.

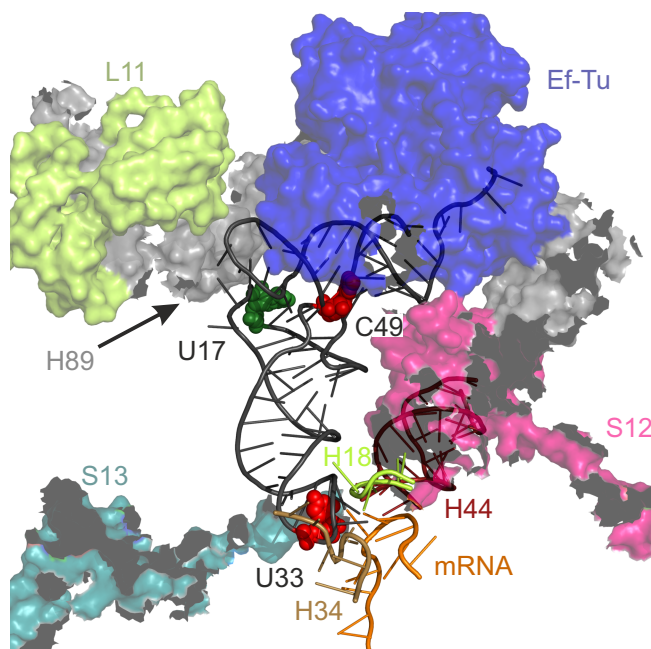


Figure 5.2.: Arrival of an EF-Tu(GTP)-tRNA ternary complex at the A site of the ribosome (detail of a crystal structure from *T. thermophilus*, PDB IDs 2WRN and 2WRO). Gray surface rRNA of the large subunit, colored surfaces represent protein components. Dye labeling positions in black tRNA are depicted by colored spheres (U33 and C49 red, U17 green). E and P site tRNAs are omitted for clarity.

5.2. SmFRET reveals two conformations of hmt tRNA^{Leu(CUN)}

5.2.1. Construct design and idea

Previous smFRET experiments on freely diffusing human mitochondrial tRNA^{Lys} revealed three different conformations the abundance of which were dependent in ionic strength and tRNA modification level [46, 158, 262, 263]. For a similar construct of human mitochondrial (hmt) tRNA^{Leu(CUN)} [179] no such confor-

mational equilibrium could be observed [264]. To verify these observations, a tRNA^{Leu(CUN)} construct carrying Cy3 at U3, 5FU27 and Cy5 at U31 was extended with a non-canonical biotinylated 3'-tail (see Fig.5.3) by splinted ligation. The potential structural impact of this extension was minimized by using an RNA strand derived from anti-eGFP siRNA [265], which lacks any sequence complementarity with the tRNA.

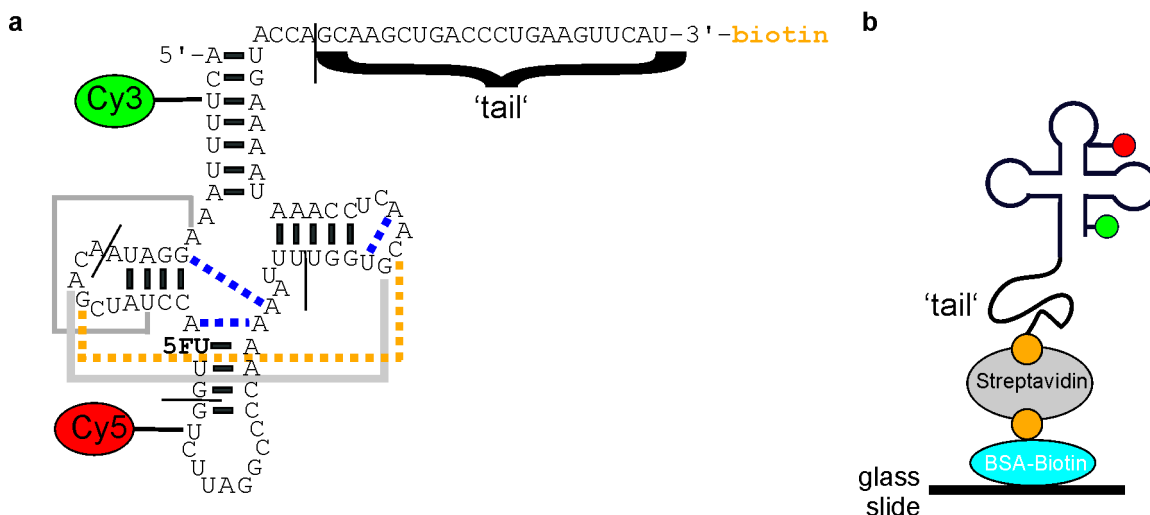


Figure 5.3.: Construct design and immobilization procedure for smFRET. **a** Sequence of the investigated human mitochondrial tRNA^{Leu(CUN)} construct. Labeling sites of Cy3, Cy5 and biotin are indicated. **b** Cartoon illustrating the BSA-Biotin-Streptavidin-Biotin immobilization scheme for single molecule FRET experiments.

5.2.2. At 2 mM Mg²⁺ hmt tRNA^{Leu(CUN)} is in a dynamic extended conformation

FRET dynamics of tRNA were investigated at a moderate Mg²⁺ concentration of 2 mM, as previous experiments at 10 mM Mg²⁺ showed predomination of stable high FRET states [264]. At 2 mM Mg²⁺, however, FRET efficiencies form a clear two state distribution: A low $E_{FRET} \sim 0.2$ predominated, while rare and short transitions to higher $E_{FRET} \sim 0.6$ could be observed. A FRET efficiency histogram generated from 20 single tRNA molecules is depicted in Fig.5.4.

Analysis with the tool "HAMMY" [266], yielded the following transition rates

$$k_{low \rightarrow high} = 0.27s^{-1} \text{ and } k_{high \rightarrow low} = 2.3s^{-1}.$$

which are comparable to rates independently determined by G. Hinze:

$$k_{low \rightarrow high} = 0.43s^{-1} \text{ and } k_{high \rightarrow low} = 3.4s^{-1}.$$

Reported RNA folding rates from smFRET experiments lie in a similar range, as, e.g., riboswitch aptamer domains in absence of their cognate ligand [56, 57, 60, 267, 268], artificial [269, 270] and native ribozymes [271, 272] or the pseudoknot domain of human Telomerase RNA [273].

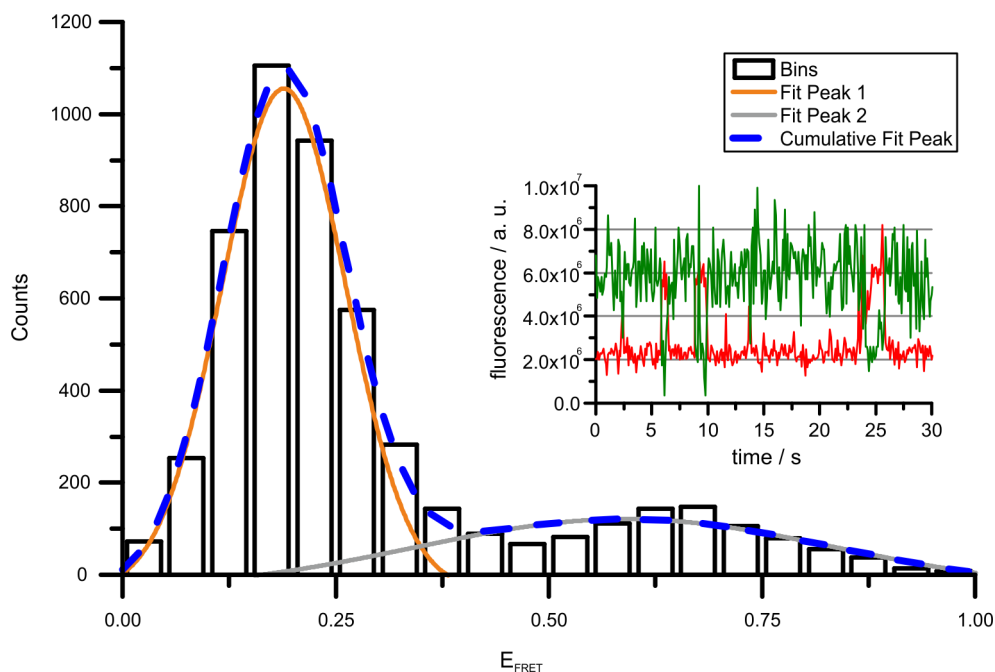


Figure 5.4.: Single molecule FRET efficiency histogram of human mitochondrial tRNA^{Leu(CUN)} at 2 mM Mg²⁺. The histogram was constructed from 20 individual molecules and fitted to a dual gaussian. Each count represents one time point of data recorded in 100 ms intervals. The inset shows a typical single molecule trace of donor and acceptor fluorescence: The low FRET state predominates and only rarely and for short intervals acceptor fluorescence increases while donor fluorescence decreases, resulting in high E_{FRET} .

If the predominating low FRET state was to be attributed to an unknown extended tRNA conformation, one should note that tertiary interactions in hmt tRNA^{Leu(CUN)} comprise only some of the interactions present in canonical tRNAs [43] (see Fig.5.5 a+b). An interesting feature of this tRNA, called 'T slip', was proposed by Rui Hao et al. based on structural probing experiments [274]. In this conformational change U48, marked with a rose circle in Fig.5.5 slips into the T stem [274]. This event results in a 1 bp larger T loop, changing the secondary structures to those depicted in Fig.5.5c+d. Further structural probing experiments on mutants indicate that the T stem slip changes D-T-loop interactions [274] by an yet unknown mechanism.

It is tempting to hypothesize that the two-state distribution with favored low FRET (Fig. 5.4) is caused by a weakened D loop T loop interaction, presumably due to a T slip. Since earlier experiments with unmodified hmt tRNA^{Leu(CUN)} at 10 mM Mg²⁺ did show a preference of high FRET [264], the T slip would have to be considerably favored at 2 mM Mg²⁺, resulting in weakened tertiary interactions and low FRET.

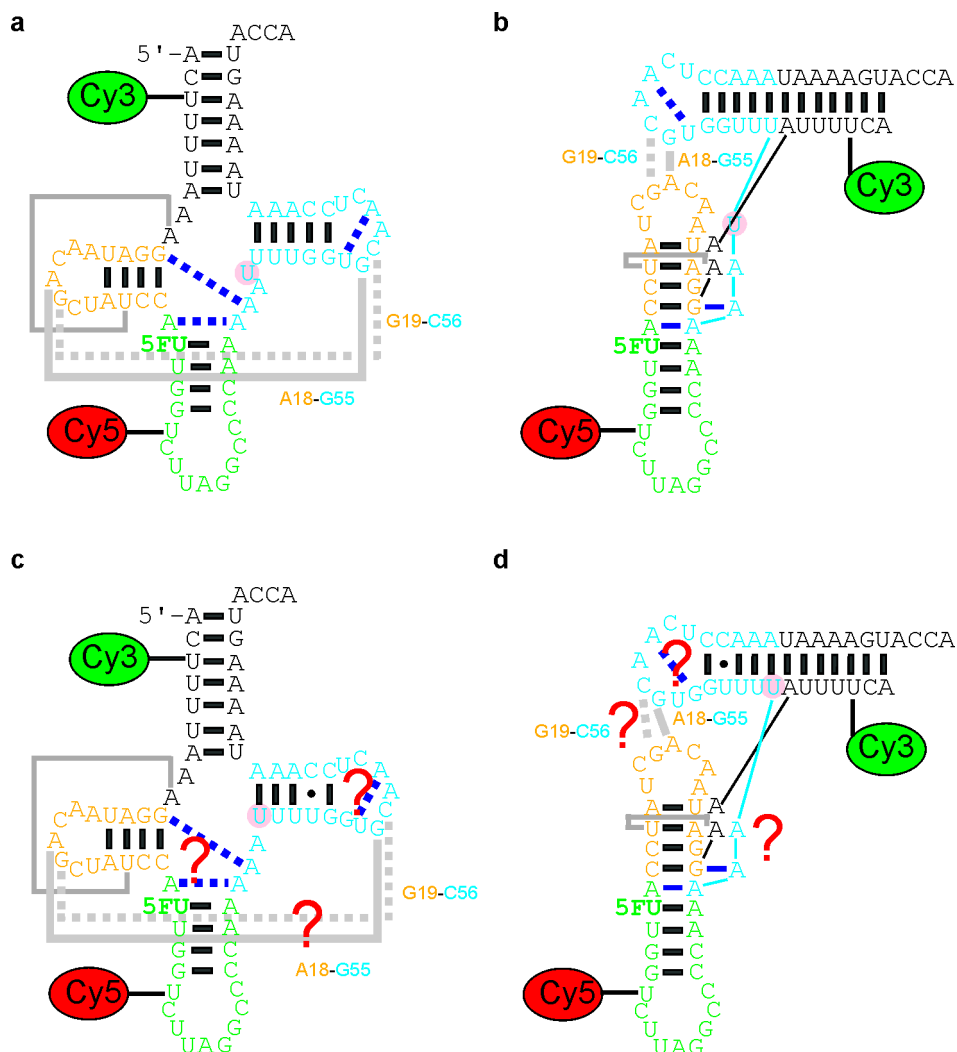


Figure 5.5.: Tertiary interaction in hmt tRNA^{Leu(CUN)} in the cloverleaf representation (a) or in the canonical L-shape (b). U48 is marked by a rose circle, since it was proposed to participate in the so called 'T slip', resulting in the structures shown in c and d. The 'T slip' could influence the tertiary interactions marked with '?'.

A U48C mutant, which should be unable to perform a T slip, is aminoacylated more efficiently than the wild type [274]. Consequently, if the T slip exists and is

significantly influenced by Mg^{2+} , aminoacylation efficiency should be similarly dependent on Mg^{2+} , which is not the case [274].

Further evidence is provided by previous smFRET experiments at 10 mM Mg^{2+} on constructs harboring a mismatch mutation in the T stem: The histogram resembles Fig.5.4 [264], indicating that low E_{FRET} could result from disruption of the canonical L-fold caused by weakened interactions between the D loop and the T loop.

To fully characterize the two state distribution determined here and to determine whether a 'T slip' is indeed responsible, additional experiments are required. In particular FRET assays at other Mg^{2+} concentrations and with different T slip mutants as in [274] should be conducted. Additionally structural probing assays [275] would be helpful, as RNA secondary structure algorithms like 'RNA structure' [276] or 'mfold' [277] are unsuitable for tRNA.

6. Conclusion & Outlook

6.1. Conclusion

6.1.1. Microscale thermophoresis on RNA

In the first part of this thesis the general applicability of microscale thermophoresis titrations to various questions in RNA research was addressed. MST turned out to be a fast and robust method that was generally applicable to Cy5 labeled RNAs. The method allowed to detect small molecule ligand binding by the *B. subtilis* SAM-I riboswitch and revealed specific responses to Mg^{2+} concentration for different structural mutants of human mitochondrial tRNA^{Lys}.

Furthermore, a high tolerance of fluorescently labeled tRNAs by modification enzymes could be demonstrated: Binding affinity is mostly independent of the label's position relative to the enzyme's substrate site and independent of whether the tRNA is treated as a substrate or not. For the case of *Thermotoga maritima* TruB very subtle differences in affinity (two- to five-fold) between label variants could be identified. Labeling at C49 yielded the lowest binding affinity, while the disturbance significantly depends on the specific manner of attachment: Labeling at the ribose via a 2'-amino group is better tolerated than a label at position 5 of the pyrimidine.

Although several readouts of MST traces responded to binding in most cases, neither the exact physical basis for this responsiveness, nor a divergence in binding affinities determined from different readouts can be explained at present.

6.1.2. Protein induced fluorescence enhancement

Binding of modification enzymes to Cy5-labeled tRNA generally caused an increase in fluorescence intensity. The effect's magnitude was mostly independent

of the label's position relative to the enzyme's substrate site, similar to the trends obtained for binding affinity. This seemingly contradicts the present model for the related cyanine Cy3, which depicts the PIFE as highly sensitive to label-protein distance [125]. It can be assumed that the PIFE is not only highly distance dependent but also unique for a given protein due to individual dye-amino acid interactions, a topic unaddressed so far. Furthermore, for the particular case of labeled tRNA a superposition of PIFE with effects related to dye-RNA interaction [123] can be expected.

6.1.3. 5FU55-tRNA TruB interaction

A combination of binding assays using either fluorescence or thermophoresis with electrophoretic mobility shift assays and turnover assays consistently disproved that a stable, irreversible and covalent inhibition of pseudouridine synthase *Thermotoga maritima* TruB by 5FU55-labeled tRNA occurs on a biochemically relevant timescale. Remarkably, tRNA labeled at U33, far away from TruB's substrate site 55, exhibits a significantly stronger spectroscopic response to binding than a label at C49, close to position 55. Until now, it is neither understood what exactly causes this difference in responsiveness, nor why U55-tRNA labeled at U33 is almost not turned over by the enzyme even under harsh reaction conditions. In the current hypothesis the U33 label interferes with TruB turnover by preventing a long-range intramolecular rearrangement of the tRNA [202].

6.1.4. Single molecule FRET

Single molecule FRET experiments revealed a remarkable tolerance of labeled tRNAs in ribosome binding assays, matching the tolerance in MST enzyme binding assays. In the course of this work a single molecule FRET setup was established that provided the so far unique possibility to record spectra of single dye labeled tRNAs. Initial experiments with this setup revealed human mitochondrial tRNA^{Leu(CUN)} to fluctuate between two conformational states at 2 mM Mg²⁺ with transition rates typical for RNA.

6.2. Outlook

6.2.1. MST on hmt tRNA^{Lys}

The influence of Mg^{2+} on different mutants of hmt tRNA^{Lys} detected by MST essentially reproduces previous results from single molecule FRET experiments [46, 182]. Since smFRET could also reveal individual responses to Mg^{2+} for differentially modified tRNA^{Lys} constructs [46, 158, 262, 263], future MST titrations might complement these studies. Such experiments bear the potential to generate a conclusive picture of how nucleoside modifications alter the conformational equilibrium of this particular tRNA.

6.2.2. Single molecule fluorescence studies of tRNA-TruB interaction

TruB binding to Cy5-labeled tRNA was detectable via each of four different spectroscopic parameters that were monitored. This extensive spectroscopic responsiveness renders the interaction particularly interesting for single molecule fluorescence studies. Provided that the dynamics of the interaction are slow (time resolution ~ 1 s), bathochromic shifts of single Cy5-labeled tRNAs should allow to determine on- and off-rates of tRNA-TruB binding. Potential differences in on- and off-rates for different label variants and for U55 vs. 5FU55 could allow important conclusions on the respective tRNA-TruB interactions. In addition, it would be interesting to use fluorescence lifetime as readout, similarly as reported for the related cyanine Cy3 [212, 278, 279]. Both approaches would require molecule-by-molecule measurements and would therefore profit from two improvements:

1. lower acidification by pyranose oxidase compared to glucose oxidase [280]
2. the use of extremely photostable Cy5 derivatives [281], which are not commercially available so far.

6.2.3. Turnover studies and binding kinetics on tRNA-TruB interaction

Although binding of TruB tolerated a wide range of fluorescent labels, the two label variants for which turnover efficiency was determined were either severely impaired in turnover (C49) or even almost not turned over at all (U33). Consequently, assessing the turnover efficiency of other label variants used in this work might reveal interesting details of TruB's tRNA recognition mechanism. Moreover, spectroscopic response of all label variants to TruB binding should be determined, since preliminary experiments indicate a responsiveness of a Cy3-U17-label. Identification of label-related effects in different steps of TruB binding might be able by:

1. combining cyanine labels with other TruB binding assays [117, 201] and
2. binding kinetics in bulk using a stopped flow apparatus [117].

Michaelis Menten kinetics should be carried out to characterized tRNA turnover by *Thermotoga maritima* TruB, as well as potential inhibition by 5FU55. Finally, it would be interesting to determine turnover of 5FU to 5Fh Ψ by TruB. After all 5Fh Ψ was detected previously in the cocrystal [103, 104] and in biochemical characterization of other Ψ synthases [110].

7. Experimental Details

7.1. Material

7.1.1. Buffers:

MST

TruB MST 1x buffer: 20 mM Tris pH7.5, 60 mM KCl, 0.02% Tween-20

KL buffer: 50 mM Tris-HCl (pH 7.4), with or without 10 mM MgCl

SAM-I buffer: 50 mM Tris-HCl pH8.5, 100 mM KCl, 20 mM MgCl₂

Pus1p buffer: 0.1 M Tris-HCl pH 8.0, 10 mM MgCl₂, 0.1 M NH₄OAc, 0.1 mM EDTA, 0.5 mM DTT

Pus X buffer: 0.1 M Tris-HCl pH 8.0, 10 mM MgCl₂, 0.1 M NH₄OAc, 0.1 mM EDTA, 0.5 mM DTT, 0.02 mM Triton-X 100

PAGE

Denaturing loading dye: 1x TBE (diluted from 10x), 90% (v/v) formamide

Colored loading dye: 1x TBE (diluted from 10x), 90% (v/v) formamide, 0.1% bromophenol blue, 0.1% xylene cyanol

Native loading dye: 10% glycerol, 1x TBE final

Protein synthesis

LB medium: 20 g Lennox LB-Broth mix was added to final 1 L distilled before autoclaving

Phosphate buffered saline: 137 mM NaCl, 2.7 mM KCl, 10 mM Na₂HPO₄, 1.76 mM KH₂PO₄, pH 7.4

TruB His buffer A: 100 mM Tris pH 8.0

TruB His buffer B: 100 mM Tris pH 8.0, 500 mM Imidazol

TruB SEC buffer: 500 mM KCl 50 mM TrisHCl pH7.5

RNA Synthesis

Strasbourg buffer: 40 mM Tris-HCl (pH 8.1), 1 mM spermidine, 5 mM DTT, 0.01 % Triton X-100

KL buffer: 50 mM Tris-HCl (pH 7.4), 10 mM MgCl₂

7.1.2. Enzymes

Table 7.1.: Enzymes used in this work.

Enzyme	Manufacturer
biotinylated Bovine Serum Albumin	Sigma-Aldrich (Steinheim, Germany)
BstNI (10000 U/ μ l)	New England Biolabs (Frankfurt am Main, Germany)
Catalase from bovine liver	Merck Germany CalBiochem
DNase 1 (50U/ μ l)	Fermentas (St. Leon-Rot, Germany)
hDnm2	expressed and purified in our lab
Glucose Oxidase from Aspergillus Niger	Sigma-Aldrich (Steinheim, Germany)
mouse Pu1p	expressed and purified in our lab
yeast Pus4p	expressed and purified in our lab
pabTrmi	expressed and purified in our lab
yeast Trm4p	expressed and purified in our lab
T4 DNA ligase (30U/ μ l)	Fermentas (St. Leon-Rot, Germany)
T4 Polynucleotide kinase (10 U/ μ l)	Fermentas (St. Leon-Rot, Germany)
T7 RNA-polymerase various mg/ml	expressed and purified in our lab
T4 RNA Ligase 2	expressed and purified in our lab
<i>Thermotoga maritima</i> TruB	expressed and purified in the course of this work
E. coli total tRNA (10 μ g/ μ l)	Roche Diagnostics (Mannheim, Germany)
Plasmid containing tRNA ^{Phe} template	expressed and purified in our lab
Streptavidin	New England Biolabs (Frankfurt am Main, Germany)
E. coli Rosetta pLysS DE3 competent cells	Merck Novagen (Darmstadt, Germany)

7.1.3. Consumables

Chemicals and other consumables used in this work.

7.1 Material

Compound	Manufacturer
Ammonium Acetate p. a. for HPLC	Carl Roth (Karlsruhe, Germany)
Ammonium peroxydisulfate (APS)	Carl Roth (Karlsruhe, Germany)
ATP	Fermentas (St. Leon-Rot, Germany)
Bovine Serum Albumine (20 mg/ml)	Fermentas (St. Leon-Rot, Germany)
Bromphenolblue	Sigma Aldrich (Steinheim, Germany)
Chloramphenicol	Carl Roth (Karlsruhe, Germany)
Coverslips	A. Hartenstein (Würzburg, Germany)
Coomassie Brilliant blue G-250	Carl Roth (Karlsruhe, Germany)
Dichloromethylsilane	Sigma-Aldrich (Steinheim, Germany)
Diethylether, for HPLC, $\geq 99\%$	Sigma-Aldrich (Steinheim, Germany)
Dithiothreitol	Fermentas (St. Leon-Rot, Germany)
DNA ladder 100bp plus	Fermentas (St. Leon-Rot, Germany)
dNTP mix (10 mM)	Fermentas (St. Leon-Rot, Germany)
Eppendorf tubes (Silanized)	Carl Roth (Karlsruhe, Germany)
Ethanol $>99,5\%$ Ph.Eur.	Carl Roth (Karlsruhe, Germany)
Ethylenediaminetetraacetic acid (EDTA)	Carl Roth (Karlsruhe, Germany)
Formamide $>99,5\%$ RNase/DNase-free	Carl Roth (Karlsruhe, Germany)
Glycerol	Sigma-Aldrich (Steinheim, Germany)
Glucose	Sigma-Aldrich (Steinheim, Germany)
HCl, 37%	Sigma-Aldrich (Steinheim, Germany)
Hellmanex	Hellma (Müllheim, Germany)
HisTrap HP 1 ml column	GE Healthcare (Munich, Germany)
LB Broth mix Lennox	Carl Roth (Karlsruhe, Germany)
Imidazole 99%	Carl Roth (Karlsruhe, Germany)
Isopropanol	Sigma Aldrich (Steinheim, Germany)
Isopropyl β -D-1-thiogalactopyranoside (IPTG)	Carl Roth (Karlsruhe, Germany)
Kanamycin	Carl Roth (Karlsruhe, Germany)
Magnesiumchloride	Carl Roth (Karlsruhe, Germany)
NEBuffer 2	New England Biolabs (Frankfurt am Main, Germany)
N,N,N',N'-Tetramethylethylenediamine (TEMED)	Carl Roth (Karlsruhe, Germany)
Potassium chloride (KCl)	Carl Roth (Karlsruhe, Germany)
KH_2PO_4	Carl Roth (Karlsruhe, Germany)

Pall Nanosep 0.45 μm	Sigma-Aldrich (Steinheim, Germany)
Pipet tips, with filter, sterile RNase/DNase free	Greiner Bio-One
Roti-Phenol	Carl Roth (Karlsruhe, Germany)
Rotiphorese 10x TBE buffer	Carl Roth (Karlsruhe, Germany)
Rotiphorese sequencing gel buffer concentrate	Carl Roth (Karlsruhe, Germany)
Rotiphorese sequencing gel concentrate 25% denaturing	Carl Roth (Karlsruhe, Germany)
Rotiphorese Gel 40 19:1, 40% non-denaturing	Carl Roth (Karlsruhe, Germany)
Rotiphorese sequencing gel diluent	Carl Roth (Karlsruhe, Germany)
Rotiphorese SDS 10x running buffer	Carl Roth (Karlsruhe, Germany)
S-Adenosyl-L-methionine (SAM)	New England Biolabs (Frankfurt am Main, Germany)
SeaKem LE Agarose	Lonza (Basel, Switzerland)
Na_2HPO_4	Carl Roth (Karlsruhe, Germany)
Syringe filters 13 mm diameter, nylon, pore: 0.2 μm	Carl Roth (Karlsruhe, Germany)
Suprasil quartz glass cuvette, 50 μl , 3mm light pass	Hellma (Müllheim, Germany)
Superdex 200 10/300 GL 200	GE Healthcare (Munich, Germany)
Sodium Chloride	Carl Roth (Karlsruhe, Germany)
Sodiumdodecylsulfate	Sigma Aldrich (Steinheim, Germany)
SYBR Gold	Invitrogen
Tris	Carl Roth (Karlsruhe, Germany)
Trolox	Sigma Aldrich (Steinheim, Germany)
Tris-Hcl	Carl Roth (Karlsruhe, Germany)
Triton X-100	Sigma Aldrich (Steinheim, Germany)
Tween-20	Sigma Aldrich (Steinheim, Germany)
Vivaspin 20, molecular weight cutoff 10,000 Da	Sartorius Stedim Biotech (Göttingen, Germany)
Xylene Cyanol	Sigma Aldrich (Steinheim, Germany)

7.1.4. Instruments

Table 7.3.: Instruments used in this work.

Instrument	Manufacturer
Bioer non-mixing heatblock	Biozym (Oldendorf, Germany)
Centrifuge 1-15 PK	Sigma (Osterode am Harz, Germany)
Centrifuge 5810R	Eppendorf (Hamburg, Germany)
Centrifuge Avanti J20	Beckman Coulter (Krefeld, Germany)
Digital Heatblock	VWR (Darmstadt, Germany)
Electrophoresis Chamber	CBS Scientific, VWR (Darmstadt, Germany)
FPLC Biologic DuoFlow	BIORAD (Munich, Germany)
Nanodrop ND 2000 Spectrophotometer	PeqLab (Erlangen, Germany)
Monolith NT.115	Nanotemper (Munich, Germany)
pH-Meter FE20/EL20	Mettler Toledo (Gießen, Germany)
SpeedVac Concentrator Plus	Eppendorf (Hamburg, Germany)
Thermomixer comfort	Eppendorf (Hamburg, Germany)
Typhoon 9400 variable mode imager	GE Healthcare (Munich, Germany)
Ultrapure Water Purification System	Milli-Q, Millipore (Schwalbach, Germany)
UV lamp 254 nm	Herolab Molekulare Trenntechnik (Wiesloch, Germany)

7.2. RNA ligation constructs

All oligonucleotides were purchased from IBA GmbH (Göttingen, Germany), except MH165, MH166, MH172, MH449 and MH450 were synthesized by Dharmacon Inc. (Chicago, USA), MH379 was synthesized by Dagmar Graber in the lab of Ronald Micura, Innsbruck University, Austria and MH578 and MH579 were synthesized by Biomers GmbH (Ulm, Germany).

7.2.1. Yeast tRNA^{Phe}

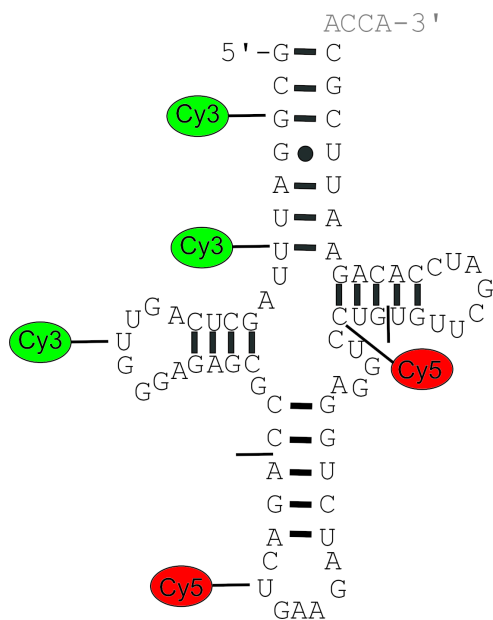


Figure 7.1.: Secondary structure representation of yeast tRNA^{Phe}, indicated are respective dye positions and boundaries of ligation fragments.

7.2 RNA ligation constructs

Table 7.4.: Oligonucleotides applied in yeast tRNA^{Phe} synthesis.

MH	Fragment #	Sequence 5'-3'	Modification	dye linker
449	1	pGCG GAU UUA GCU CAG UUG GGA GAG CGC C	none	none
213	1	GCG* GAU UUA GCU CAG UUG GGA GAG CGC C	Cy3@dG3	C8-6-amino-dG
521	1	GCG GAU U*UA GCU CAG UUG GGA GAG CGC C	Cy3@U7	2'-NH ₂
518	1	GCG GAU UUA GCU CAG U*G GGA GAG CGC C	Cy3@U17	C-5-6-amino-U
450	2	AGA CUG AAG AUC UGG AGG UCC UG	none	none
214	2	AGA C*U*G AAG AUC UGG AGG UCC UG	Cy5@U33	C-5-6-amino-U
522	2	AGA CUG AAG AUC UGG AGG UCC* UG	Cy5@C49	2'-NH ₂
675	2	AGA CUG AAG AUC UGG AGG UCC* UG used in chapter 4 as substitute for out-of-stock 2'-NH ₂ -C	Cy5@C49	C-5-6-amino-dC
215	3	UGU UCG AUC CAC AGA AUU CGC ACC A	none	none
379	3	pUGU <u>UCG</u> AUC CAC AGA AUU CGC ACC A	<u>5FU55</u>	none
216	DNA splint	TGG TGC GAA TTC TGT GGA TCG AAC ACA GGA CCT CCA GAT CTT CAG TCT GGC GCT CTC CCA ACT GAG CTA AAT CCG C		

7.2.2. Human mitochondrial tRNA^{Lys}

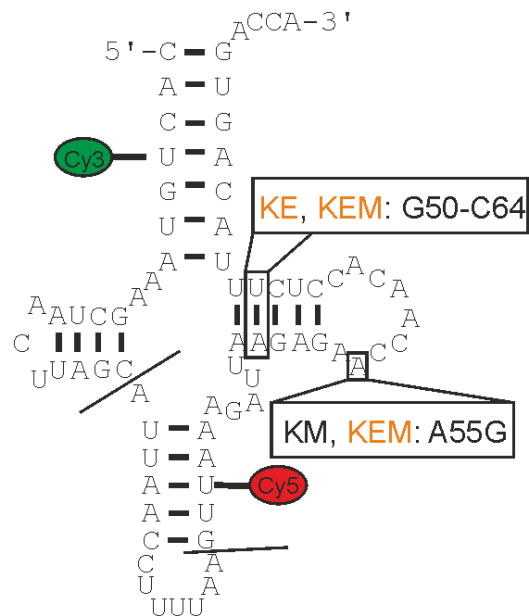
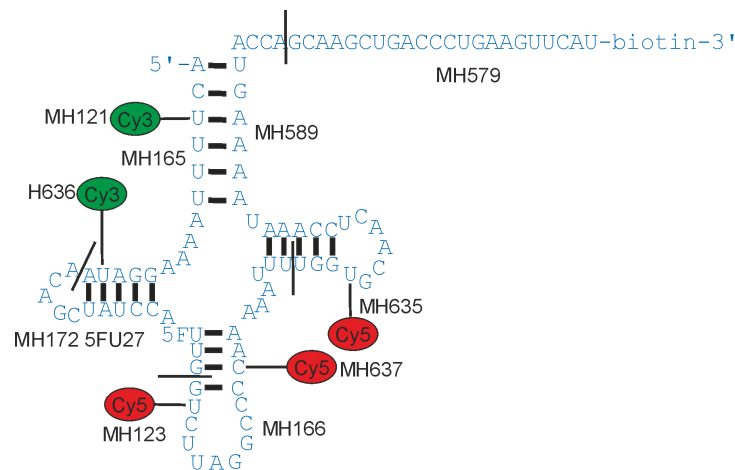


Figure 7.2.: Secondary structure representation of human mitochondrial tRNA^{Lys}, indicated are respective dye positions, mutations (cloverleaf mutants in orange) and ligation fragments.

Table 7.5.: Oligonucleotides applied in human mitochondrial tRNA^{Lys} synthesis.

MH	Fragment #	Sequence 5'-3'	Mutation	Dye linker
182	1	CAC t ⁺ GU AAA GCU AAC UUA GC	none	T4-Cy3-C5-6-amino-dT
242	2	AUU AAC CUU UUA A	none	none
137	3	GUt ⁺ AAA GAU UAA GAG AAC CAA CAC CUC UUU ACA GUG ACC A	none	T41-Cy5- C5-6-amino-dT
177	3	GUt ⁺ AAA GAU UAG GAG AAC CAA CAC CUC CUU ACA GUG ACC A	KE: A50G, U64C; 3'-biotin	T41-Cy5- C5-6-amino-dT
178	3	GUt ⁺ AAA GAU UAG GAG AGC CAA CAC CUC CUU ACA GUG ACC A	KEM: A50G, A55G U64C; 3'-biotin	
316	3	GUt ⁺ AAA GAU UAA GAG AGC CAA CAC CUC UUU ACA GUG ACC A	KM mutation: A55G	C5-6-amino-dT
78	DNA splint	TGG TCA CTG TAA GAG GTG TTG GTT CTC TTA ATC TTT AAC TTA AAA AGG TTA ATG CTA AGT TAG CTT TAC AGT G		

7.2.3. Human mitochondrial tRNA^{Leu(CUN)}

**Figure 7.3.:** Secondary structure representation of human mitochondrial tRNA^{Leu(CUN)}, indicated are respective dye positions, modifications and ligation fragments.

7.3 Methods

Table 7.6.: Oligonucleotides applied in human mitochondrial tRNA^{Leu(CUN)} synthesis.

MH	Fragment #	Sequence 5'-3'	Modification	dye linker	5'-P
165	1	pACU UUU AAA GGA UA	none	none	yes
121	1	AC ⁶ UUU AAA GGA UA	Cy3@U3	C-5-6-amino-T	no
636	1	ACU UUU AAA GGA U ⁶ A	Cy3@U13	C-5-6-amino-U	no
172	2	ACA GCU AUC CAU UG	5FU27	none	yes
166	3	UC UUA GGC CCC AAA AAU UU	none	none	yes
123	3	G ⁶ C UUA GGC CCC AAA AAU UU	Cy5@U31	C-5-6-amino-T	no
637	3	GUC UUA GGC CCd ⁶ C ⁶ AAA AAU UU	Cy5@C41	C-5-6-amino-dC	no
634	4	UGG UGC AAC UCC AAA U ⁶ AA AAG UAC CA	Cy3@U66	C-5-6-amino-U	no
635	4	UGG U ⁶ GC AAC UCC AAA UAA AAG UAC CA	Cy5@U54	C-5-6-amino-U	no
589	4	UGG UGC AAC UCC AAA UAA AAG UAC CA	none	none	no
MH129 should be identical to MH589, but cannot be ligated at the 3'-end and is too heavy in MALDI					
579	5	GCAAGCUGACCCUGAAGUUCAU	3'-biotin		no
126	DNA	TGG TAC TTT TAT TTG GAG TTG CAC CAA AAT TTT TGG GGC CTAA			
	splint	GAC CAA TGG ATA GCT GTT ATC CTT TAA AAG TTA TAG TGA GTC GTA TTA AGC TTC GCG CG			
578	DNA	ATG AAC TTC AGG GTC AGC TTG CTG GTA CTT TTA TTT GGA GTT GCA CCA AAA TTT			
	splint for 5	TTG GGG CCT AAG ACC AAT GGA TAG CTG TTA TCC TTT AAA AGT TAT AGT GAG TCG TAT TAA GCT TCG CGC G			

7.3. Methods

7.3.1. RNA synthesis

7.3.1.1. Ligations:

All handling was performed beneath aluminium foil if possible to minimize dye bleaching. Ligated tRNAs were produced from three fragments for yeast tRNA^{Phe} or hmt tRNA^{Lys} or four fragments in case of hmt tRNA^{Leu(CUN)} (five for single molecule experiments). RNAs for single molecule FRET experiments contained an additional 3'-fragment for immobilization as indicated. Ligation was basically carried out, as described previously[157].

Prior to ligation constructs that lacked a 5'-phosphate and that were not the leading fragment were phosphorylated for 1 h at 37°C using 0.75 U/ μ l Pnk, 5 mM ATP, and 5 mM DTT in KL buffer with a minimal final volume of 7 μ l, resulting

in an oligo concentration up to $\sim 26 \mu\text{M}$. Prior to enzyme addition all phosphorylations and additional oligonucleotides including the DNA splint were pooled and supplemented with additional ATP, DTT and 5x KL buffer to yield 1x KL-buffer, 5 mM ATP and 5 mM DTT as well as $\sim 7\text{-}11 \mu\text{M}$ oligo nucleotide concentration for the final reaction. Annealing was carried out by heating the mixture for 4 min at 75°C and cooling to room temperature in 15 min. Enzymes were added (1.5 U/ μl T4 DNA ligase and 0.06-0.75 $\mu\text{g}/\mu\text{l}$ T4 RNA ligase 2) and the reaction was carried out overnight at 16°C .

Ligation success was confirmed by an analytical 10% PAGE and scanning on a GE Healthcare Typhoon 9400 (excitation 532 nm, emission BP580 for Cy3, excitation 633 nm, emission BP670 for Cy5, excitation 532 nm, emission BP670 for FRET). Following 1 h digestion by $\sim 2 \text{ U}/\mu\text{l}$ DNaseI at 37°C , purification was carried out on 10% 8M urea PAGE (20-26 W) with band detection by eyesight to avoid dye bleaching. Gel bands were cut out using a scalpel, squashed and eluted into 0.5 M NH_4OAc at 20°C and 400 rpm overnight.

Gel pieces were removed by spinning through Pall Nanoseps at room temperature and precipitation was carried out by an addition of 2.5 Vol 100% -80°C cold ethanol, thorough vortexing and incubation overnight at -20°C or 2 h at -80°C . RNA was pelleted by centrifugation at 15.000 G and -5°C for 2 h followed by supernatant removal and drying in an Eppendorf SpeedVac.

The blue (Cy5), pink (Cy3) or purple (both dyes) RNA pellet was resuspended in MilliQ water and concentration determination was carried out using a ThermoScientific Nanodrop photometer's RNA program. Molar concentrations were estimated using the approximation that 1 μg are 40 pmol in case of tRNA.

7.3.1.2. Transcription:

The *in-vitro* transcript of yeast tRNA^{Phe} transcript was produced from a BstNI-digested plasmid template (original plasmid p67YF0 was a gift from O. Uhlenbeck [199]). Linearization was achieved by digesting the plasmid (0.1 $\mu\text{g}/\mu\text{l}$) with 1 U/ μl of the restriction enzyme in supplied NEBuffer 2 supplemented with 0.1 $\mu\text{g}/\mu\text{l}$ BSA for 3 h at 60°C . The linearized DNA was purified *via* phenol-diethylether extraction and precipitated by adjusting the aqueous phase to 0.5 M ammonium acetate following supplementation with 2.5 vol. absolute -80°C cold

ethanol. After thorough vortexing and incubation for at least 3 h at -20°C DNA was pelleted as described for RNA above. The pellet was washed once in 80% ethanol, dried, and resuspended in MilliQ water, concentration determination was carried out using a ThermoScientific Nanodrop photometer.

Transcription reactions were performed in 0.4-1 ml final volume of Strasbourg buffer containing 40 ng/ μ l linearized plasmid, supplemented with 30 mM MgCl₂, 5 mM NTPs, 5 mM DTT, and 2 μ g/ml BSA. Transcription was started by an addition of 0.05 μ g/ μ l of in-house-prepared T7 RNA-polymerase and the reaction was kept at 37°C for 4 h. In the last quarter of the reaction time pyrophosphate tends to form a white precipitate, thereby indicating a successful reaction. Transcript purification was carried out on 10% Urea-PAGE using UV shadowing for RNA detection. Gel bands were cut out, squashed and eluted into 0.5 M NH₄OAc over night at 20°C. Gel pieces were removed by spinning through Pall Nanoseps at room temperature and precipitation was carried out by an addition of 2.5x Vol 100% -80°C cold EtOH, thorough vortexing and incubation overnight at -20°C. RNA was pelleted by centrifugation at 15.000 g and -5°C for 2 h followed by supernatant removal and drying in an Eppendorf SpeedVac. The RNA pellet was resuspended in MilliQ water and concentration determination was carried out using a ThermoScientific Nanodrop photometer.

7.3.2. Protein synthesis

An *E. coli* rosetta 2 (DE3) strain containing a lac-operon controlled pET28 vector encoding C-terminal His₆-tagged *Thermotoga maritima* TruB was used for protein expression (the plasmid was a gift of R. Stroud [103]). The expression culture was grown in LB-medium (Lennox) supplemented with 34 μ g/ml chloramphenicol and 50 μ g/ml kanamycin to select pET28-TruB positive cells carrying the pLysS plasmid. TruB expression was induced by addition of 0.5 mM IPTG at an OD₆₀₀ of ~0.8. After 4 h, cells were harvested by centrifugation (at 2200 g and 4°C) and resuspended in PBS. Cells were centrifuged again in PBS and the supernatants disposed. Cell pellets were shock-frozen in liquid nitrogen and stored at -80°C. For purification the cell pellets were thawed and resuspended in 100 mM Tris pH 8.0, lysed with lysozyme, centrifuged (30 min 20000 g, 4°C) and the supernatant was boiled for 20 min at 70°C.

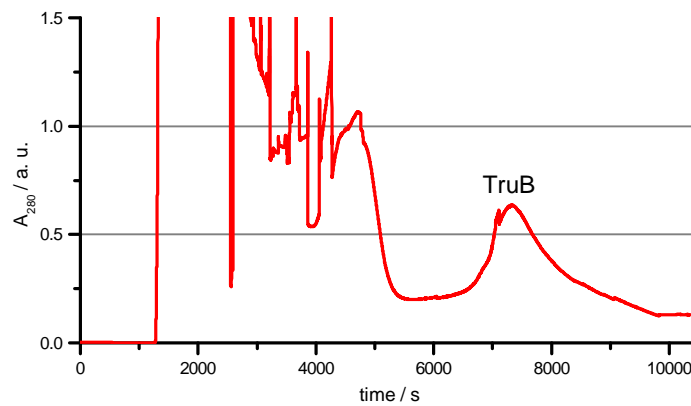


Figure 7.4.: Chromatograms from passing TruB preparations through the through a GE Healthcare HisTrap Ni²⁺-NTA column. TruB exhibits unusually strong binding for a His₆-tagged protein and elutes only at ~100% buffer B (500 mM imidazole).

After a second centrifugation step to remove denatured *E. coli* protein (30 min 20000 g, 4°C) the protein was captured using a GE Healthcare HisTrapHP Ni²⁺-NTA column. A typical chromatogram can be seen in Fig.7.4. Following reconcentration by Vivaspins purification was completed by passing the protein through a GE Healthcare Superdex 200 10/300 GL 200 size exclusion column using 500 mM KCl 50 mM TrisHCl pH 7.5 buffer (see Fig.7.5).

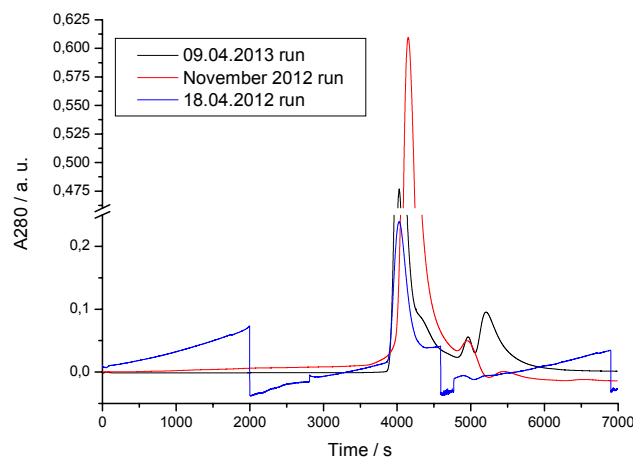


Figure 7.5.: Chromatograms from passing His-Tag purified TruB preparations through the GE Healthcare Superdex 200 10/300 GL 200 SEC column. The largest peak eluting at ~4200 s contained the protein.

Using a Vivaspin spinfilter the protein was reconcentrated and changed into MST1x buffer, purity was verified by SDS PAGE. Finally concentration determination was carried out using a Nanodrop photometer and an extinction coefficient calculated from the model of Gill and coworkers [282], the sample was parted into aliquots and shock frozen in liquid N₂.

7.3.3. Microscale thermophoresis

7.3.3.1. Derivatization of a 1:1 binding model

Measuring of complexation by thermophoresis requires a 1:1 binding model, which shall be derived here. Complex formation of the two reaction partners A and B proceeds as follows:



If this reaction is in equilibrium the fraction of formed complex can be described by the law of mass action:

$$K_D = \frac{A \cdot B}{AB} \quad (7.2)$$

By considering that a fraction of unbound molecules went into the complex, meaning $A = A_0 - AB$ and $B = B_0 - AB$ Eq.7.2 can be rewritten as

$$K_D = \frac{(A_0 - AB) \cdot (B_0 - AB)}{AB} = \frac{A_0 \cdot B_0 - A_0 \cdot AB - B_0 \cdot AB + AB^2}{AB} \quad (7.3)$$

resulting in the quadratic equation

$$0 = AB^2 - AB \cdot (A_0 + B_0 + K_D) + A_0 \cdot B_0 \quad (7.4)$$

The 'fraction bound' $\frac{AB}{A_0}$ is used at final readout. To get to this, the above equation

has to be solved for AB , resulting in

$$AB = \frac{K_D + A_0 + B_0 \pm \sqrt{(A_0 + B_0 + K_D)^2 - 4 \cdot A_0 \cdot B_0}}{AB} \quad (7.5)$$

If the 'fraction bound', meaning thereby all A molecules occupied in an AB complex, is introduced, the 1:1 binding model fit used in this work is derived

$$Fraction\ bound = \frac{AB}{A_0} = \frac{K_D + A_0 + B_0 - \sqrt{(A_0 + B_0 + K_D)^2 - 4 \cdot A_0 \cdot B_0}}{2 \cdot A_0} \quad (7.6)$$

Microscale thermophoresis changes the fluorescence observed from a value f_0 into a value f by either increasing or decreasing the fluorophore concentration inside the observation volume, resulting in the readout $\frac{f}{f_0}$ (one of the ratios given in Fig.1.15b). This readout can be used to derive the fraction of bound fluorescently labeled molecules, provided that $\left(\frac{f}{f_0}\right)_A \neq \left(\frac{f}{f_0}\right)_{AB}$ or, in words, provided that the observed ratio changes at all with binding, which results in [204]:

$$\frac{f}{f_0} (Fraction\ bound) = \left(\frac{f}{f_0}\right)_A + \left(\left(\frac{f}{f_0}\right)_{AB} - \left(\frac{f}{f_0}\right)_A \right) \cdot Fraction\ bound \quad (7.7)$$

7.3.3.2. Protein screen

Buffer of all proteins was changed into Pus1p 1x buffer using Vivaspins. Prior to enzyme addition tRNA was folded by heating for 4 min at 75°C in water and cooling to room temperature in 15 min after addition of Pus1p buffer (to 1x final). Aliquots of 100 nM tRNA were titrated with an equal volume (10 µl) protein from 1:1 dilutions in MST 1x buffer (50 nM tRNA final). Measurements were performed after 30 min incubation time using standard treated capillaries, where every capillary represented a specific titration point. Experiments were conducted using a Nanotemper Monolith N.115 with red excitation and detection; settings were 70% LED, 40% MST power and 25°C temperature control setting. Data was analyzed using 'NT analysis 1.4.27' and normalized as well as fitted to a Hill model in the software.

7.3.3.3. tRNA-TruB interaction

Prior to enzyme addition tRNA was folded by heating for 4 min at 75°C in water and cooling to room temperature in 15 min after addition of MST buffer. Aliquots of 100 nM tRNA were titrated with an equal volume (10 µl) tmTruB from 1:1 dilutions in MST 1x buffer (50 nM tRNA final). Measurements were performed after 30 min incubation time using standard treated capillaries, where every capillary represented a specific titration point. Experiments were conducted using a Nanotemper Monolith N.115 with red excitation and detection; settings were 70% LED, 40% MST power and 25°C temperature control setting.

In case of the measurements given in chapter 4, one experimental set consisted of titrations of all four constructs followed by chase experiments on the same samples with yeast tRNA^{Phe} transcript, curves given in Fig. 4.6 were additionally fitted to a bi-exponential decay function in Origin 9 (OriginLab). In general the resulting data was analyzed using 'NT analysis 1.4.27' and normalized as well as fitted to a 1:1 binding model derived from [204] in the software.

7.3.3.4. tRNA-mPus1p interaction

A mPus1p preparation stored as described in [179] was exchanged in to 'Pus1 buffer' [179] containing 0.02 mM Triton-X 100 (termed PusX buffer) by Vivaspin filters. Prior to enzyme addition tRNA was folded by heating for 4 min at 75°C in water and cooling to room temperature in 15 min after addition of PusX buffer. Aliquots of 50 nM tRNA were titrated with an equal volume (10 µl) mPus1p from 1:1 dilutions in PusX buffer (ctRNA_{final} = 25 nM). Measurements were performed after 30 min incubation time using standard treated capillaries, where every capillary represented a specific titration point. Experiments were conducted using a Nanotemper Monolith N.115 with red excitation and detection; settings were 100% LED, 40% MST power and 25°C temperature control setting. The resulting data was analyzed using 'NT analysis 1.4.27' and normalized as well as fitted to a 1:1 binding model derived from [204] in the software.

7.3.3.5. tRNA-Mg²⁺ interaction

Different mutants of were folded by heating for 4 min at 75°C in water and cooling to room temperature in 15 min after addition of Mg²⁺-free 5x KL buffer (1x fi-

nal, RNA concentration 100 nM). From a near-saturated MgCl_2 -solution (~4 M) a serial dilution of 15 concentrations in Mg^{2+} -free KL buffer was generated and for every concentration 10 μl salt were mixed with 10 μl , with mixed with Mg^{2+} -free KL1x buffer serving as blank. Therefore, final concentrations were 1x KL buffer and 50 nM RNA. Experiments were conducted using a Nanotemper Monolith N.115 with red excitation and detection; settings were 70% LED, 40% MST power (or 80% MST power) and 25°C temperature control setting. One experimental set consisted of titration of all four constructs. The resulting data was analyzed using 'NT analysis 1.4.27' for the normal thermophoresis (MST) regime.

7.3.3.6. SAM-I-riboswitch

Riboswitch constructs were folded in 1x SAMI buffer by heating for 2 min at 70°C and cooling to room temperature in 10 min. From a fresh batch SAM solution (32 nM) a serial dilution down to 32 μM was performed using SAMI-1x buffer as diluent. Fifteen 10 μl aliquots of all the six riboswitch constructs were titrated with 10 μl of serial 1:1 dilutions of the pre-diluted SAM stock with RNA mixed with I 1x buffer serving as blank (highest final SAM concentration 16 μM , final RNA concentration 50 nM, 1x SAMI buffer final). MST experiments were conducted using red excitation and detection; settings were 100% LED, 70% MST power and 25°C temperature control setting. One experimental set consisted of titration of all six constructs. The resulting data was analyzed using 'NT analysis 1.4.27' and normalized as well as fitted to a 1:1 binding model derived from[204] in the same software.

7.3.4. Gel shift experiments

Prior to enzyme addition tRNA was folded by heating for 4 min at 75°C in water and cooling to room temperature in 15 min after addition of MST buffer. All reactions were incubated for the times indicated, following 5 min incubation in 0.5 x the respective loading dye at either 25 °C or 95 °C. All gels, either 20x30 cm 10% 8 M Urea PAGE , 10x10 cm or 20x10 cm 10% SDS PAGE with 6% stacking gel (casted resolving gel was overlaid with isopropanol during polymerization), were run at 100 V and room temperature. Gels were first scanned with a GE Healthcare Typhoon 9400 for Cy5 (excitation 633 nm, emission 670BP30) and then

stained with SYBR Gold (Invitrogen), scanned for SYBR Gold (excitation 488 nm, emission 520BP40) and, if indicated, FRET from SYBR Gold to Cy5 (excitation 488 nm, emission 670BP30), followed by Coomassie G-250 staining and detection by a xerox copy machine (tif saved on USB stick).

Table 7.7.: Recipe for 6% stacking and 10% resolving SDS PAGE.

Component	6% Stacking	10% Resolving
Total volume / ml	3	10
H ₂ O / ml	2.1645	4.646
40% acrylamide 19:1 / ml	0.3825	2.55
1.5 M Tris-Cl pH8.8 / ml	0	2.6
1 M Tris-Cl pH6.8 / ml	0.39	0
10% SDS / ml	0.03	0.1
10% APS / ml	0.03	0.1
TEMED / ml	0.003	0.004

7.3.5. Coomassie staining procedure

Colloidal Coomassie was prepared by resuspending ~60-80 mg Coomassie G-250 in 1000 ml MilliQ water (mixing for 1 h) and adding 3 ml 37% HCl afterwards. Prior to staining SDS was removed from the SDS gel by three cycles of washing: (1) boiling the gel in MilliQ water in the microwave for 1 min, (2) shaking 3 min, (3) exchange water for fresh water, (4) repeat. SDS removal is the most crucial parameter for the sensitivity of the stain. Most efficient was incubation of the gel in 25% isopropanol, 75% TBE at 4°C overnight: SDS precipitates. If the gel is relatively free of SDS and/or the protein concentration is high, bands are usually visible already after several minutes staining time. Longest staining duration applied was 60 min. Weak background can be removed by incubating the gel in MilliQ water with tissues.

7.3.6. Bulk fluorescence measurements

Experiments were performed, as described in [283], using 50 μ l 200 nM tRNA solutions in 50 μ l Quartz cuvette (Hellma analytics) employing a Fluorolog-3 spectrofluorometer (HORIBA Jobin-Yvon). Emission spectra were recorded upon excitation at 647 nm from 651 – 690 nm (increment 1 nm, slits at excitation 3 nm

and at emission 1 nm). Excitation spectra were recorded at 668 nm while exciting from 630 to 663 nm (increment 1 nm, slits at excitation 1 nm and at emission 3 nm). Fluorescence lifetime measurements have been performed with the same spectrometer using a pulsed Fianium laser (Fianium, Sc400_2PP, 20 MHz) for excitation at 647 nm. A single photon detector (PMA Hybrid 50, PicoQuant) in conjunction with a PicoHarp 300 module (PicoQuant) allowed for time correlated single photon counting (TCSPC). For every titration point photons were collected in histogram mode up to a peak maximum of 65000 counts. Two different polarization geometries VV and VH have been used to separate fluorescence lifetime from molecular reorientation effects. The resulting data was analyzed using self-written scripts in Matlab (MathWorks) and Origin (OriginLab) and subjected to a self-normalizing 1:1 binding-model fit derived from [204]. Intensity decay data was fitted globally to extract lifetime and anisotropy data for every titration point, thereby generating a titration curve. For spectra titration curves were generated by fitting the spectral maxima to a single Gaussian.

Chase experiments were performed by measuring 200 nM RNA alone, adding TruB to >5 μ M final concentration, measuring the instantaneous binding and, after an incubation time of ~40 min due to the measurement, adding 5.5 μ M transcript and measuring the instantaneous displacement of fluorescent tRNA from the complex.

7.3.7. Single molecule fluorescence measurements

7.3.7.1. Sample preparation

Measurement chambers were prepared as described previously [284]. Measurements were performed in 0.2x DTT-free Pus1 buffer final (meaning 0.02 M Tris-HCl at pH 8.0, 2 mM MgCl₂, 0.02M NH₄OA, 0.02 mM EDTA, but WITHOUT 0.1 mM DTT final) as imaging buffer. This was initially an honest error as 5x Pus1 buffer is labeled with the composition of 1x Pus1 buffer in Hengesbach et al. [179].

Prior to any incubation the tRNA (20 pM final in 50 μ l, 20 pM) was folded by heating for 4 min at 75°C in water with subsequent addition of 1x Pus1 buffer to 0.2x final in 50 μ l total volume. Preparation of the measurement chamber for tRNA

immobilization was carried out during a 15 min period that allowed cooling to room temperature:

- 5 min incubation with pure BSA-Biotin in PBS
- Wash with PBS (2x 100 μ l)
- 30s-60s incubation with Streptavidin (0.2 mg/ml in PBS)
- Wash with PBS(2x 100 μ l)
- Wash with Imaging buffer (2x100 μ l)
- 5 min incubation with 50 μ l 20 pM tRNA solution in imaging buffer
- Wash with 2x100 μ l imaging buffer
- Exchange against 100 μ l “Gloxy” buffer directly before measurement

“Gloxy” buffer was prepared as follows: (1) Trolox buffer: 1 microspatula tip of Trolox was dissolved in a solution consisting of 550 μ l MilliQ water, 250 μ l 40% glucose and 200 μ l Pus1 1x buffer (for 0.2x final), vortexed for 2 min and filtered through two stacked nylon syringe filters (450 nm pore size). (2) Enzymes: 0.2 μ g/ μ l catalase, 100 μ g/ μ l Glucose oxidase in Pus 0.2x final, fingertip instead of vortexing until dissolved (3) add 1.5 μ l of the enzyme stock to 100 μ l Trolox buffer, inject the buffer into the measurement chamber.

The sample chamber was sealed with Parafilm and mounted directly onto the microscope.

7.3.7.2. Microscope setup

The microscope setup was designed, assembled, maintained and calibrated by Dr. Gerald Hinze, group of Prof. Thomas Basché Institute of Physical Chemistry, Johannes Gutenberg-University Mainz, Germany. In consequence handling the microscope setup was not a central focus of this work and the component shall be described only briefly. Excitation was carried out with 1 μ W laser power at 532 nm. The signal was collected by a 1.49 NA objective, passed through a filter to eliminate scattered laser light, and parted 50:50 by a beamsplitter cube to a spectrograph (at 1 s integration per time spectrum and 50x electron multiplying mode at -70°C; ANDOR IXON) and to two Avalanche photodiodes (Perkin Elmer) detecting up to 630 nm and until 630 nm respectively with 100 ms time resolution.

7.3.7.3. Data analysis

Data analysis was carried out in Matlab programs written mainly by G. Hinze and partly by F. Spenkuch. In a first step the spectrograph data was visually inspected for start and endpoints, which were stored in files. In the final analysis spectrograph data was used to correct the relative intensities of 'green' and 'red' APD traces. Resulting traces were corrected for background and for 15% donor bleedthrough into the acceptor channel, direct acceptor excitation was neglected. FRET efficiencies were calculated from $E_{FRET} = I_{AD}/(I_{AD} + I_{DA})$ and final traces were exported for plotting in Origin (Origin Lab) and further analysis using 'HAMMY' and 'TDP' [266].

A. Appendix

A.1. Appendix to chapter 3

A.1.1. sec. 3.1.1

As explained in sec.1.5, there are several ways to analyze thermophoresis curves of a titration experiments: While the usual readout for a given titration point is the ratio of post T Jump intensity and steady state intensity, all other combinations given in sec.1.5 were also responsive to enzyme binding. Dissociation constants resulting from fits to a 1:1 binding model are given in Fig.A.1.

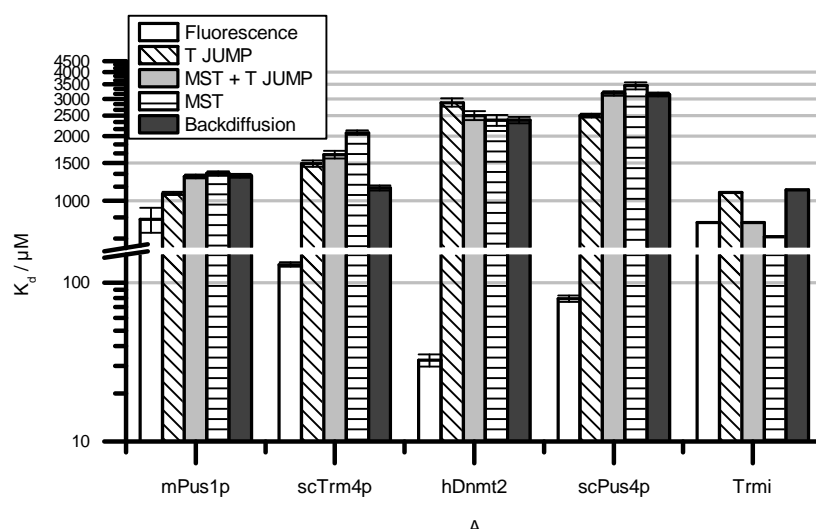


Figure A.1.: Dissociation constants of TruB and tRNA constructs as resulting from different thermophoresis curve readouts. Error bars represent the standard error of the fit as provided by the NT analysis software.

All readouts are in good agreement only for mPus1p and pabTrmi, For all other enzymes K_d value determined from absolute fluorescence intensity is 10-100-fold

lower than affinities determined from other readouts. Divergence of K_d values determined from fluorescence from the average over all readouts was also detected for other tRNA-protein interactions in this work. As discussed in the main text, mPus1p induces the largest change in fluorescence intensity, while pabT_{mi} has the smallest influence. Obviously and for yet unknown reasons an overall high signal does not necessarily correspond to well agreeing K_d values.

A.1.2. sec. 3.1.2

A.1.2.1. Chemistry of fluorescence labeling

All oligonucleotide were purchased as already labeled from IBA Göttingen. However, dyes were attached at three different bases (G, C and U), thereby requiring three different chemistries: Attachment at C5 for U, 2'-NH₂ for C and U or at G.

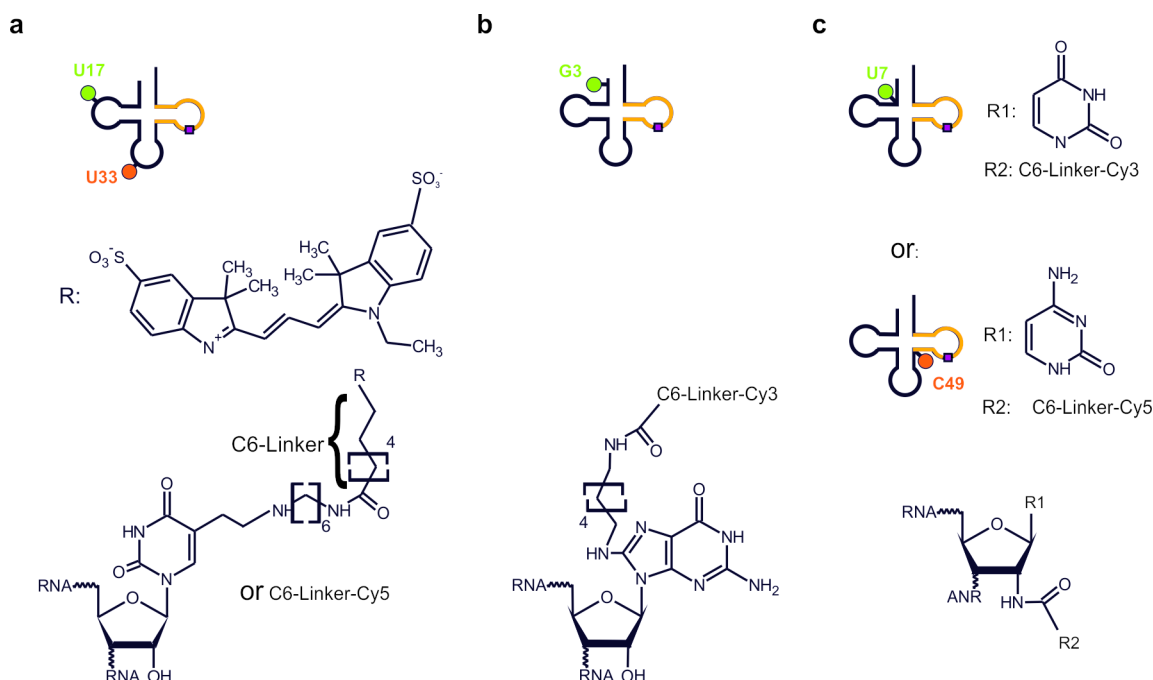


Figure A.2.: Labeling chemistries for different yeast tRNA^{Phe} constructs. All dyes at U17 and U33 were attached as shown in **a**, dyes at G3 as shown in **b** and dyes at U7 and C49 as in **c**.

A.1.2.2. Additional MST curve

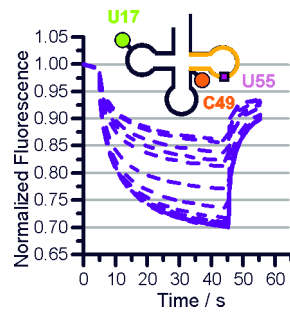


Figure A.3.: MST curve set of the C49 U17 U55 construct with the TruB minimal substrate marked in orange. Note that the curves closely resemble the C49 U17 5FU55 construct shown in the main text.

A.1.2.3. All features of MST curves are sensitive to TruB binding

As explained in sec.1.5, there are several ways to analyze thermophoresis curves of a titration experiments: While the usual readout for a given titration point is the ratio of post T Jump intensity and steady state intensity, all other combinations given in sec.1.5 were equally responsive to TruB binding. Dissociation constants resulting from fits to a 1:1 binding model are given in Fig.A.4. The only clear feature of the data are significantly higher K_d values from absolute fluorescence intensity, while values determined from other readouts vary only by a maximum factor of four.

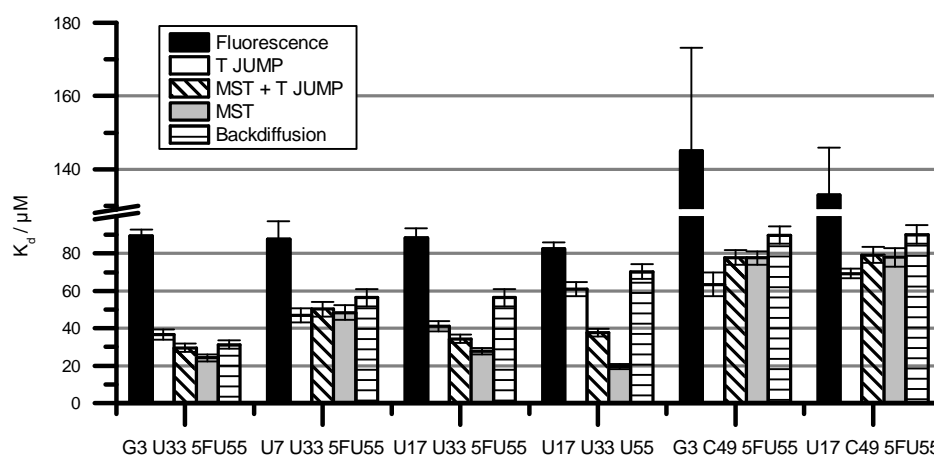


Figure A.4.: Dissociation constants of TruB and tRNA constructs as resulting from different thermophoresis curve readouts. Error bars represent the standard error of the fit as provided by the NT analysis software.

A.1.3. Appendix to sec. 1.5

As explained in sec.1.5, there are several ways to analyze thermophoresis curves of a titration experiments: While the usual readout for a given titration point is the ratio of post T Jump intensity and steady state intensity, all other combinations given in sec.1.5 were also responsive to mPus1p binding. The only clear trend in Fig.A.5 is a generally higher K_d value for thermophoresis and a generally lower K_d value for the T JUMP. However, as discussed in the main text, any further discussion remains speculation in lack of nearly quantitative binding, since the uncertainty of determined K_d values is very high.

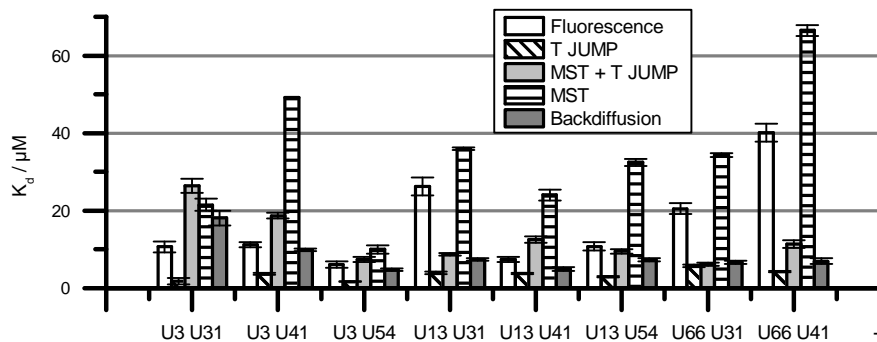


Figure A.5.: Dissociation constants of mPus1p and tRNA constructs as resulting from different thermophoresis curve readouts. Error bars represent the standard error of the fit as provided by the NT analysis software.

A.2. Appendix to chapter 4

This part of the Appendix contains representative LC-MS/MS spectra on TruB turnover, MST experiments on protein aggregation and reproducibility, an analysis of tRNA-C49-TruB interaction assessed after 10 min incubation on urea PAGE, results for all constructs after 12 h incubation at 4 °C assessed on urea and native PAGE and a SDS gel on different temperatures and incubation times for C49-5FU55-tRNA-TruB interaction.

A.2.1. Pseudouridine formation analyzed by LC-MS/MS

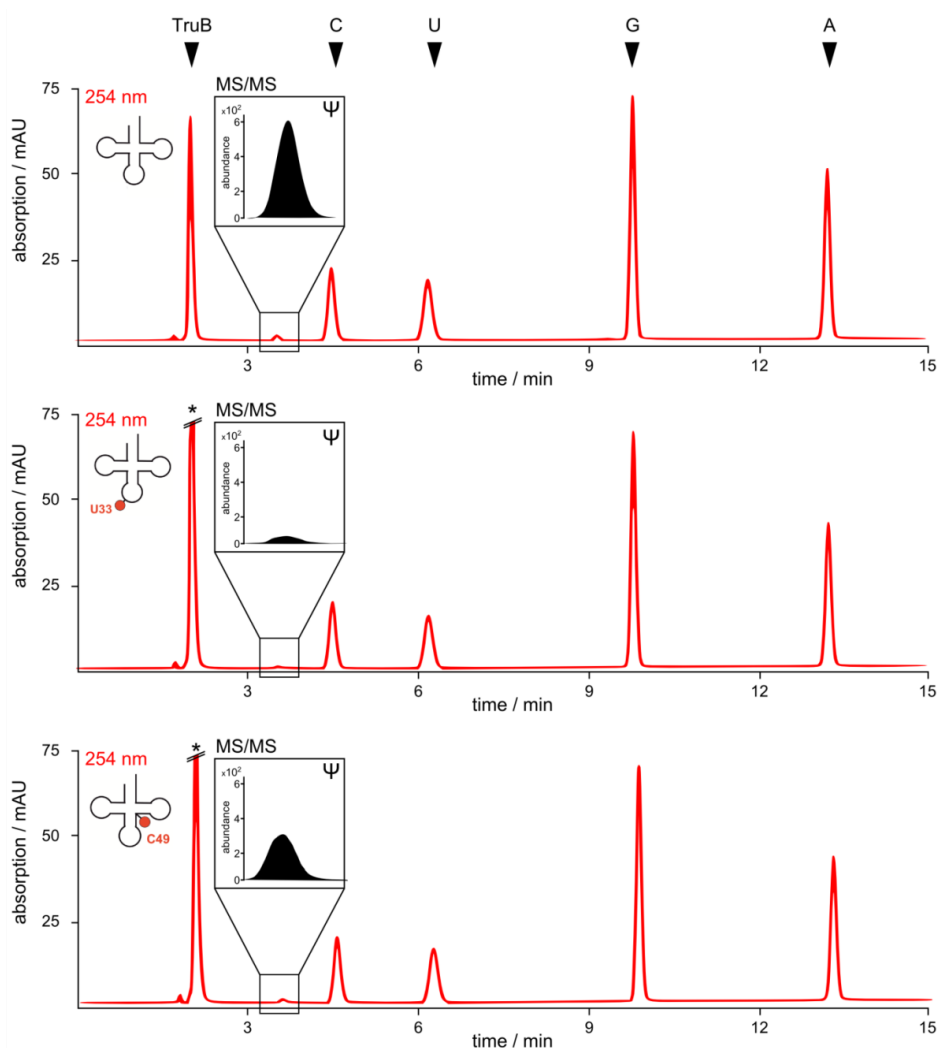


Figure A.6.: Measurements performed by LC-MS/MS analysis for verification of turnover efficiency. UV chromatograms (red) and MS signals of pseudouridine (black) of TruB incubated transcript (100% conversion), U33-U55 (6% conversion) construct and C49-U55 construct (57% conversion). No pseudouridine could be detected in the negative controls (TruB without RNA and transcript without TruB, respectively). Note that the TruB protein carries a high positive charge in the eluent with pH5.5 due to its pI of ~8.8, which results in elution near the dead time. Measurement, data analysis and figure preparation by Stefanie Kellner is gratefully acknowledged. Measurement and data analysis were performed as described in [285].

A.2.2. All features of MST curves are sensitive to TruB binding

As explained in sec.1.5, there are several ways to analyze thermophoresis curves of a titration experiments: While the usual readout for a given titration point is the ratio of post T Jump intensity and steady state intensity, all other combinations given in sec.1.5 were equally responsive to TruB binding. Dissociation constants resulting from fits to a 1:1 binding model are given in Fig. A.7. For both U33-tRNAs most K_d values are almost identical, while for the C49 constructs values determined from fluorescence and T Jump are up to ~15-fold lower than those determined from MST+T-Jump, MST or backdiffusion.

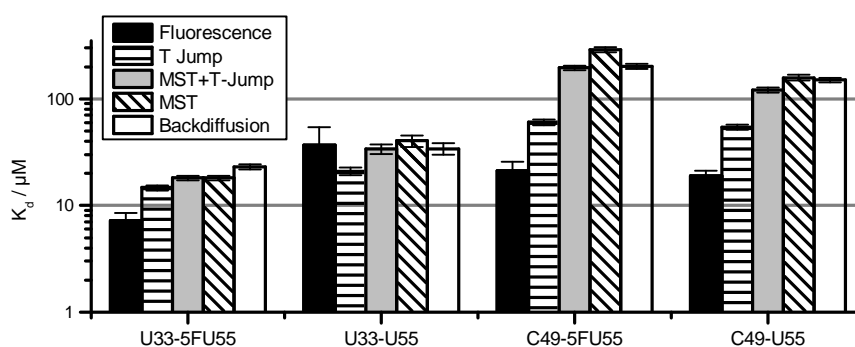


Figure A.7.: Dissociation constants of TruB and tRNA constructs as resulting from different thermophoresis curve readouts. For each readout the averaged data of three replicates were fitted. Error bars represent the standard error of the fit as provided by the NT analysis software.

The comparably large error inherent in absolute fluorescence intensity relativizes these differences somewhat, but still the following conclusion is suggested by the data:

As mentioned in the main text, upon TruB binding, the U33 label is more responsive in all spectroscopic properties than the C49 label. It might be that all readouts given in Fig. A.7 are dominated by the spectroscopic responsiveness for the U33 label, explaining the observed uniformity.

A.2.3. Additional MST experiments

Thermophoresis curves of an old, highly concentrated (~300 μM) TruB stock showed heavy fluctuations (Fig. A.8a) resulting in a titration curve lacking proper fits

with either a Hill model, or a one-to-one binding model (Fig. A.8b). Both models yielded similar, low affinities: $EC_{50} = 1592$ nM for the Hill model and $K_d = 1520$ nM for one-to-one binding. Thorough centrifugation results in smoother traces (Fig. A.8c).

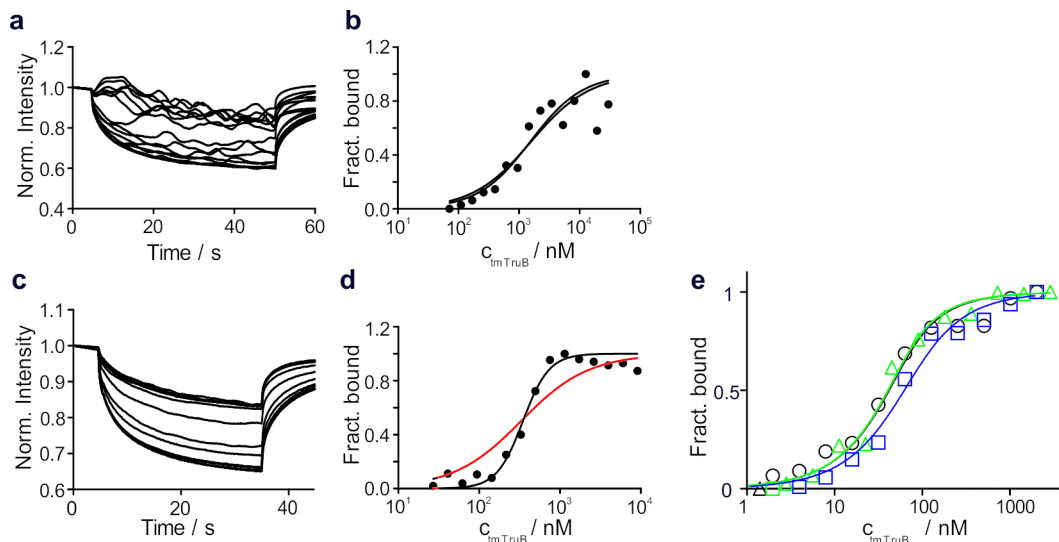


Figure A.8.: Influence of protein inhomogeneity on MST experiments. **a** Thermophoresis curves of 5 year old 300 μ M protein. **b** Titration curve resulting from a, fitted to either a one-to-one binding or to a Hill model (solid black lines). **c** Thermophoresis curves of centrifuged protein. **d** Titration curve and fits resulting from c: One-to-one binding model (red line) and Hill model (black line). **e** Longterm reproducibility of MST. Triplicate of a TruB-U33-5FU55 titration, while each run was 1 month apart from the other. K_d values as resulting from the fit to a one-to-one binding model (solid line): empty squares: 37.31 nM; empty triangles: 15.49 nM; empty circles: 16.89 nM.

However, the resulting step titration curve could not be fitted to a one-to-one binding model (red line in Fig. A.8d). A Hill fit (black line in Fig. A.8d), yielded $n = 2.68$ and $EC_{50} 347.8$ nM, more than 10x above the actual affinity. Affinity of tmTruB for the U33-5FU55 construct was measured three times over a period of three months with variations up to a factor of two and a precision value of 52%, as apparent from Fig. A.8e.

A.2.4. tRNA-TruB binding investigated by urea PAGE

Prior to gel loading complexation reactions with C49 tRNA were incubated at 2 μ M concentrations for 10 min at 25 $^{\circ}$ C, following 5 min incubation in 0.5x of the

respective loading dye (SDS buffer or 90% formamide in TBE (FA)) at either 25°C (Heat -) or 95 °C (Heat +).

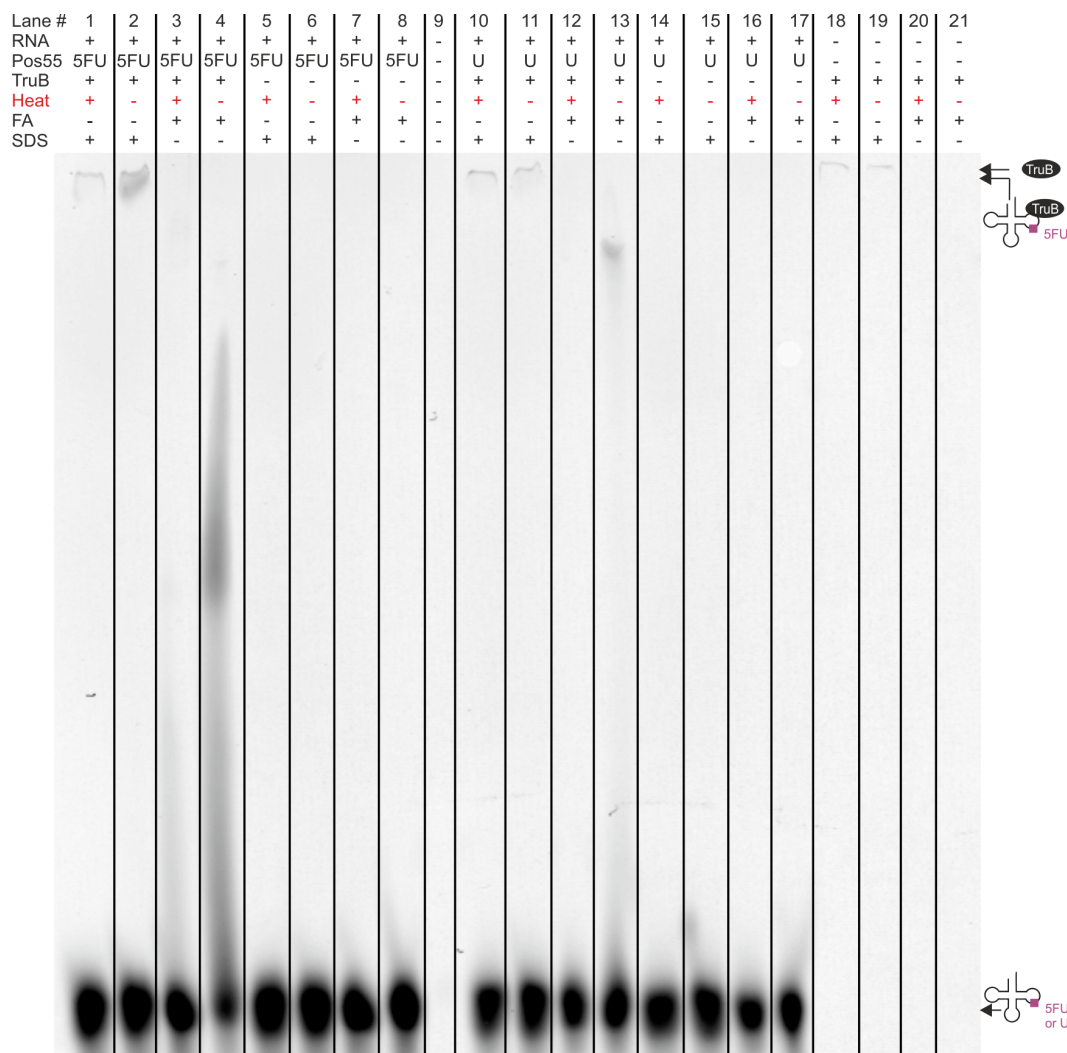


Figure A.9.: TruB-C49-tRNA interaction assessed by 8 M Urea PAGE (20x30 cm 10%, 100 V, 25 °C). Four conditions were tested: Prior to gel loading the complex reaction was either incubated for 5 min in either formamide or SDS buffer as loading dye at 25 °C or 95 °C. Detection by Cy5 scan (excitation 633 nm, emission 670 BP 30).

A Coomassie stain showed TruB incubated in FA only barely entering the gel as a diffuse streak on similar height as TruB in SDS buffer (data not shown). The Cy5 scan of the same gel is given in Fig.A.9 and allows the following observations:

- (1) Very weak autofluorescence of TruB can be detected, if SDS buffer is used (lanes 1, 10, 11, 18 and 19),
- (2) no complex formation with U55-tRNA occurs (lanes 10-13),
- (3) no complex for 5FU55-tRNA, if the reaction is heated to 95 °C prior to

gel loading (lanes 1+3), (4) as with SDS PAGE, the complex is 5FU55-specific, but detectable in only ~1% yield in SDS loading buffer (lane 2), a stark contrast to the ~40% detectable complex on SDS PAGE (Figure 3 in the main text), (5) in formamide buffer dissociation of the 5FU55-tRNA TruB complex is evident from heavy smearing (lane 4). In summary the 'stable' complex is neither resistant to urea, nor to formamide and therefore an SDS-related artifact.

Following 12 h incubation at 4 °C ($c_{\text{tRNA}} = 1 \mu\text{M}$, $c_{\text{TruB}} = 2.5 \mu\text{M}$), the complexation reaction was incubated in 90% formamide loading dye and analyzed on 10% urea PAGE (Fig.A.10). The gel shows intense smearing specific to 5FU55-TruB complexes, as in Fig. A.9, and weak autofluorescence of TruB for U55-tRNAs.

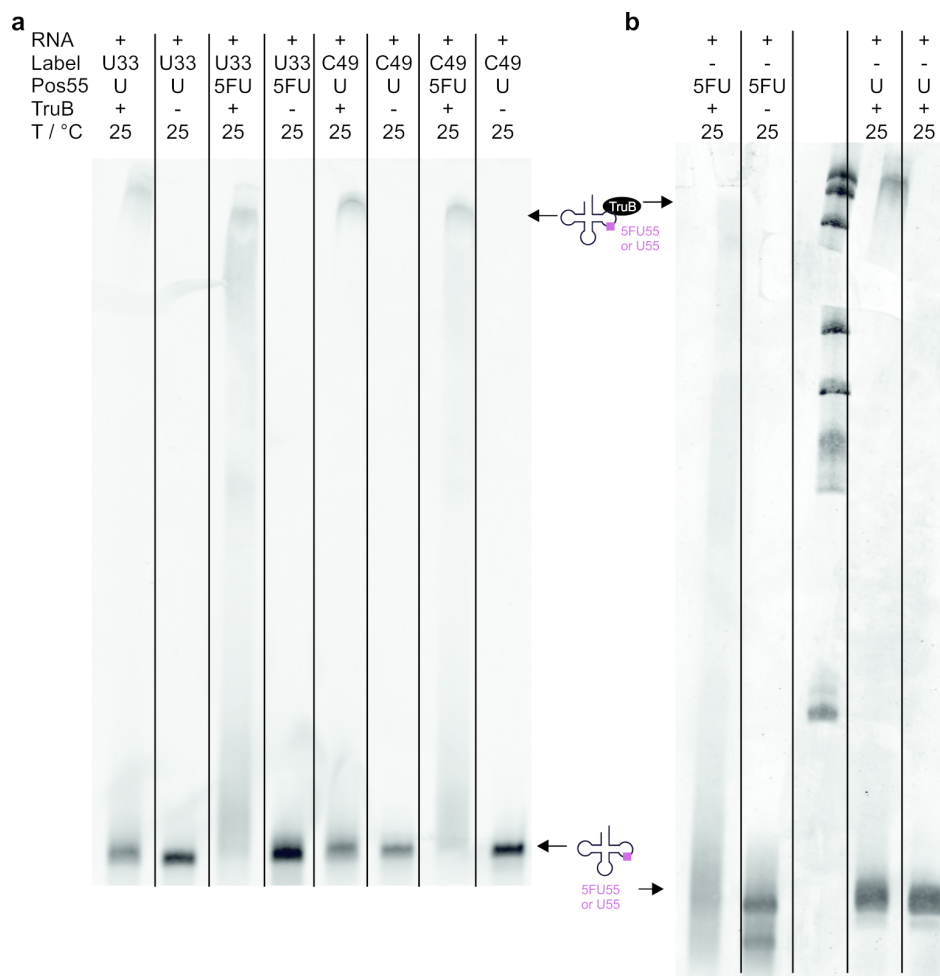


Figure A.10.: TruB-tRNA interaction assessed by urea PAGE (20x30 cm 10%, 16 W, 25 °C). All constructs were analyzed on the same gel: a) Cy5 scan of the gel half containing fluorescent constructs (excitation 633 nm, emission 670 BP 30), b) scan for SYBR Gold stain of unlabeled RNA (other gel half, excitation: 488 nm, emission: 526 SP).

An additional aliquot of the reactions shown in Fig.A.10 was analyzed on 10% native PAGE, revealing (except for some degradation) identical behavior of all constructs (Fig.A.11).

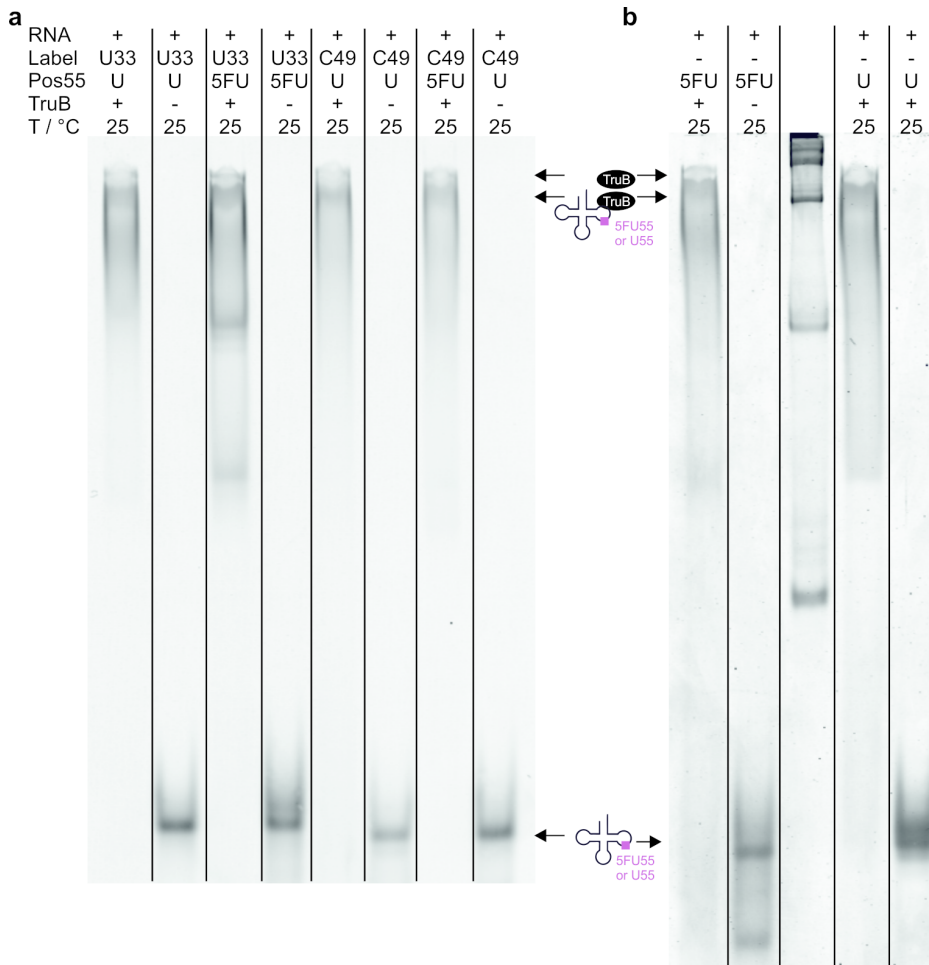


Figure A.11.: TruB-tRNA interaction assessed by native PAGE (20x30 cm 10%, 6 W, 25 °C). All constructs were analyzed on the same gel: a) Cy5 scan of the gel half containing fluorescent constructs (excitation 633 nm, emission BP670), b) scan for SYBR Gold stain of unlabeled RNA (other gel half, excitation: 488 nm, emission: SP526).

A.2.5. tRNA-TruB interactions investigated on SDS PAGE

Incubation of C49-5FU55-tRNA and TruB at 1 μ M and various temperatures for 2 or 18 h did not result in a significantly different complex yield, as is evident from the gel in Fig. A.12. However, RNA degradation is visible for high temperatures and/or long incubation times.

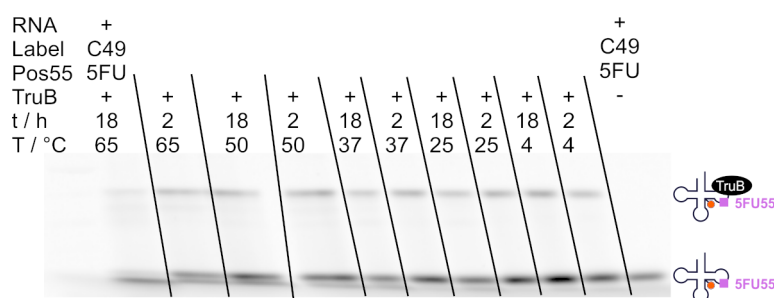


Figure A.12.: TruB-C49-5FU55-tRNA interaction assessed by SDS PAGE for the different incubation times and temperatures indicated. Note that the tRNA band shows a double band for elongated incubation and elevated temperatures, indicating degradation. Typhoon Cy5 scan excitation 633 nm, emission 670BP30.

A.2.6. Spectra on tRNA-TruB interaction

As mentioned in the main text, spectroscopic changes were larger for U33 vs. C49 labeled tRNAs. Representative spectra of all tRNA constructs are given in Fig. A.13.

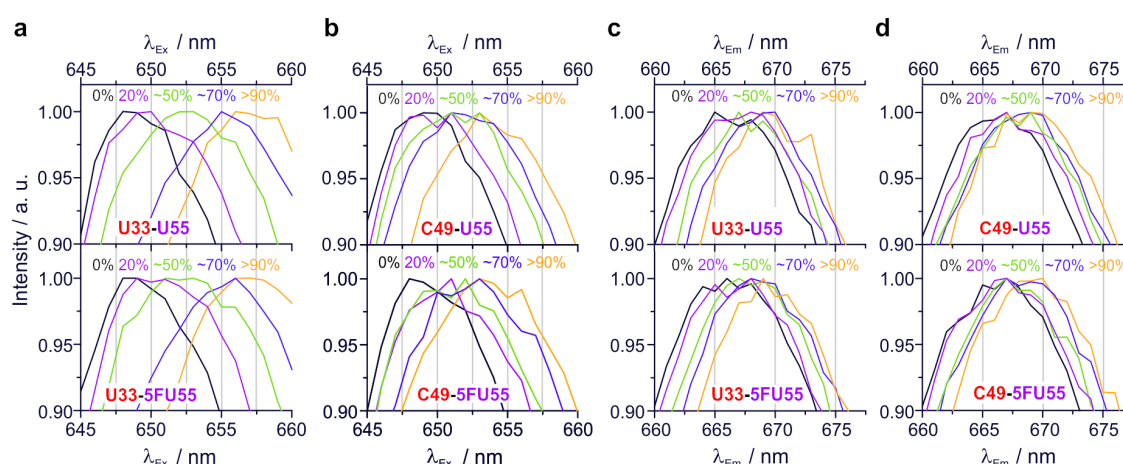


Figure A.13.: Representative spectra from tRNA TruB titrations. Protein binding ($\sim\%$ binding is given) causes bathochromic shifts of excitation (a, b, U55 above, 5FU55 below, $\lambda_{Em} = 668nm$) and emission spectra (c, d, U55 above, 5FU55 below, $\lambda_{Ex} = 647nm$).

A.2.7. Effects of tRNA-TruB binding on fluorescence anisotropy

Since the sample contains populations that differ in fluorescence life time, as well as rotational correlation times, time resolved fluorescence data has to be treated as a so called associated anisotropy decay to allow for deconvolution of anisotropy decay and fluorescence lifetimes [286]. Since systems with more than two correlation times are difficult to address [286] and could therefore let us interpret too much into our data, we chose a simple two component system, where components differ from each other in both, fluorescence lifetime and correlation time. The parallel and the perpendicular component are described by the following equations:

$$I_{\parallel} = A_1(1 - F)e^{-\frac{t}{\tau_{F1}}} \left[1 + 2r_1e^{-\frac{t}{\tau_{A1}}} \right] + A_2e^{-\frac{t}{\tau_{F2}}} \left[1 + 2r_2e^{-\frac{t}{\tau_{A2}}} \right] \quad (\text{A.1})$$

$$I_{\perp} = A_1(1 - F)e^{-\frac{t}{\tau_{F1}}} \left[1 + r_1e^{-\frac{t}{\tau_{A1}}} \right] + A_2e^{-\frac{t}{\tau_{F2}}} \left[1 + r_2e^{-\frac{t}{\tau_{A2}}} \right] \quad (\text{A.2})$$

Here (1-F) and F describe the fractional abundance of the two components, A_1 and A_2 are scaling amplitudes for both data sets and , τ_{F1} and τ_{F2} the fluorescence decay times, anisotropy amplitudes are given by r_1 and r_2 corresponding to rotational correlation times τ_{A1} and τ_{A2} , respectively. Anisotropy values for all constructs are given in Tab.A.1.

Table A.1.: Changes in anisotropy upon TruB binding

RNA	τ_{A1} / ns	τ_{A2} / ns	r_1	r_2
U33-U55	0.56	22.4	0.23	0.11
U33-5FU55	0.66	21.1	0.22	0.14
C49-U55	0.52	31.7	0.21	0.05
C49-5FU55	0.53	20.2	0.20	0.03

One component shows a fast anisotropic rotation, the other shows a rotational correlation time typical for a dye trapped in a protein complex [286]. The rotational correlation times are remarkably similar for all constructs with a slightly faster τ_{A1} for U33-tRNA. The amplitudes differ not for 5FU55 vs. U55, but for the

dye label position: For U33-tRNA the amplitudes of both components are similar, while the slow rotating component is nearly negligible for C49-tRNA.

The tRNA-TruB docking model [76] might explain at least one half of the observations: As is shown in Fig. A.14, C49 (depicted as a red structure) lies 'on top' of the enzyme shown as gray surface. The red inset in Fig. A.14 shows that the dye is attached to the 'C-H edge' of C49, positioning it towards the RNA backbone. The position marked with a blue arrow corresponds to the circle in the crystal structure, thereby depicting the dye attachment site. Considering the long linker attaching the dye to the base, one could imagine a quite undisturbed rotation of the dye 'above' the tRNA-TruB complex. Consistent with this hypothesis, we propose that r_2 of C49-tRNA is low, because the dye is still highly mobile in the complex and the resulting fast (almost isotropic) rotation cancels out the slow component. In reverse a larger r_2 for U33-tRNA implies an effective low mobility of the enzyme-bound U33-label, presumably due to long distance intramolecular rearrangement, as discussed in the main text. In lack of a cocrystal containing a full tRNA, specific effects of the U33 label cannot be discussed in more detail.

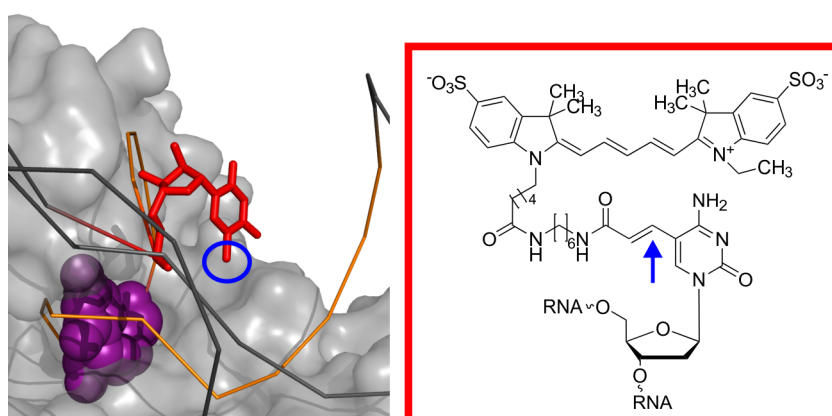


Figure A.14.: Detail of tRNA-TruB docking model [76]: TruB gray surface, tRNA represented as a black ribbon, minimal substrate is shown in orange and substrate position 55 as a purple sphere. The red structure shows m^5C49 native to yeast tRNA^{Phe} with the methyl group at position 5 marked by a blue circle. Cy5 attached to the base dC as inset. A blue arrow marks the position corresponding to the blue circle, thereby depicting the dye attachment site.

Bibliography

- [1] Lander, E. S. (2011) Initial impact of the sequencing of the human genome. *Nature* **470**, 187–197.
- [2] Crick, F et al. (1970) Central dogma of molecular biology. *Nature* **227**, 561–563.
- [3] Conaway, J. W. (2012) Introduction to theme chromatin, epigenetics, and transcription. *Annual review of biochemistry* **81**, 61–64.
- [4] Tollervey, J. R & Lunyak, V. V. (2012) Epigenetics: Judge, jury and executioner of stem cell fate. *Epigenetics* **7**, 823–840.
- [5] Esteller, M. (2011) Non-coding RNAs in human disease. *Nature Reviews Genetics* **12**, 861–874.
- [6] Fabian, M. R, Sonenberg, N, & Filipowicz, W. (2010) Regulation of mrna translation and stability by micrnas. *Annual review of biochemistry* **79**, 351–379.
- [7] Luco, R. F, Allo, M, Schor, I. E, Kornblihtt, A. R, & Misteli, T. (2011) Epigenetics in alternative pre-mrna splicing. *Cell* **144**, 16–26.
- [8] Cedar, H & Bergman, Y. (2012) Programming of dna methylation patterns. *Annual review of biochemistry* **81**, 97–117.
- [9] Rinn, J. L & Chang, H. Y. (2012) Genome regulation by long noncoding rnas. *Annual review of biochemistry* **81**, 145–166.
- [10] Shilatifard, A. (2012) The compass family of histone h3k4 methylases: mechanisms of regulation in development and disease pathogenesis. *Annual review of biochemistry* **81**, 65–95.
- [11] Fu, Y, Dominissini, D, Rechavi, G, & He, C. (2014) Gene expression regulation mediated through reversible m6a rna methylation. *Nature Reviews Genetics* **15**, 293–306.
- [12] Zhou, Q, Li, T, & Price, D. H. (2012) Rna polymerase ii elongation control. *Annual review of biochemistry* **81**, 119–143.
- [13] Carell, T, Brandmayr, C, Hienzsch, A, Müller, M, Pearson, D, Reiter, V, Thoma, I, Thumbs, P, & Wagner, M. (2012) Structure and function of noncanonical nucleobases. *Angewandte Chemie International Edition Engl* **51**, 7110–31.
- [14] Machnicka, M. a, Milanowska, K, Osman Oglou, O, Purta, E, Kurkowska, M, Olchowik, A, Januszewski, W, Kalinowski, S, Dunin-Horkawicz, S, Rother, K. M, Helm, M, Bujnicki, J. M, & Grosjean, H. (2013) Modomics: a database of rna modification pathways–2013 update. *Nucleic Acids Research* **41**, D262–7.
- [15] Kellner, S, Neumann, J, Rosenkranz, D, Lebedeva, S, Ketting, R. F, Zischler, H, Schneider, D, & Helm, M. (2014) Profiling of rna modifications by multiplexed stable isotope labelling. *Chemical Communications* **50**, 3516–3518.

- [16] Fabian, M. R & Sonenberg, N. (2012) The mechanics of mirna-mediated gene silencing: a look under the hood of mirisc. *Nature structural & molecular biology* **19**, 586–593.
- [17] Tuorto, F, Liebers, R, Musch, T, Schaefer, M, Hofmann, S, Kellner, S, Frye, M, Helm, M, Stoecklin, G, & Lyko, F. (2012) Rna cytosine methylation by dnmt2 and nsun2 promotes trna stability and protein synthesis. *Nature structural & molecular biology* **19**, 900–905.
- [18] Blanco, S, Dietmann, S, Flores, J. V, Hussain, S, Kutter, C, Humphreys, P, Lukk, M, Lombard, P, Treps, L, Popis, M, et al. (2014) Aberrant methylation of trnas links cellular stress to neuro-developmental disorders. *The EMBO journal* DOI: [10.15252/embj.201489282](https://doi.org/10.15252/embj.201489282).
- [19] Amort, T, Soulière, M. F, Wille, A, Jia, X.-Y, Fiegl, H, Wörle, H, Micura, R, & Lusser, A. (2013) Long non-coding rnas as targets for cytosine methylation. *RNA Biology* **10**, 0–1.
- [20] Karijolich, J & Yu, Y.-T. (2011) Converting nonsense codons into sense codons by targeted pseudouridylation. *Nature* **474**, 395–398.
- [21] Fernández, I. S, Ng, C. L, Kelley, A. C, Wu, G, Yu, Y.-T, & Ramakrishnan, V. (2013) Unusual base pairing during the decoding of a stop codon by the ribosome. *Nature* **500**, 107–110.
- [22] Serganov, A & Nudler, E. (2013) A decade of riboswitches. *Cell* **152**, 17–24.
- [23] Carreras, C. W & Santi, D. V. (1995) The catalytic mechanism and structure of thymidylate synthase. *Annual review of biochemistry* **64**, 721–762.
- [24] Kruger, K, Grabowski, P. J, Zaug, A. J, Sands, J, Gottschling, D. E, & Cech, T. R. (1982) Self-splicing rna: autoexcision and autocyclization of the ribosomal rna intervening sequence of tetrahymena. *Cell* **31**, 147–157.
- [25] Guerrier-Takada, C, Gardiner, K, Marsh, T, Pace, N, & Altman, S. (1983) The rna moiety of ribonuclease p is the catalytic subunit of the enzyme. *Cell* **35**, 849–857.
- [26] Cech, T. R. (2012) The rna worlds in context. *Cold Spring Harbor perspectives in biology* **4**, a006742.
- [27] Batey, R. T, Rambo, R. P, & Doudna, J. A. (1999) Tertiary motifs in rna structure and folding. *Angewandte Chemie International Edition* **38**, 2326–2343.
- [28] Görlich, D & Kutay, U. (1999) Transport between the cell nucleus and the cytoplasm. *Annual review of cell and developmental biology* **15**, 607–660.
- [29] Knoop, V. (2011) When you can't trust the dna: Rna editing changes transcript sequences. *Cellular and Molecular Life Sciences* **68**, 567–586.
- [30] Su, A & Randau, L. (2011) A-to-i and c-to-u editing within transfer rnas. *Biochemistry (Moscow)* **76**, 932–937.
- [31] Smith, C. K, Withka, J. M, & Regan, L. (1994) A thermodynamic scale for the beta.-sheet forming tendencies of the amino acids. *Biochemistry* **33**, 5510–5517.
- [32] Kim, C. A & Berg, J. M. (1993) Thermodynamic β -sheet propensities measured using a zinc-finger host peptide. *Nature* **362**, 267–270.
- [33] Li, S.-C, Goto, N. K, Williams, K. A, & Deber, C. M. (1996) Alpha-helical, but not beta-sheet, propensity of proline is determined by peptide environment. *Proceedings of the National Academy of Sciences of the United States of America* **93**, 6676–6681.
- [34] Butcher, S. E & Pyle, A. M. (2011) The molecular interactions that stabilize rna tertiary structure: Rna motifs, patterns, and networks. *Accounts of chemical research* **44**, 1302–1311.

- [35] Dethoff, E. A, Chugh, J, Mustoe, A. M, & Al-Hashimi, H. M. (2012) Functional complexity and regulation through rna dynamics. *Nature* **482**, 322–330.
- [36] Jovine, L, Djordjevic, S, & Rhodes, D. (2000) The crystal structure of yeast phenylalanine tRNA at 2.0 Å resolution: cleavage by Mg(2+) in 15-year old crystals. *Journal of Molecular Biology* **301**, 401–14.
- [37] SHI, H & MOORE, P. B. (2000) The crystal structure of yeast phenylalanine trna at 1.93 [angstrom capital a, ring] resolution: A classic structure revisited. *RNA* **6**, 1091–1105.
- [38] Müller-Esterl, W. (2004) Biochemie. *Eine Einführung für Mediziner und Naturwissenschaftler. Spektrum.*
- [39] Motorin, Y & Helm, M. (2010) trna stabilization by modified nucleotides. *Biochemistry* **49**, 4934–4944.
- [40] Shi, H & Moore, P. B. (2000) The crystal structure of yeast phenylalanine tRNA at 1.93 Å resolution : a classic structure revisited . The crystal structure of yeast phenylalanine tRNA at 1.93 Å resolution : A classic structure revisited. *RNA* **6**, 1091–1105.
- [41] Xiong, Y & Steitz, T. A. (2004) Mechanism of transfer rna maturation by cca-adding enzyme without using an oligonucleotide template. *Nature* **430**, 640–645.
- [42] Wilusz, J. E, Whipple, J. M, Phizicky, E. M, & Sharp, P. A. (2011) trnas marked with ccacca are targeted for degradation. *Science* **334**, 817–821.
- [43] Helm, M, Brulé, H, Friede, D, Giegé, R, Pütz, D, & Florentz, C. (2000) Search for characteristic structural features of mammalian mitochondrial trnas. *RNA* **6**, 1356–1379.
- [44] Gray, M. W, Burger, G, & Lang, B. F. (2001) The origin and early evolution of mitochondria. *Genome Biol* **2**, 1018–1.
- [45] Helm, M, Brulé, H, Degoul, F, Cepanec, C, Leroux, J.-P, Giegé, R, & Florentz, C. (1998) The presence of modified nucleotides is required for cloverleaf folding of a human mitochondrial trna. *Nucleic Acids Research* **26**, 1636–1643.
- [46] Kobitski, A. Y, Hengesbach, M, Helm, M, & Nienhaus, G. U. (2008) Sculpting an RNA Conformational Energy Landscape by a Methyl Group Modification - A Single-Molecule FRET Study. *Angewandte Chemie International Edition* **47**, 4326–4330.
- [47] Helm, M, Giegé, R, & Florentz, C. (1999) A watson-crick base-pair-disrupting methyl group (m1a9) is sufficient for cloverleaf folding of human mitochondrial trnals. *Biochemistry* **38**, 13338–13346.
- [48] Ellington, A. D & Szostak, J. W. (1990) In vitro selection of rna molecules that bind specific ligands. *Nature* **346**, 818–822.
- [49] Tuerk, C & Gold, L. (1990) Systematic evolution of ligands by exponential enrichment: Rna ligands to bacteriophage t4 dna polymerase. *Science* **249**, 505–510.
- [50] Winkler, W, Nahvi, A, & Breaker, R. R. (2002) Thiamine derivatives bind messenger rnas directly to regulate bacterial gene expression. *Nature* **419**, 952–956.
- [51] Mandal, M, Boese, B, Barrick, J. E, Winkler, W. C, & Breaker, R. R. (2003) Riboswitches control fundamental biochemical pathways in bacillus subtilis and other bacteria. *Cell* **113**, 577–586.
- [52] Lu, C, Ding, F, Chowdhury, A, Pradhan, V, Tomsic, J, Holmes, W. M, Henkin, T. M, & Ke,

- A. (2010) Sam recognition and conformational switching mechanism in the bacillus subtilis yitj s box/sam-i riboswitch. *Journal of Molecular Biology* **404**, 803–818.
- [53] Wallace, A. C, Laskowski, R. A, & Thornton, J. M. (1995) Ligplot: a program to generate schematic diagrams of protein-ligand interactions. *Protein engineering* **8**, 127–134.
- [54] Haller, A, Rieder, U, Aigner, M, Blanchard, S. C, & Micura, R. (2011) Conformational capture of the SAM-II riboswitch. *Nature chemical biology* **7**, 393–400.
- [55] Heppell, B, Blouin, S, Dussault, A.-M, Mulhbach, J, Ennifar, E, Penedo, J. C, & Lafontaine, D. A. (2011) Molecular insights into the ligand-controlled organization of the sam-i riboswitch. *Nature chemical biology* **7**, 384–392.
- [56] Wood, S, Ferré-D'Amaré, A. R, & Rueda, D. (2012) Allosteric tertiary interactions preorganize the c-di-GMP riboswitch and accelerate ligand binding. *ACS Chemical Biology* **7**, 920–7.
- [57] Fiegand, L. R, Garst, A. D, Batey, R. T, & Nesbitt, D. J. (2012) Single-molecule studies of the lysine riboswitch reveal effector-dependent conformational dynamics of the aptamer domain. *Biochemistry* **51**, 9223–33.
- [58] Haller, A, Altman, R. B, Soulière, M. F, Blanchard, S. C, & Micura, R. (2013) Folding and ligand recognition of the TPP riboswitch aptamer at single-molecule resolution. *Proceedings of the National Academy of Sciences of the United States of America* **110**, 4188–4193.
- [59] Soulière MF, Altman RB, S. V. H. A. B. S. M. R. (2013) Tuning a riboswitch response through structural extension of a pseudoknot. *Proceedings of the National Academy of Sciences of the United States of America* **110**, E3256–64.
- [60] Dalgarno, P. a, Bordello, J, Morris, R, St-Pierre, P, Dubé, A, Samuel, I. D. W, Lafontaine, D. a, & Penedo, J. C. (2013) Single-molecule chemical denaturation of riboswitches. *Nucleic Acids Research* **41**, 4253–65.
- [61] Winkler, W. C, Nahvi, A, Sudarsan, N, Barrick, J. E, & Breaker, R. R. (2003) An mrna structure that controls gene expression by binding s-adenosylmethionine. *Nature Structural & Molecular Biology* **10**, 701–707.
- [62] Lim, J, Winkler, W. C, Nakamura, S, Scott, V, & Breaker, R. R. (2006) Molecular-recognition characteristics of sam-binding riboswitches. *Angewandte Chemie International Edition* **45**, 964–968.
- [63] Tomšič, J, McDaniel, B. A, Grundy, F. J, & Henkin, T. M. (2008) Natural variability in s-adenosylmethionine (sam)-dependent riboswitches: S-box elements in bacillus subtilis exhibit differential sensitivity to sam in vivo and in vitro. *Journal of Bacteriology* **190**, 823–833.
- [64] Davis, F. F & Allen, F. W. (1957) Ribonucleic acids from yeast which contain a fifth nucleotide. *Journal of Biological Chemistry* **227**, 907–915.
- [65] Mueller, E. G & Ferre-D'Amare, A. R. (2009) Pseudouridine formation, the most common transglycosylation in rna. *DNA and RNA Modification Enzymes: Structure, Mechanism, Function and Evolution* pp. 363–376.
- [66] Davis, D. R. (1995) Stabilization of rna stacking by pseudouridine. *Nucleic Acids Research* **23**, 5020–5026.
- [67] Hall, K. B & McLaughlin, L. W. (1992) Properties of pseudouridine n1 imino protons located in the major groove of an a-form rna duplex. *Nucleic Acids Research* **20**, 1883–1889.

- [68] Newby, M. I & Greenbaum, N. L. (2002) Sculpting of the spliceosomal branch site recognition motif by a conserved pseudouridine. *Nature Structural & Molecular Biology* **9**, 958–965.
- [69] Newby, M. I & Greenbaum, N. L. (2002) Investigation of overhauser effects between pseudouridine and water protons in rna helices. *Proceedings of the National Academy of Sciences* **99**, 12697–12702.
- [70] Kierzek, E, Malgowska, M, Lisowiec, J, Turner, D. H, Gdaniec, Z, & Kierzek, R. (2014) The contribution of pseudouridine to stabilities and structure of rnas. *Nucleic Acids Research* **42**, 3492–3501.
- [71] Arnez, J. G & Steitz, T. A. (1994) Crystal structure of unmodified trnagln complexed with glutamyl-trna synthetase and atp suggests a possible role for pseudo-uridines in stabilization of rna structure. *Biochemistry* **33**, 7560–7567.
- [72] Charette, M & Gray, M. W. (2000) Pseudouridine in rna: what, where, how, and why. *IUBMB life* **49**, 341–351.
- [73] Hamma, T & Ferré-D'Amaré, A. R. (2006) Pseudouridine synthases. *Chemistry & biology* **13**, 1125–1135.
- [74] Ge, J & Yu, Y.-T. (2013) RNA pseudouridylation: new insights into an old modification. *Trends in biochemical sciences* **38**, 210–8.
- [75] Spenkuch, F, Motorin, Y, & Helm, M. (2014) Pseudouridine: Still mysterious, but never a fake (uridine)! *invited to RNA Biology*.
- [76] Hoang, C & Ferré-d'Aamaré, A. R. (2001) Cocrystal structure of a tRNA Psi55 pseudouridine synthase: Nucleotide flipping by an RNA-modifying enzyme. *Cell* **107**, 929–939.
- [77] Nobles, K. N, Yarian, C. S, Liu, G, Guenther, R. H, & Agris, P. F. (2002) Highly conserved modified nucleosides influence Mg²⁺-dependent tRNA folding. *Nucleic Acids Research* **30**, 4751–4760.
- [78] Berg, Jeremy M and Tymoczko, John L and Stryer, Lubert, ed. (2002) *Biochemistry*. (WH Freeman, New York).
- [79] Matthews, D, Villafranca, J, Janson, C, Smith, W, Welsh, K, & Freer, S. (1990) Stereochemical mechanism of action for thymidylate synthase based on the x-ray structure of the covalent inhibitory ternary complex with 5-fluoro-2'-deoxyuridylate and 5, 10-methylenetetrahydrofolate. *Journal of molecular biology* **214**, 937–948.
- [80] Reinisch, K. M, Chen, L, Verdine, G. L, & Lipscomb, W. N. (1995) The crystal structure of haelll methyltransferase covalently complexed to dna: An extrahelical cytosine and rearranged base pairing. *Cell* **82**, 143–153.
- [81] Lee, T. T, Agarwalla, S, & Stroud, R. M. (2005) A unique rna fold in the ruma-rna-cofactor ternary complex contributes to substrate selectivity and enzymatic function. *Cell* **120**, 599–611.
- [82] Alian, A, Lee, T. T, Griner, S. L, Stroud, R. M, & Finer-Moore, J. (2008) Structure of a trma-rna complex: A consensus rna fold contributes to substrate selectivity and catalysis in m5u methyltransferases. *Proceedings of the National Academy of Sciences of the United States of America* **105**, 6876–6881.
- [83] Motorin, Y, Lyko, F, & Helm, M. (2010) 5-methylcytosine in rna: detection, enzymatic formation and biological functions. *Nucleic Acids Research* **38**, 1415–1430.

- [84] Longley, D. B, Harkin, D. P, & Johnston, P. G. (2003) 5-fluorouracil: mechanisms of action and clinical strategies. *Nature Reviews Cancer* **3**, 330–338.
- [85] Santi, D. V & Hardy, L. W. (1987) Catalytic mechanism and inhibition of trna (uracil-5-) methyltransferase: evidence for covalent catalysis. *Biochemistry* **26**, 8599–8606.
- [86] Gu, X & Santi, D. V. (1992) Covalent adducts between trna (m5u54)-methyltransferase and rna substrates. *Biochemistry* **31**, 10295–10302.
- [87] Osterman, D. G, DePillis, G. D, Wu, J. C, Matsuda, A, & Santi, D. V. (1988) 5-fluorocytosine in dna is a mechanism-based inhibitor of hhai methylase. *Biochemistry* **27**, 5204–5210.
- [88] Friedman, S & Ansari, N. (1992) Binding of the ecorii methyltransferase to 5-fluorocytosine-containing dna. isolation of a bound peptide. *Nucleic Acids Research* **20**, 3241–3248.
- [89] Klimasauskas, S, Kumar, S, Roberts, R. J, & Cheng, X. (1994) Hhal methyltransferase flips its target base out of the dna helix. *Cell* **76**, 357–369.
- [90] Liu, Y & Santi, D. V. (2000) m5c rna and m5c dna methyl transferases use different cysteine residues as catalysts. *Proceedings of the National Academy of Sciences of the United States of America* **97**, 8263–8265.
- [91] Walbott, H, Husson, C, Auxilien, S, & Golinelli-Pimpaneau, B. (2007) Cysteine of sequence motif vi is essential for nucleophilic catalysis by yeast trna m5c methyltransferase. *RNA* **13**, 967–973.
- [92] Tiraby, M, Cazaux, C, Baron, M, Drocourt, D, Reynes, J.-P, & Tiraby, G. (1998) Concomitant expression of e. coli cytosine deaminase and uracil phosphoribosyltransferase improves the cytotoxicity of 5-fluorocytosine. *FEMS microbiology letters* **167**, 41–49.
- [93] Vermes, A, Guchelaar, H.-J, & Dankert, J. (2000) Flucytosine: a review of its pharmacology, clinical indications, pharmacokinetics, toxicity and drug interactions. *Journal of Antimicrobial Chemotherapy* **46**, 171–179.
- [94] Pritchard, D. M, Watson, A. J, Potten, C. S, Jackman, A. L, & Hickman, J. A. (1997) Inhibition by uridine but not thymidine of p53-dependent intestinal apoptosis initiated by 5-fluorouracil: evidence for the involvement of rna perturbation. *Proceedings of the National Academy of Sciences* **94**, 1795–1799.
- [95] Gustavsson, M & Ronne, H. (2008) Evidence that trna modifying enzymes are important in vivo targets for 5-fluorouracil in yeast. *RNA* **14**, 666–674.
- [96] Pettersen, H. S, Visnes, T, Vågbo, C. B, Svaasand, E. K, Dosest, B, Slupphaug, G, Kavli, B, & Krokan, H. E. (2011) Ung-initiated base excision repair is the major repair route for 5-fluorouracil in dna, but 5-fluorouracil cytotoxicity depends mainly on rna incorporation. *Nucleic acids research* **39**, 8430–8444.
- [97] Kammen, H. O, Marvel, C. C, Hardy, L, & Penhoet, E. E. (1988) Purification, structure, and properties of escherichia coli trna pseudouridine synthase i. *Journal of Biological Chemistry* **263**, 2255–2263.
- [98] Samuelsson, T. (1991) Interactions of transfer RNA pseudouridine synthases with RNAs substituted with fluorouracil. *Nucleic Acids Research* **19**, 6139–6144.
- [99] Patton, J. R. (1993) Ribonucleoprotein particle assembly and modification of u2 small nuclear rna containing 5-fluorouridine. *Biochemistry* **32**, 8939–8944.

- [100] L Huang, M Pookanjanatavip, X. G. D. V. S. (1998) A conserved aspartate of trna pseudouridine synthase is essential for activity and a probable nucleophilic catalyst. *Biochemistry* **37**, 344–51.
- [101] Gu, X, Liu, Y, & Santi, D. V. (1999) The mechanism of pseudouridine synthase I as deduced from its interaction with 5-fluorouracil-tRNA. *Proceedings of the National Academy of Sciences of the United States of America* **96**, 14270–5.
- [102] Kamalampeta, R, Keffer-Wilkes, L. C, & Kothe, U. (2013) trna binding, positioning, and modification by the pseudouridine synthase pus10. *Journal of Molecular Biology* **425**, 3863–3874.
- [103] Pan, H, Agarwalla, S, Moustakas, D. T, Finer-Moore, J, & Stroud, R. M. (2003) Structure of tRNA pseudouridine synthase TruB and its RNA complex: RNA recognition through a combination of rigid docking and induced fit. *Proceedings of the National Academy of Sciences of the United States of America* **100**, 12648–53.
- [104] Phannachet, K & Huang, R. H. (2004) Conformational change of pseudouridine 55 synthase upon its association with RNA substrate. *Nucleic Acids Research* **32**, 1422–9.
- [105] Phannachet, K, Elias, Y, & Huang, R. H. (2005) Dissecting the roles of a strictly conserved tyrosine in substrate recognition and catalysis by pseudouridine 55 synthase. *Biochemistry* **44**, 15488–94.
- [106] Hoang, C, Chen, J, Vizthum, C. a, Kandel, J. M, Hamilton, C. S, Mueller, E. G, & Ferré-D'Amaré, A. R. (2006) Crystal structure of pseudouridine synthase RluA: indirect sequence readout through protein-induced RNA structure. *Molecular cell* **24**, 535–45.
- [107] Alian, A, DeGiovanni, A, Griner, S. L, Finer-Moore, J. S, & Stroud, R. M. (2009) Crystal structure of an rluf-rna complex: A base-pair rearrangement is the key to selectivity of rluf for u2604 of the ribosome. *Journal of Molecular Biology* **388**, 785–800.
- [108] Spedalieri, C. J. (2004) Not all pseudouridine synthases are potently inhibited by RNA containing 5-fluorouridine. *RNA* **10**, 192–199.
- [109] Hamilton, C. S, Greco, T. M, Vizthum, C. A, Ginter, J. M, Johnston, M. V, & Mueller, E. G. (2006) Mechanistic investigations of the pseudouridine synthase RluA using RNA containing 5-fluorouridine. *Biochemistry* **45**, 12029–12038.
- [110] McDonald, M. K, Miracco, E. J, Chen, J, Xie, Y, & Mueller, E. G. (2011) The handling of the mechanistic probe 5-fluorouridine by the pseudouridine synthase TruA and its consistency with the handling of the same probe by the pseudouridine synthases TruB and RluA. *Biochemistry* **50**, 426–36.
- [111] Chan, C. M & Huang, R. H. (2009) Enzymatic characterization and mutational studies of TruD—the fifth family of pseudouridine synthases. *Archives of biochemistry and biophysics* **489**, 15–9.
- [112] Miracco, E. J & Mueller, E. G. (2011) The products of 5-fluorouridine by the action of the pseudouridine synthase trub disfavor one mechanism and suggest another. *Journal of the American Chemical Society* **133**, 11826–9.
- [113] Czudnochowski, N, Ashley, G. W, Santi, D. V, Alian, A, Finer-Moore, J, & Stroud, R. M. (2014) The mechanism of pseudouridine synthases from a covalent complex with rna, and

- alternate specificity for u2605 versus u2604 between close homologs. *Nucleic Acids Research* **42**, 2037–2048.
- [114] Liang, B, Zhou, J, Kahen, E, Terns, R. M, Terns, M. P, & Li, H. (2009) Structure of a functional ribonucleoprotein pseudouridine synthase bound to a substrate rna. *Nature structural & molecular biology* **16**, 740–746.
- [115] Spedaliere, C. J, Hamilton, C. S, & Mueller, E. G. (2000) Functional importance of motif I of pseudouridine synthases: mutagenesis of aligned lysine and proline residues. *Biochemistry* **39**, 9459–65.
- [116] Sibert, B. S, Fischel-Ghodsian, N, & Patton, J. R. (2008) Partial activity is seen with many substitutions of highly conserved active site residues in human pseudouridine synthase 1. *RNA* **14**, 1895–1906.
- [117] Friedt, J, Leavens, F. M, Mercier, E, Wieden, H.-J, & Kothe, U. (2014) An arginine-aspartate network in the active site of bacterial trub is critical for catalyzing pseudouridine formation. *Nucleic Acids Research* **42**, 3857–3870.
- [118] Marmé, N, Knemeyer, J.-P, Sauer, M, & Wolfrum, J. (2003) Inter-and intramolecular fluorescence quenching of organic dyes by tryptophan. *Bioconjugate chemistry* **14**, 1133–1139.
- [119] Brismar, H, Trepte, O, & Ulfhake, B. (1995) Spectra and fluorescence lifetimes of lis-samine rhodamine, tetramethylrhodamine isothiocyanate, texas red, and cyanine 3.18 fluorophores: influences of some environmental factors recorded with a confocal laser scanning microscope. *Journal of Histochemistry & Cytochemistry* **43**, 699–707.
- [120] Buschmann, V, Weston, K. D, & Sauer, M. (2003) Spectroscopic study and evaluation of red-absorbing fluorescent dyes. *Bioconjugate chemistry* **14**, 195–204.
- [121] Rasnik, I, Myong, S, Cheng, W, Lohman, T. M, & Ha, T. (2004) Dna-binding orientation and domain conformation of the e. coli rep helicase monomer bound to a partial duplex junction: single-molecule studies of fluorescently labeled enzymes. *Journal of Molecular Biology* **336**, 395–408.
- [122] Cao, J, Wu, T, Hu, C, Liu, T, Sun, W, Fan, J, & Peng, X. (2012) The nature of the different environmental sensitivity of symmetrical and unsymmetrical cyanine dyes: an experimental and theoretical study. *Physical chemistry chemical physics : PCCP* **14**, 13702–8.
- [123] Levitus, M & Ranjit, S. (2011) Cyanine dyes in biophysical research: the photophysics of polymethine fluorescent dyes in biomolecular environments. *Quarterly Reviews of Biophysics* **44**, 123–151.
- [124] Widengren, J & Schwille, P. (2000) Characterization of Photoinduced Isomerization and Back-Isomerization of the Cyanine Dye Cy5 by Fluorescence Correlation Spectroscopy. *The Journal of Physical Chemistry A* **104**, 6416–6428.
- [125] Hwang, H & Myong, S. (2014) Protein induced fluorescence enhancement (pife) for probing protein–nucleic acid interactions. *Chemical Society Reviews* **43**, 1221–1229.
- [126] Gatzogiannis, E, Chen, Z, Wei, L, Wombacher, R, Kao, Y.-T, Yefremov, G, Cornish, V. W, & Min, W. (2012) Mapping protein-specific micro-environments in live cells by fluorescence lifetime imaging of a hybrid genetic-chemical molecular rotor tag. *Chemical Communications* **48**, 8694–8696.
- [127] Hwang, H, Kim, H, & Myong, S. (2011) Protein induced fluorescence enhancement as a

- single molecule assay with short distance sensitivity. *Proceedings of the National Academy of Sciences of the United States of America* **108**, 7414–7418.
- [128] Norman, D. G, Grainger, R. J, Uhrin, D, & Lilley, D. M. (2000) Location of cyanine-3 on double-stranded dna: importance for fluorescence resonance energy transfer studies. *Biochemistry* **39**, 6317–6324.
- [129] Iqbal, A, Wang, L, Thompson, K. C, Lilley, D. M, & Norman, D. G. (2008) The structure of cyanine 5 terminally attached to double-stranded dna: Implications for fret studies. *Biochemistry* **47**, 7857–7862.
- [130] Ouellet, J, Schorr, S, Iqbal, A, Wilson, T. J, & Lilley, D. M. J. (2011) Orientation of cyanine fluorophores terminally attached to DNA via long, flexible tethers. *Biophysical Journal* **101**, 1148–54.
- [131] Urnavicius, L, McPhee, S. a, Lilley, D. M. J, & Norman, D. G. (2012) The structure of sulfoindocarbocyanine 3 terminally attached to dsDNA via a long, flexible tether. *Biophysical Journal* **102**, 561–8.
- [132] Harvey, B. J & Levitus, M. (2009) Nucleobase-specific enhancement of cy3 fluorescence. *Journal of Fluorescence* **19**, 443–448.
- [133] Sanborn, M. E, Connolly, B. K, Gurunathan, K, & Levitus, M. (2007) Fluorescence properties and photophysics of the sulfoindocyanine Cy3 linked covalently to DNA. *The Journal of Physical Chemistry. B* **111**, 11064–74.
- [134] Harvey, B. J, Perez, C, & Levitus, M. (2009) DNA sequence-dependent enhancement of Cy3 fluorescence. *Photochemical & photobiological sciences : Official journal of the European Photochemistry Association and the European Society for Photobiology* **8**, 1105–10.
- [135] Spiriti, J, Binder, J. K, Levitus, M, & van der Vaart, A. (2011) Cy3-DNA stacking interactions strongly depend on the identity of the terminal basepair. *Biophysical Journal* **100**, 1049–57.
- [136] Stennett, E. M, Ma, N, van der Vaart, A, & Levitus, M. (2013) Photophysical and dynamical properties of doubly linked cy3–dna constructs. *The Journal of Physical Chemistry B* **118**, 152–163.
- [137] Sabanayagam, C. R, Eid, J. S, & Meller, A. (2005) Using fluorescence resonance energy transfer to measure distances along individual DNA molecules: corrections due to nonideal transfer. *The Journal of Chemical Physics* **122**, 061103.
- [138] Milas, P, Gamari, B. D, Parrot, L, Krueger, B. P, Rahmanseresht, S, Moore, J, & Goldner, L. S. (2013) Indocyanine dyes approach free rotation at the 3' terminus of a-rna: A comparison with the 5' terminus and consequences for fluorescence resonance energy transfer. *The Journal of Physical Chemistry B* **117**, 8649–8658.
- [139] Ludwig, C, Staatsdruckerei, K. H.-u, & Braumüller, W. (1856) *Diffusion zwischen ungleich erwärmten Orten gleich zusammengesetzter Lösung*. (Aus der KK Hof-und Staatsdruckerei, in Commission bei W. Braumüller, Buchhändler des KK Hofes und der K. Akademie der Wissenschaften).
- [140] Jerabek-Willemsen, M, Wienken, C. J, Braun, D, Baaske, P, & Duhr, S. (2011) Molecular interaction studies using microscale thermophoresis. *Assay and drug development technologies* **9**, 342–353.

- [141] Duhr, S & Braun, D. (2006) Why molecules move along a temperature gradient. *Proceedings of the National Academy of Sciences of the United States of America* **103**, 19678–19682.
- [142] Misra, V. K & Draper, D. E. (2001) A thermodynamic framework for mg²⁺ binding to rna. *Proceedings of the National Academy of Sciences of the United States of America* **98**, 12456–12461.
- [143] Herzog, M. (2012) Ph.D. thesis (Ludwig-Maximilians-University Munich, Germany).
- [144] Schaefer, M, Pollex, T, Hanna, K, Tuorto, F, Meusburger, M, Helm, M, & Lyko, F. (2010) Rna methylation by dnmt2 protects transfer rnas against stress-induced cleavage. *Genes & development* **24**, 1590–1595.
- [145] Helm, M & Alfonzo, J. D. (2014) Posttranscriptional rna modifications: Playing metabolic games in a cell's chemical legoland. *Chemistry & biology* **21**, 174–185.
- [146] Motorin, Y & Helm, M. (2010) tRNA stabilization by modified nucleotides. *Biochemistry* **49**, 4934–44.
- [147] Neumann, P, Lakomek, K, Naumann, P-T, Erwin, W. M, Lauhon, C. T, & Ficner, R. (2014) Crystal structure of a 4-thiouridine synthetase–rna complex reveals specificity of trna u8 modification. *Nucleic acids research* **42**, 6673–6685.
- [148] Gu, X, Yu, M, Ivanetich, K. M, & Santi, D. V. (1998) Molecular recognition of tRNA by tRNA pseudouridine 55 synthase. *Biochemistry* **37**, 339–43.
- [149] Randau, L, Stanley, B. J, Kohlway, A, Mechta, S, Xiong, Y, & Söll, D. (2009) A cytidine deaminase edits c to u in transfer rnas in archaea. *Science* **324**, 657–659.
- [150] Tanaka, Y, Yamagata, S, Kitago, Y. U, Yamada, Y, Chimnaronk, S, Yao, M. I. N, & Tanaka, I. (2009) Deduced RNA binding mechanism of ThiI based on structural and binding analyses of a minimal RNA ligand. *RNA* **15**, 1498–1506.
- [151] Yamagami, R, Yamashita, K, Nishimasu, H, Tomikawa, C, Ochi, A, Iwashita, C, Hirata, A, Ishitani, R, Nureki, O, & Hori, H. (2012) The tRNA recognition mechanism of folate/FAD-dependent tRNA methyltransferase (TrmFO). *The Journal of biological chemistry* **287**, 42480–94.
- [152] McCleverty, C. J, Hornsby, M, Spraggon, G, & Kreuzsch, A. (2007) Crystal structure of human pus10, a novel pseudouridine synthase. *Journal of molecular biology* **373**, 1243–1254.
- [153] Jurkowski, T. P, Shanmugam, R, Helm, M, & Jeltsch, A. (2012) Mapping the trna binding site on the surface of human dnmt2 methyltransferase. *Biochemistry* **51**, 4438–4444.
- [154] Czudnochowski, N, Wang, A. L, Finer-Moore, J, & Stroud, R. M. (2013) In Human Pseudouridine Synthase 1 (hPus1), a C-Terminal Helical Insert Blocks tRNA from Binding in the Same Orientation as in the Pus1 Bacterial Homologue TruA, Consistent with Their Different Target Selectivities. *Journal of Molecular Biology* **1**, 1–13.
- [155] Ishitani, R, Nureki, O, Nameki, N, Okada, N, Nishimura, S, & Yokoyama, S. (2003) Alternative tertiary structure of tRNA for recognition by a posttranscriptional modification enzyme. *Cell* **113**, 383–94.
- [156] Hur, S & Stroud, R. M. (2007) How U38, 39, and 40 of many tRNAs become the targets for pseudouridylation by TruA. *Molecular cell* **26**, 189–203.
- [157] Kurschat, W. C, Müller, J, Wombacher, R, Helm, M, & Mu, J. (2005) Optimizing splinted ligation of highly structured small RNAs Optimizing splinted ligation of highly structured small RNAs. *RNA* **11**, 1909–1914.

- [158] Kobitski, A. Y, Hengesbach, M, Seidu-Larry, S, Dammertz, K, Chow, C. S, van Aerschot, A, Nienhaus, G. U, & Helm, M. (2011) Single-molecule FRET reveals a cooperative effect of two methyl group modifications in the folding of human mitochondrial tRNA(Lys). *Chemistry & Biology* **18**, 928–36.
- [159] Chen, J & Patton, J. R. (1999) Cloning and characterization of a mammalian pseudouridine synthase. *RNA* **5**, 409–419.
- [160] Motorin, Y & Grosjean, H. (1999) Multisite-specific trna: m5c-methyltransferase (trm4) in yeast *saccharomyces cerevisiae*: identification of the gene and substrate specificity of the enzyme. *RNA* **5**, 1105–1118.
- [161] Becker, H, Motorin, Y, Planta, R, & Grosjean, H. (1997) The yeast gene ynl292w encodes a pseudouridine synthase (pus4) catalyzing the formation of ψ 55 in both mitochondrial and cytoplasmic trnas. *Nucleic Acids Research* **25**, 4493–4499.
- [162] Roovers, M, Wouters, J, Bujnicki, J. M, Tricot, C, Stalon, V, Grosjean, H, & Droogmans, L. (2004) A primordial rna modification enzyme: the case of trna (m1a) methyltransferase. *Nucleic Acids Research* **32**, 465–476.
- [163] Guelorget, A, Roovers, M, Guérineau, V, Barbey, C, Li, X, & Golinelli-Pimpaneau, B. (2010) Insights into the hyperthermostability and unusual region-specificity of archaeal *pyrococcus abyssi* trna m1a57/58 methyltransferase. *Nucleic Acids Research* **38**, 6206–6218.
- [164] Weiss, J. N. (1997) The hill equation revisited: uses and misuses. *The FASEB Journal* **11**, 835–841.
- [165] Dong, A, Yoder, J. A, Zhang, X, Zhou, L, Bestor, T. H, & Cheng, X. (2001) Structure of human dnmt2, an enigmatic dna methyltransferase homolog that displays denaturant-resistant binding to dna. *Nucleic Acids Research* **29**, 439–448.
- [166] Arluison, V, Buckle, M, & Grosjean, H. (1999) Pseudouridine synthetase Pus1 of *Saccharomyces cerevisiae*: kinetic characterisation, tRNA structural requirement and real-time analysis of its complex with tRNA. *Journal of Molecular Biology* **289**, 491–502.
- [167] Hamilton, C. S, Spedaliere, C. J, Ginter, J. M, Johnston, M. V, & Mueller, E. G. (2005) The roles of the essential Asp-48 and highly conserved His-43 elucidated by the pH dependence of the pseudouridine synthase TruB. *Archives of biochemistry and biophysics* **433**, 322–34.
- [168] Teimer, R. (2010) Master's thesis (Ruprecht-Karls-University Heidelberg, Germany).
- [169] Nelson, K. E, Clayton, R. A, Gill, S. R, Gwinn, M. L, Dodson, R. J, Haft, D. H, Hickey, E. K, Peterson, J. D, Nelson, W. C, Ketchum, K. A, et al. (1999) Evidence for lateral gene transfer between archaea and bacteria from genome sequence of *thermotoga maritima*. *Nature* **399**, 323–329.
- [170] Bykhovskaya, Y, Casas, K, Mengesha, E, Inbal, A, & Fischel-Ghodsian, N. (2004) Missense mutation in pseudouridine synthase 1 (pus1) causes mitochondrial myopathy and sideroblastic anemia (mlasa). *The American Journal of Human Genetics* **74**, 1303–1308.
- [171] Patton, J. R, Bykhovskaya, Y, Mengesha, E, Bertolotto, C, & Fischel-Ghodsian, N. (2005) Mitochondrial myopathy and sideroblastic anemia (mlasa) missense mutation in the pseudouridine synthase 1 (pus1) gene is associated with the loss of trna pseudouridylation. *Journal of Biological Chemistry* **280**, 19823–19828.

- [172] Zhao, X, Patton, J. R, Davis, S. L, Florence, B, Ames, S. J, & Spanjaard, R. A. (2004) Regulation of nuclear receptor activity by a pseudouridine synthase through posttranscriptional modification of steroid receptor rna activator. *Molecular cell* **15**, 549–558.
- [173] Zhao, X, Patton, J. R, Ghosh, S. K, Fischel-Ghodsian, N, Shen, L, & Spanjaard, R. A. (2007) Pus3p-and pus1p-dependent pseudouridylation of steroid receptor rna activator controls a functional switch that regulates nuclear receptor signaling. *Molecular Endocrinology* **21**, 686–699.
- [174] Huet, T, Miannay, F-A, Patton, J. R, & Thore, S. (2014) Steroid receptor rna activator (sra) modification by the human pseudouridine synthase 1 (hpus1p): Rna binding, activity, and atomic model. *PLoS one* **9**, e94610.
- [175] Motorin, Y, Keith, G, Simon, C, Foiret, D, Simos, G, Hurt, E, & Grosjean, H. (1998) The yeast trna: pseudouridine synthase pus1p displays a multisite substrate specificity. *RNA* **4**, 856–869.
- [176] Massenet, S, Motorin, Y, Lafontaine, D. L, Hurt, E. C, Grosjean, H, & Branlant, C. (1999) Pseudouridine mapping in the *Saccharomyces cerevisiae* spliceosomal u small nuclear rnas (snrnas) reveals that pseudouridine synthase pus1p exhibits a dual substrate specificity for u2 snrna and trna. *Molecular and cellular biology* **19**, 2142–2154.
- [177] Behm-Ansmant, I, Massenet, S, Immel, F, Patton, J. R, Motorin, Y, & Branlant, C. (2006) A previously unidentified activity of yeast and mouse rna: pseudouridine synthases 1 (pus1p) on trnas. *RNA* **12**, 1583–1593.
- [178] Sibert, B. S & Patton, J. R. (2012) Pseudouridine synthase 1: a site-specific synthase without strict sequence recognition requirements. *Nucleic Acids Research* **40**, 2107–18.
- [179] Hengesbach, M, Voigts-Hoffmann, F, Hofmann, B, & Helm, M. (2010) Formation of a stalled early intermediate of pseudouridine synthesis monitored by real-time FRET. *RNA* **16**, 610–620.
- [180] Sissler, M, Helm, M, Frugier, M, Giegé, R, & Florentz, C. (2004) Aminoacylation properties of pathology-related human mitochondrial trnalys variants. *RNA* **10**, 841–853.
- [181] Hofmann, B. (2010) Master's thesis (Ruprecht-Karls-University Heidelberg, Germany).
- [182] Hengesbach, M. (2009) Ph.D. thesis (Ruprecht-Karls-University Heidelberg, Germany).
- [183] Serebrov, V, Vassilenko, K, Kholod, N, Gross, H. J, & Kisselev, L. (1998) Mg²⁺ binding and structural stability of mature and in vitro synthesized unmodified *Escherichia coli* trnaphe. *Nucleic Acids Research* **26**, 2723–2728.
- [184] Motorin, Y, Burhenne, J, Teimer, R, Koynov, K, Willnow, S, Weinhold, E, & Helm, M. (2011) Expanding the chemical scope of rna: methyltransferases to site-specific alkylation of rna for click labeling. *Nucleic acids research* **39**, 1943–1952.
- [185] Phang, S & Stokes, R. (1980) Density, viscosity, conductance, and transference number of concentrated aqueous magnesium chloride at 25 c. *Journal of Solution Chemistry* **9**, 497–505.
- [186] Dhont, J. K, Wiegand, S, Duhr, S, & Braun, D. (2007) Thermodiffusion of charged colloids: Single-particle diffusion. *Langmuir* **23**, 1674–1683.
- [187] Tsutomu, S, Asutaka, N, & Takeo, S. (2011) Human mitochondrial diseases caused by lack of taurine modification in mitochondrial trnas. *Wiley Interdisciplinary Reviews: RNA* **2**, 376–386.

- [188] Boyapati, V. K, Huang, W, Spedale, J, & Aboul-ela, F. (2012) Basis for ligand discrimination between on and off state riboswitch conformations: The case of the sam-i riboswitch. *RNA* **18**, 1230–1243.
- [189] Samanta, A. (2012) Ph.D. thesis (Heidelberg University).
- [190] Dominissini, D, Moshitch-Moshkovitz, S, Schwartz, S, Salmon-Divon, M, Ungar, L, Osenberg, S, Cesarkas, K, Jacob-Hirsch, J, Amariglio, N, Kupiec, M, Sorek, R, & Rechavi, G. (2012) Topology of the human and mouse m6A RNA methylomes revealed by m6A-seq. *Nature* **485**, 201–206.
- [191] Meyer, K, Saletore, Y, Zumbo, P, Elemento, O, Mason, C, & Jaffrey, S. (2012) Comprehensive analysis of mrna methylation reveals enrichment in 3' utrs and near stop codons. *Cell* **149**, 1635–1646.
- [192] Urbonavicius, J, Durand, J. M, & Bjork, G. R. (2002) Three modifications in the D and T arms of tRNA influence translation in Escherichia coli and expression of virulence genes in Shigella flexneri. *Journal of Bacteriology* **184**, 5348–5357.
- [193] Wu, G, Yu, A. T, Kantartzis, A, & Yu, Y.-T. (2011) Functions and mechanisms of spliceosomal small nuclear RNA pseudouridylation. *Wiley Interdisciplinary Reviews: RNA* **2**, 571–581.
- [194] Ishida, K, Kunibayashi, T, Tomikawa, C, Ochi, A, Kanai, T, Hirata, A, Iwashita, C, & Hori, H. (2011) Pseudouridine at position 55 in tRNA controls the contents of other modified nucleotides for low-temperature adaptation in the extreme-thermophilic eubacterium Thermus thermophilus. *Nucleic Acids Research* **39**, 2304–2318.
- [195] Sakakibara, Y & Chow, C. S. (2012) Role of Pseudouridine in Structural Rearrangements of Helix 69 During Bacterial Ribosome Assembly. *ACS Chemical Biology* **7**, 871–878.
- [196] Santi, D. V, McHenry, C. S, & Sommer, H. (1974) Mechanism of interaction of thymidylate synthetase with 5-fluorodeoxyuridylate. *Biochemistry* **13**, 471–481.
- [197] Friendewey, D. A, Kladianos, D. M, Moore, V. G, & Kaiser, I. I. (1982) Loss of trna 5-methyluridine methyltransferase and pseudouridine synthetase activities in 5-fluorouracil and 1-(tetrahydro-2-furanyl)-5-fluorouracil (ftorafur)-treated escherichia coli. *Biochimica et Biophysica Acta (BBA)-Gene Structure and Expression* **697**, 31–40.
- [198] Huang, L, Pookanjanatavip, M, Gu, X, & Santi, D. V. (1998) A conserved aspartate of trna pseudouridine synthase is essential for activity and a probable nucleophilic catalyst. *Biochemistry* **37**, 344–351.
- [199] Sampson, J. R & Uhlenbeck, O. C. (1988) Biochemical and physical characterization of an unmodified yeast phenylalanine transfer RNA transcribed in vitro. *Proceedings of the National Academy of Sciences of the United States of America* **85**, 1033–7.
- [200] Huber, R, Langworthy, T. A, König, H, Thomm, M, Woese, C. R, Sleytr, U. B, & Stetter, K. O. (1986) Thermotoga maritima sp. nov. represents a new genus of unique extremely thermophilic eubacteria growing up to 90 c. *Archives of Microbiology* **144**, 324–333.
- [201] Wright, J. R, Keffer-Wilkes, L. C, Dobing, S. R, & Kothe, U. (2011) Pre-steady-state kinetic analysis of the three Escherichia coli pseudouridine synthases TruB, TruA, and RluA reveals uniformly slow catalysis. *RNA* **17**, 2074–84.
- [202] Uter, N. T & Perona, J. J. (2004) Long-range intramolecular signaling in a trna synthetase

- complex revealed by pre-steady-state kinetics. *Proceedings of the National Academy of Sciences of the United States of America* **101**, 14396–14401.
- [203] Rodríguez-Hernández, A & Perona, J. J. (2011) Heat maps for intramolecular communication in an rnp enzyme encoding glutamine. *Structure* **19**, 386–396.
- [204] Baaske, P, Wienken, C. J, Reineck, P, Duhr, S, & Braun, D. (2010) Optical thermophoresis for quantifying the buffer dependence of aptamer binding. *Angewandte Chemie (International ed. in English)* **49**, 2238–41.
- [205] Seidel, S. a. I, Dijkman, P. M, Lea, W. a, van den Bogaart, G, Jerabek-Willemsen, M, Lazic, A, Joseph, J. S, Srinivasan, P, Baaske, P, Simeonov, A, Katritch, I, Melo, F. a, Ladbury, J. E, Schreiber, G, Watts, A, Braun, D, & Duhr, S. (2012) Microscale thermophoresis quantifies biomolecular interactions under previously challenging conditions. *Methods* **59**, 301–315.
- [206] Puglisi, J. D & Tinoco Jr, I. (1989) [22] absorbance melting curves of rna. *Methods in enzymology* **180**, 304–325.
- [207] Hoang, C, Hamilton, C. S, G Mueller, E, & Ferré-D'Amaré, A. R. (2005) Precursor complex structure of pseudouridine synthase trub suggests coupling of active site perturbations to an rna-sequestering peripheral protein domain. *Protein science* **14**, 2201–2206.
- [208] Ramamurthy, V, Swann, S. L, Paulson, J. L, Spedaliere, C. J, & Mueller, E. G. (1999) Critical aspartic acid residues in pseudouridine synthases. *The Journal of Biological Chemistry* **274**, 22225–30.
- [209] Daher, M & Rueda, D. (2012) Fluorescence characterization of the transfer RNA-like domain of transfer messenger RNA in complex with small binding protein B. *Biochemistry* **51**, 3531–8.
- [210] Pagano, J. M, Clingman, C. C, & Ryder, S. P. (2011) Quantitative approaches to monitor protein-nucleic acid interactions using fluorescent probes. *RNA* **17**, 14–20.
- [211] Steimer, L, Wurm, J. P, Linden, M. H, Rudolph, M. G, Wöhnert, J, & Klostermeier, D. (2013) Recognition of two distinct elements in the RNA substrate by the RNA-binding domain of the T. thermophilus DEAD box helicase Hera. *Nucleic Acids Research* **41**, 6259–6272.
- [212] Sorokina, M, Koh, H.-r, Patel, S. S, & Ha, T. (2009) Fluorescent Lifetime Trajectories of a Single Fluorophore Reveal Reaction. *Journal of the American Chemical Society* **131**, 9630–9631.
- [213] Grohmann, D, Klose, D, Klare, J. P, Kay, C. W. M, Steinhoff, H.-J, & Werner, F. (2010) RNA-binding to archaeal RNA polymerase subunits F/E: a DEER and FRET study. *Journal of the American Chemical Society* **132**, 5954–5.
- [214] Hsieh, J, Koutmou, K. S, Rueda, D, Koutmos, M, Walter, N. G, & Fierke, C. a. (2010) A divalent cation stabilizes the active conformation of the B. subtilis RNase P x pre-tRNA complex: a role for an inner-sphere metal ion in RNase P. *Journal of Molecular Biology* **400**, 38–51.
- [215] Cristóvão, M, Sisamakís, E, Hingorani, M. M, Marx, A. D, Jung, C. P, Rothwell, P. J, Seidel, C. a. M, & Friedhoff, P. (2012) Single-molecule multiparameter fluorescence spectroscopy reveals directional MutS binding to mismatched bases in DNA. *Nucleic Acids Research* **40**, 5448–64.
- [216] Doetsch, M, Stampfl, S, Fürtig, B, Beich-Frandsen, M, Saxena, K, Lybecker, M, & Schroeder,

- R. (2013) Study of *E. coli* Hfq's RNA annealing acceleration and duplex destabilization activities using substrates with different GC-contents. *Nucleic Acids Research* **41**, 487–97.
- [217] Kealey, J. T & Santi, D. V. (1991) Identification of the catalytic nucleophile of trna (m5u54) methyltransferase. *Biochemistry* **30**, 9724–9728.
- [218] Hamdane, D, Argentini, M, Cornu, D, Myllykallio, H, Skouloubris, S, Hui-Bon-Hoa, G, & Golinelli-Pimpaneau, B. (2011) Insights into folate/fad-dependent trna methyltransferase mechanism role of two highly conserved cysteines in catalysis. *Journal of Biological Chemistry* **286**, 36268–36280.
- [219] Chen, L, MacMillan, A. M, Chang, W, Ezaz-Nikpay, K, Lane, W. S, & Verdine, G. L. (1991) Direct identification of the active-site nucleophile in a dna (cytosine-5)-methyltransferase. *Biochemistry* **30**, 11018–11025.
- [220] Smith, S. S, Kaplan, B. E, Sowers, L. C, & Newman, E. M. (1992) Mechanism of human methyl-directed dna methyltransferase and the fidelity of cytosine methylation. *Proceedings of the National Academy of Sciences of the United States of America* **89**, 4744–4748.
- [221] Hanck, T, Schmidt, S, & Fritz, H.-J. (1993) Sequence-specific and mechanism-based crosslinking of dcm dna cytosine-c5 methyltransferase of *e. coli* k-12 to synthetic oligonucleotides containing 5-fluoro-2'-deoxycytidine. *Nucleic Acids Research* **21**, 303–309.
- [222] Vilkaitis, G, Serva, S, Weinhold, E, Klimašauskas, S, et al. (2001) The mechanism of dna cytosine-5 methylation kinetic and mutational dissection of hhai methyltransferase. *Journal of Biological Chemistry* **276**, 20924–20934.
- [223] Matthews, D, Appelt, K, Oatley, S, & Xuong, N. H. (1990) Crystal structure of *escherichia coli* thymidylate synthase containing bound 5-fluoro-2'-deoxyuridylate and 10-propargyl-5, 8-dideazafolate. *Journal of Molecular Biology* **214**, 923–936.
- [224] Reinisch, K. M, Chen, L, Verdine, G. L, & Lipscomb, W. N. (1994) Crystallization and preliminary crystallographic analysis of a dna (cytosine-5)-methyltransferase from *haemophilus aegyptius* bound covalently to dna. *Journal of Molecular Biology* **238**, 626–629.
- [225] Urbonavičius, J, Jäger, G, & Björk, G. R. (2007) Amino acid residues of the *escherichia coli* trna (m5u54) methyltransferase (trma) critical for stability, covalent binding of trna and enzymatic activity. *Nucleic Acids Research* **35**, 3297–3305.
- [226] Müller, S, Windhof, I. M, Maximov, V, Jurkowski, T, Jeltsch, A, Förstner, K. U, Sharma, C. M, Gräf, R, & Nellen, W. (2013) Target recognition, rna methylation activity and transcriptional regulation of the *dictyostelium discoideum* dnmt2-homologue (dnma). *Nucleic Acids Research* **41**, 8615–8627.
- [227] Stengl, B, Reuter, K, & Klebe, G. (2005) Mechanism and substrate specificity of trna-guanine transglycosylases (tgts): trna-modifying enzymes from the three different kingdoms of life share a common catalytic mechanism. *Chembiochem* **6**, 1926–1939.
- [228] Garcia, G. A, Chervin, S. M, & Kittendorf, J. D. (2009) Identification of the rate-determining step of trna-guanine transglycosylase from *escherichia coli*. *Biochemistry* **48**, 11243–11251.
- [229] Xie, W, Liu, X, & Huang, R. H. (2003) Chemical trapping and crystal structure of a catalytic trna guanine transglycosylase covalent intermediate. *Nature Structural & Molecular Biology* **10**, 781–788.

- [230] Bhuyan, A. K. (2010) On the mechanism of sds-induced protein denaturation. *Biopolymers* **93**, 186–199.
- [231] Otzen, D. (2011) Protein–surfactant interactions: a tale of many states. *Biochimica et Biophysica Acta (BBA)-Proteins and Proteomics* **1814**, 562–591.
- [232] Reshetnyak, Y. K & Burstein, E. A. (2001) Decomposition of protein tryptophan fluorescence spectra into log-normal components. ii. the statistical proof of discreteness of tryptophan classes in proteins. *Biophysical Journal* **81**, 1710–1734.
- [233] Nielsen, M. M, Andersen, K. K, Westh, P, & Otzen, D. E. (2007) Unfolding of beta-sheet proteins in sds. *Biophysical Journal* **92**, 3674–3685.
- [234] Tokuda, T, Calero, M, Matsubara, E, Vidal, R, Kumar, A, Permanne, B, Zlokovic, B, Smith, J, Ladu, M, Rostagno, A, et al. (2000) Lipidation of apolipoprotein e influences its isoform-specific interaction with alzheimer’s amyloid beta peptides. *Biochemical Journal* **348**, 359–365.
- [235] Dovey, H, John, V, Anderson, J, Chen, L, de Saint Andrieu, P, Fang, L, Freedman, S, Folmer, B, Goldbach, E, Holsztynska, E, et al. (2001) Functional gamma-secretase inhibitors reduce beta-amyloid peptide levels in brain. *Journal of neurochemistry* **76**, 173–181.
- [236] Lüders, J, Pyrowolakis, G, & Jentsch, S. (2003) The ubiquitin-like protein hub1 forms sds-resistant complexes with cellular proteins in the absence of atp. *EMBO Reports* **4**, 1169–1174.
- [237] Feig, C, Tchikov, V, Schütze, S, & Peter, M. E. (2007) Palmitoylation of cd95 facilitates formation of sds-stable receptor aggregates that initiate apoptosis signaling. *The EMBO Journal* **26**, 221–231.
- [238] Henkins, K. M, Sokolow, S, Miller, C. A, Vinters, H. V, Poon, W. W, Cornwell, L. B, Saing, T, & Gylys, K. H. (2012) Extensive p-tau pathology and sds-stable p-tau oligomers in alzheimer’s cortical synapses. *Brain Pathology* **22**, 826–833.
- [239] Oberoi, R, Beg, Q. K, Puri, S, Saxena, R, & Gupta, R. (2001) Characterization and wash performance analysis of an sds-stable alkaline protease from a bacillus sp. *World Journal of Microbiology and Biotechnology* **17**, 493–497.
- [240] Joo, H.-S, Kumar, C, Park, G.-C, Paik, S, & Chang, C.-S. (2003) Oxidant and sds-stable alkaline protease from bacillus clausii i-52: production and some properties. *Journal of applied microbiology* **95**, 267–272.
- [241] Wang, J, Sanchez-Rosello, M, Acena, J. L, del Pozo, C, Sorochinsky, A. E, Fustero, S, Soloshonok, V. A, & Liu, H. (2013) Fluorine in pharmaceutical industry: Fluorine-containing drugs introduced to the market in the last decade (2001–2011). *Chemical reviews* **114**, 2432–2506.
- [242] Müller, K, Faeh, C, & Diederich, F. (2007) Fluorine in pharmaceuticals: looking beyond intuition. *Science* **317**, 1881–1886.
- [243] Breiten, B, Lockett, M. R, Sherman, W, Fujita, S, Al-Sayah, M, Lange, H, Bowers, C. M, Heroux, A, Krilov, G, & Whitesides, G. M. (2013) Water networks contribute to enthalpy/entropy compensation in protein–ligand binding. *Journal of the American Chemical Society* **135**, 15579–15584.
- [244] Ren, J, He, Y, Chen, W, Chen, T, Wang, G, Wang, Z, Xu, Z, Luo, X, Zhu, W, Jiang, H, et al. (2014) Thermodynamic and structural characterization of halogen bonding in protein–

- ligand interactions: A case study of pde5 and its inhibitors. *Journal of Medicinal Chemistry* **57**, 3588–3593.
- [245] Champion, C, Guianvarc'h, D, Sénamaud-Beaufort, C, Jurkowska, R. Z, Jeltsch, A, Ponger, L, Arimondo, P. B, & Guieysse-Peugeot, A.-L. (2010) Mechanistic insights on the inhibition of c5 dna methyltransferases by zebularine. *PloS one* **5**, e12388.
- [246] Aitken, C. E, Petrov, A, & Puglisi, J. D. (2010) Single ribosome dynamics and the mechanism of translation. *Annual review of biophysics* **39**, 491–513.
- [247] Chen, J, Tsai, A, O'Leary, S. E, Petrov, A, & Puglisi, J. D. (2012) Unraveling the dynamics of ribosome translocation. *Current opinion in structural biology* **22**, 804–814.
- [248] Petrov, A, Chen, J, O'Leary, S, Tsai, A, & Puglisi, J. D. (2012) Single-molecule analysis of translational dynamics. *Cold Spring Harbor perspectives in biology* **4**, a011551.
- [249] Schmeing, T. M, Voorhees, R. M, Kelley, A. C, Gao, Y.-G, Murphy, F. V, Weir, J. R, & Ramakrishnan, V. (2009) The crystal structure of the ribosome bound to ef-tu and aminoacyl-trna. *Science* **326**, 688–694.
- [250] Blanchard, S. C, Kim, H. D, Gonzalez, R. L, Puglisi, J. D, & Chu, S. (2004) trna dynamics on the ribosome during translation. *Proceedings of the National Academy of Sciences of the United States of America* **101**, 12893–12898.
- [251] Munro, J. B, Altman, R. B, O'Connor, N, & Blanchard, S. C. (2007) Identification of two distinct hybrid state intermediates on the ribosome. *Molecular cell* **25**, 505–517.
- [252] Munro, J. B, Altman, R. B, Tung, C.-S, Cate, J. H. D, Sanbonmatsu, K. Y, & Blanchard, S. C. (2010) Spontaneous formation of the unlocked state of the ribosome is a multistep process. *Proceedings of the National Academy of Sciences of the United States of America* **107**, 709–14.
- [253] Tsai, A, Petrov, A, Marshall, R. A, Korlach, J, Uemura, S, & Puglisi, J. D. (2012) Heterogeneous pathways and timing of factor departure during translation initiation. *Nature* **487**, 390–393.
- [254] Fei, J, Kosuri, P, MacDougall, D. D, & Gonzalez Jr, R. L. (2008) Coupling of ribosomal l1 stalk and trna dynamics during translation elongation. *Molecular cell* **30**, 348–359.
- [255] Pan, D, Qin, H, & Cooperman, B. S. (2009) Synthesis and functional activity of trnas labeled with fluorescent hydrazides in the d-loop. *RNA* **15**, 346–354.
- [256] Kaur, J, Raj, M, & Cooperman, B. S. (2011) Fluorescent labeling of trna dihydrouridine residues: Mechanism and distribution. *RNA* **17**, 1393–1400.
- [257] Chen, C, Stevens, B, Kaur, J, Cabral, D, Liu, H, Wang, Y, Zhang, H, Rosenblum, G, Smilansky, Z, Goldman, Y. E, & Cooperman, B. S. (2011) Single-molecule fluorescence measurements of ribosomal translocation dynamics. *Molecular cell* **42**, 367–77.
- [258] Peterson, E. T & Uhlenbeck, O. C. (1992) Determination of recognition nucleotides for escherichia coli phenylalanyl-trna synthetase. *Biochemistry* **31**, 10380–10389.
- [259] Nissen, P, Kjeldgaard, M, Thirup, S, Polekhina, G, Reshetnikova, L, Clark, B. F, & Nyborg, J. (1995) Crystal structure of the ternary complex of phe-trnaphe, ef-tu, and a gtp analog. *Science* **270**, 1464–1472.
- [260] Yusupov, M. M, Yusupova, G. Z, Baucom, A, Lieberman, K, Earnest, T. N, Cate, J, & Noller, H. F. (2001) Crystal structure of the ribosome at 5.5 Å resolution. *Science* **292**, 883–896.

- [261] Villa, E, Sengupta, J, Trabuco, L. G, LeBarron, J, Baxter, W. T, Shaikh, T. R, Grassucci, R. A, Nissen, P, Ehrenberg, M, Schulten, K, et al. (2009) Ribosome-induced changes in elongation factor tu conformation control gtp hydrolysis. *Proceedings of the National Academy of Sciences of the United States of America* **106**, 1063–1068.
- [262] Voigts-Hoffmann, F, Hengesbach, M, Kobitski, A. Y, Van Aerschot, A, Herdewijn, P, Nienhaus, G. U, & Helm, M. (2007) A methyl group controls conformational equilibrium in human mitochondrial trnals. *Journal of the American Chemical Society* **129**, 13382–13383.
- [263] Dammertz K, Hengesbach M, H. M. N. G. K. A. (2011) Single-molecule FRET studies of counterion effects on the free energy landscape of human mitochondrial lysine tRNA. *Biochemistry* **50**, 3107–15.
- [264] Voigts-Hoffmann, F. (2006) Master's thesis (Ruprecht-Karls-University Heidelberg, Germany).
- [265] Hirsch, M, Ziroli, V, Helm, M, & Massing, U. (2009) Preparation of small amounts of sterile sirna-liposomes with high entrapping efficiency by dual asymmetric centrifugation (dac). *Journal of Controlled Release* **135**, 80–88.
- [266] McKinney, S. A, Joo, C, & Ha, T. (2006) Analysis of single-molecule fret trajectories using hidden markov modeling. *Biophysical Journal* **91**, 1941–1951.
- [267] Brenner, M. D, Scanlan, M. S, Nahas, M. K, Ha, T, & Silverman, S. K. (2010) Multivector fluorescence analysis of the xpt guanine riboswitch aptamer domain and the conformational role of guanine. *Biochemistry* **49**, 1596–1605.
- [268] Tremblay, R, Lemay, J.-F, Blouin, S, Mulhbacher, J, Bonneau, E, Legault, P, Dupont, P, Penedo, J. C, & Lafontaine, D. a. (2011) Constitutive regulatory activity of an evolutionarily excluded riboswitch variant. *The Journal of Biological Chemistry* **286**, 27406–15.
- [269] De Silva, C & Walter, N. G. (2009) Leakage and slow allostery limit performance of single drug-sensing aptazyme molecules based on the hammerhead ribozyme. *RNA* **15**, 76–84.
- [270] Keller, B. G, Kobitski, A, Jäschke, A, Nienhaus, G. U, & Noe, F. (2014) Complex rna folding kinetics revealed by single-molecule fret and hidden markov models. *Journal of the American Chemical Society* **136**, 4534–4543.
- [271] McDowell, S. E, Jun, J. M, & Walter, N. G. (2010) Long-range tertiary interactions in single hammerhead ribozymes bias motional sampling toward catalytically active conformations. *RNA* **16**, 2414–26.
- [272] Greenfeld, M, Solomatin, S. V, & Herschlag, D. (2011) Removal of covalent heterogeneity reveals simple folding behavior for p4-p6 rna. *Journal of Biological Chemistry* **286**, 19872–19879.
- [273] Hengesbach, M, Kim, N.-K, Feigon, J, & Stone, M. D. (2012) Single-molecule FRET reveals the folding dynamics of the human telomerase RNA pseudoknot domain. *Angewandte Chemie (International ed. in English)* **51**, 5876–9.
- [274] Hao, R, Zhao, M.-W, Hao, Z.-X, Yao, Y.-N, & Wang, E.-D. (2005) A t-stem slip in human mitochondrial trnaleu (cun) governs its charging capacity. *Nucleic Acids Research* **33**, 3606–3613.
- [275] Weeks, K. M. (2010) Advances in rna structure analysis by chemical probing. *Current opinion in structural biology* **20**, 295–304.

- [276] Bellaousov, S, Reuter, J. S, Seetin, M. G, & Mathews, D. H. (2013) Rnastructure: web servers for rna secondary structure prediction and analysis. *Nucleic Acids Research* **41**, W471–W474.
- [277] Zuker, M. (2003) Mfold web server for nucleic acid folding and hybridization prediction. *Nucleic Acids Research* **31**, 3406–3415.
- [278] Markiewicz, R. P, Vrtis, K. B, Rueda, D, & Romano, L. J. (2012) Single-molecule microscopy reveals new insights into nucleotide selection by dna polymerase i. *Nucleic Acids Research* **40**, 7975–84.
- [279] Vrtis, K. B, Markiewicz, R. P, Romano, L. J, & Rueda, D. (2013) Carcinogenic adducts induce distinct DNA polymerase binding orientations. *Nucleic Acids Research* **41**, 7843–7853.
- [280] Swoboda, M, Henig, J, Cheng, H.-M, Brugger, D, Haltrich, D, Plumeré, N, & Schlierf, M. (2012) Enzymatic oxygen scavenging for photostability without ph drop in single-molecule experiments. *ACS nano* **6**, 6364–6369.
- [281] Juette, M. F, Terry, D. S, Wasserman, M. R, Zhou, Z, Altman, R. B, Zheng, Q, & Blanchard, S. C. (2014) The bright future of single-molecule fluorescence imaging. *Current opinion in chemical biology* **20**, 103–111.
- [282] Gill, S. C & Von Hippel, P. H. (1989) Calculation of protein extinction coefficients from amino acid sequence data. *Analytical biochemistry* **182**, 319–326.
- [283] Spenkuch, F., H. G. K. S. T. K. M. R. B. T. H. M. (2014) in revision at. *Nucleic Acids Research*.
- [284] Spenkuch, Felix and Domingo, Olwen and Hinze, Gerald and Basché, Thomas and Helm, Mark. (2014) *Handbook of RNA Biochemistry: Second, Completely Revised and Enlarged Edition*, eds. Roland K. Hartmann, Albrecht Bindereif, A. S & Westhof, E. (Wiley Online Library), pp. 499–526.
- [285] Kellner, S, Ochel, A, Thüring, K, Spenkuch, F, Neumann, J, Sharma, S, Entian, K.-D, Schneider, D, & Helm, M. (2014) Absolute and relative quantification of rna modifications via biosynthetic isotopomers. *Nucleic acids research* p. doi: 10.1093/nar/gku733.
- [286] Lakowicz, J. R. (2009) *Principles of fluorescence spectroscopy*. (Springer).

B. Publications

1. Spenkuch, F (2013) How do Pseudouridine Synthases work? *JUnQ* 3, 2
2. Spenkuch, F, Hinze, G, Domingo, O, Basché, T, & Helm, M (2014) Studying RNA Using Single Molecule Fluorescence Resonance Energy Transfer., in Handbook of RNA Biochemistry: Second, Completely Revised and Enlarged Edition (eds Hartmann, R, K, Bindereif, A, Schön, A, & Westhof E), Wiley-VCH, Weinheim, Germany
3. Kellner, S, Ochel, A, Thüring, K, Spenkuch, F, Neumann, J, Schneider, D, & Helm, M (2014) Absolute and relative quantification of RNA modifications via biosynthetic isotopomers. *Nucleic Acids Research* 42, e142.
4. Spenkuch, F, Hinze, G, Kellner, S, Thüring, K, Micura, R, Basché, T, & Helm, M (2014) Dye label interference with RNA modification reveals 5-fluorouridine as non-covalent inhibitor. *Nucleic Acids Research* doi: 10.1093/nar/gku908
5. Spenkuch, F, Motorin, Y, & Helm, M Pseudouridine - Still mysterious but never a fake (uridine)! Accepted *RNA Biology* as of 10/2014